# Technology Development for Iron and Cobalt Fischer-Tropsch Catalysts

Quarterly Report

January1, 1999 to March 31, 1999

Burtron H. Davis

Enrique Iglesia (UC/B Subcontract)

April 30, 1999

DE-FC26-98FT40308--02

University of Kentucky Research Foundation

201 Kinkead Hall

Lexington, KY 40506

University of California-Berkelely (Subcontract)

Laboratory for the Science and Application of Catalysis

Department of Chemical Engineering

University of California at Berkeley

Berkeley, CA 94720

Abstract

CAER

The impact of activation procedure on the phase composition of precipitated iron Fischer-Tropsch (FT) catalysts has been studied. Catalyst samples taken during activation and FT synthesis have been characterized by Mössbauer spectroscopy. Formation of iron carbide is necessary for high FT activity. Hydrogen activation of precipitated iron catalysts results in reduction to predominantly metallic iron and $Fe_3O_4$. Metallic iron is not stable under FT conditions and is rapidly converted to $\epsilon'$-$Fe_{2.2}C$. Activation with carbon monoxide or syngas with low hydrogen partial pressure reduces catalysts to $\chi$-$Fe_5C_2$ and a small amount of superparamagnetic carbide. Exposure to FT conditions partially oxidizes iron carbide to $Fe_3O_4$; however, catalysts promoted with potassium or potassium and copper maintain a constant carbide content and activity after the initial oxidation. An unpromoted iron catalyst which was activated with carbon monoxide to produce 94% $\chi$-$Fe_5C_2$, deactivated rapidly as the carbide was oxidized to $Fe_3O_4$. No difference in activity, stability or deactivation rate was found for $\chi$-$Fe_5C_2$ and $\epsilon'$-$Fe_{2.2}C$.

UC/B

The temperature-programmed surface reaction (TPSR) of Fe-Zn and Fe-Zn-K-Cu oxides in CO showed that the reduction and carburization of Fe-Zn-K-Cu oxides proceeded in three steps: $Fe_2O_3$ was first reduced to $Fe_3O_4$; Then, $Fe_3O_4$ was reduced to metallic Fe followed by carburization to a mixture of $\chi$-$Fe_{2.5}C$ and $Fe_3C$. The reduction and carburization of Fe oxides shifted to higher temperatures at higher Zn contents; K slightly inhibited both the reduction and carburization of Fe oxides; Cu decreased not only the temperature required for the reduction but also that for carburization. In-situ X-ray absorption studies at Fe K-edge for Fe-Zn-K-Cu oxide in CO showed progressive shifts of the edge energy from 7123 eV ($Fe^{3+}$) to 7112 eV ($Fe^0$) along with changes in the near-edge and fine structure regions while increasing the carburization temperature up to 500 $^oC$. The Fischer-Tropsch synthesis (FTS) on Fe-Zn oxide showed that the addition of potassium (2 ~ 4 at.%) significantly increased FTS and water-gas shift reaction rates, decreased the selectivity to methane and increased selectivities to high molecular weight hydrocarbons and to olefins. $CO_2$ addition experiments showed that the addition of $CO_2$ inhibited the formation of $CO_2$ via water-gas shift reactions but did not affect the FTS reaction. FTS reaction rates and selectivities at different space velocities on $Co/SiO_2$ catalysts showed that CO conversion and $C_{5+}$ selectivity increased while $CH_4$ selectivity and $\alpha$-olefin to *n*-paraffin ratio decreased with increasing bed residence time. Also, FTS reaction rates increased with increasing bed residence time. Water increased FTS rates and selectivities to $C_{5+}$ and olefins. CO conversion rates increased with increasing water partial pressure. $D_2O$ tracer studies showed that water dissociation was not quasi-equilibrated in Co-catalyzed FTS. The kinetic isotope effect (KIE) experiments on Co catalysts suggested that hydrogen dissociation involved in the rate-determining step and that chain termination to olefins was larger for deuterium containing chains.

Table of Contents

Executive Summary

CAER

Formation of an iron carbide is necessary for high activity with precipitated iron catalysts. A precipitated iron catalyst (100Fe/4.6Si/2.7Cu/1.0K) which was activated with hydrogen at 220$^{O}$C and ambient pressure was partially reduced to metallic iron and $Fe_3O_4$. Metallic iron was not stable under FT conditions and exposure to syngas ($H_2$/CO=0.7) at 270ºC and 1.3 MPa converted all of the metallic iron to $\epsilon'$-$Fe_{2.2}C$. Catalysts activated with carbon monoxide (unpromoted iron and 100Fe/8.9Cu/1.9K/67kaolin) or syngas with low hydrogen partial pressure (100Fe/3.6Si/0.7K) at 270$^{O}$C produced predominantly $\chi$-$Fe_5C_2$ and had high initial syngas conversion. Activation with syngas at 270$^{O}$C and 1.3 MPa partially reduced the 100Fe/3.6Si/0.7K catalyst to 100% $Fe_3O_4$ which resulted in low FT activity. Iron carbides produced by carbon monoxide and syngas activation of promoted catalysts were partially oxidized to $Fe_3O_4$ during the first 24 hours of FT synthesis; however, these catalysts deactivated slowly. There was no difference in the activity, stability or deactivation characteristics of $\epsilon'$-$Fe_{2.2}C$ and $\chi$-$Fe_5C_2$ under the FT conditions employed in this study. Catalysts with stable activity maintained a constant iron carbide level. An unpromoted iron catalyst deactivated more rapidly than iron catalysts promoted with potassium, copper and a nonreducible metal oxide. The deactivation of the unpromoted iron catalyst was caused by oxidation of active iron carbide to inactive/less active $Fe_3O_4$.

The presence of iron carbides and $Fe_3O_4$ together can be explained by inhomogeneity of gases within individual catalyst particles. Water and carbon dioxide produced by conversion of syngas within catalyst particles can cause the environment inside a particle to be oxidizing while the surface is exposed to reducing conditions of the reactor atmosphere. This would result in the formation of a $Fe_3O_4$ core and an iron carbide outer layer. Another possibility is that under typical FT conditions the redox potential of the reactor atmosphere lies within the narrow region of the C/H/O/Fe phase diagram where $Fe_3O_4$ and iron carbides can coexist.

UC/B

During this reporting period, we have continued to investigate the temperature-programmed surface reaction (TPSR) of Fe-Zn and Fe-Zn-K-Cu oxides with CO in order to determine the temperatures required for the reduction and carburization of the oxides, the rates at which Fe carbides are formed and the amount of Fe oxide that is reduced or carburized. Generally, the reduction and carburization of the oxides proceeded in three steps: $Fe_2O_3$ was first reduced to $Fe_3O_4$ at about 270ºC; Then, $Fe_3O_4$ was reduced to metallic Fe followed by carburization to a mixture of $\chi$-$Fe_{2.5}C$ and $Fe_3C$ between 270 ~ 450ºC. Above 450ºC, CO disproportionation (Boudouard reaction) occurred, leading to the formation of excess free carbon. X-ray diffraction measurements showed that a phase transformation from $\chi$-$Fe_{2.5}C$ to $Fe_3C$ occurred at about 450ºC.

The TPSR studies on the effects of Zn, K and Cu on the reduction and carburization of the Fe oxides showed that Zn did not appreciably influence the reduction and carburization of Fe oxides at low Zn contents (<0.2). However, the reduction and carburization on the sample with high Zn content (e.g., 0.4 Zn/Fe) shifted to higher temperatures because $ZnFe_2O_4$ is more stable against reduction than $Fe_2O_3$; K slightly inhibited both the reduction and carburization of Fe

oxides; Cu decreased not only the temperature required for the reduction but also that for carburization. Cu appeared to facilitate the incorporation of carbon within Fe to form Fe carbides.

In-situ X-ray absorption studies on Fe-based catalyst were conducted at the Stanford Synchrotron Research Laboratory (SSRL) during this reporting period. X-ray absorption near-edge spectra (XANES) and extended X-ray absorption fine structure spectra (EXAFS) at Fe K-edge for Fe-Zn-K-Cu oxide (Zn/Fe = 0.1, 2 at.% K, 1 at.% Cu) were recorded in flowing $H_2$, CO and synthesis gas at different temperatures. Fe K-edge spectra for the Fe-Zn-K-Cu oxide in CO showed progressive shifts of the edge energy from 7123 eV ($Fe^{3+}$) to 7112 eV ($Fe^0$) along with changes in the near-edge and fine structure regions while increasing the temperature up to 500°C. A principal component analysis of the near-edge spectra is being carried out in order to quantify the relative concentration of various oxide, carbide and metal phases during FTS.

The effects of potassium on Fischer-Tropsch synthesis (FTS) were examined on Fe-based catalysts (Zn/Fe = 0.1, 1 at.% Cu) with different K contents (0 ~ 4 at.%). The addition of potassium (2 ~ 4 at.%) increased FTS and water-gas shift reaction rates, decreased the selectivity to methane and increased selectivities to high molecular weight hydrocarbons and to olefins. Potassium levels above 2 at.% had only small effects on FTS rates and selectivities. Also, the promotion effect of K was more evident at 235°C and 21.4 atm than at 270°C and 5 atm for all K contents.

The effects of $CO_2$ addition on the rate of water-gas shift reaction and on the selectivities to $CO_2$ and hydrocarbons were investigated by adding $CO_2$ on a K-free sample (Zn/Fe = 0.1, 1 at.% Cu) at 270°C and 5 atm. Addition of $CO_2$ inhibited the formation of $CO_2$ via water-gas shift but did not affect the FTS reaction because both the CO conversion rate and $CO_2$ net formation rate decreased when $CO_2$ was added but FTS rates did not depend on $CO_2$ pressure. The inhibit effect of $CO_2$ on the water-gas shift reaction was less evident on a K-containing sample (Zn/Fe = 0.07, 2 at.% K and 1 at.% Cu) for FTS that was run at 235°C and 21.4 atm since the water-gas shift reaction is more thermodynamically favorable at lower temperatures. Although addition of $CO_2$ can be used to decrease $CO_2$ yields during FTS, the elimination of net $CO_2$ formation may well require levels of $CO_2$ that are impractical because of separation and re-compression costs.

Co catalysts were prepared by incipient wetness impregnation of $SiO_2$ with Co nitrate solution (12.7 wt.% and 21.9 wt.%). FTS reaction rates and selectivities at different space velocities showed that CO conversion and $C_{5+}$ selectivity increased while $CH_4$ selectivity and $\alpha$-olefin to *n*-paraffin ratio decreased with increasing bed residence time. FTS reaction rates also increased with increasing bed residence time. Water, one of the reaction products, appeared to have an accelerating effect on FTS rates. Water effects on FTS rates and selectivities were examined by adding $H_2O$ (2 ~ 8 atm) to synthesis gas feeds at low CO conversions. CO conversion rates increased with increasing water partial pressure. The selectivity to desired $C_{5+}$ products increased and the olefin content in products also increased with increasing water partial pressure. The beneficial effect of water on the FTS rate and product distribution reflects an increase in the rate of chain growth and in chain termination to $\alpha$-olefins.

$D_2O$ tracer studies are being carried out on Co catalysts by co-feeding 2 atm $D_2O$ with 20 atm synthesis gas (13.8 % D in the feed). The D contents in the primary products ($C_4$-$C_8$) and in the $H_2$ isotopomers increased as the bed residence time increased. This indicates that water dissociation is not quasi-equilibrated in the Co-catalyzed FTS. The kinetic isotope effect (KIE) was also studied by comparing the FTS rates in flowing $H_2/CO/N_2$ (62/31/7) and $D_2/CO/N_2$ (62/31/7). The ratio of methane formation rate ($k_{CH4}/k_{CD4}$) was 1.34, suggesting the involvement

of hydrogen dissociation in the rate-determining step. In contrast, KIE were less than worthy for steps leading to the formation of higher molecular weight olefins, suggesting that chain termination to olefins is larger for deuterium containing chains. In the next report, we will discuss the mechanistic implications of these findings.

**Task 1. Iron Catalyst Preparation**

The objective of this task is to produce robust intermediate- and high-α catalysts.
No scheduled or further activity to report.

**Task 2. Catalyst Testing**

The objective of this task is to obtain catalyst performance on the catalysts prepared in Task 1.

No scheduled or further activity to report.

**Task 3. Catalyst Characterization**

The objective of this task is to obtain characterization data of the prepared catalysts using routine and selected techniques.

## Mössbauer Spectroscopy of Iron-Based Fischer-Tropsch Catalysts: Impact of Activation Procedure

Robert J. O'Brien[1], Yong-Qing Zhang[1], Shuh-Jeng Liaw[1], Hussein H. Hamdeh[2] and Burtron H. Davis[1]

1. University of Kentucky, Center for Applied Energy Research
2540 Research Park Drive
Lexington, KY 40511-8410

2. Wichita State University, Department of Physics
Wichita, KS 67260

### Abstract

The impact of activation procedure on the phase composition of precipitated iron Fischer-Tropsch (FT) catalysts has been studied. Catalyst samples taken during activation and FT synthesis have been characterized by Mössbauer spectroscopy. Formation of iron carbide is necessary for high FT activity. Hydrogen activation of precipitated iron catalysts results in reduction to predominantly metallic iron and $Fe_3O_4$. Metallic iron is not stable under FT conditions and is rapidly converted to $\epsilon'$-$Fe_{2.2}C$. Activation with carbon monoxide or syngas with low hydrogen partial pressure reduces catalysts to $\chi$-$Fe_5C_2$ and a small amount of superparamagnetic carbide. Exposure to FT conditions partially oxidizes iron carbide to $Fe_3O_4$; however, catalysts promoted with potassium or potassium and copper maintain a constant carbide content and activity after the initial oxidation. An unpromoted iron catalyst which was activated with carbon monoxide to produce 94% $\chi$-$Fe_5C_2$, deactivated rapidly as the carbide was oxidized to $Fe_3O_4$. No difference in activity, stability or deactivation rate was found for $\chi$-$Fe_5C_2$ and $\epsilon'$-$Fe_{2.2}C$.

## Introduction

Iron Fischer-Tropsch (FT) catalysts undergo numerous phase changes which may have profound effects on catalyst activity (1-3), selectivity (4), attrition (5) and deactivation (6). Precipitated and fused iron catalysts are typically oxides before use and need to be activated by reducing to the zero valent state. The activation procedure generally involves reducing with hydrogen to metallic iron or with carbon monoxide or syngas to various iron carbides. Metallic iron, produced by hydrogen activation, is rapidly converted to iron carbides when exposed to syngas under FT conditions (2,3). Additional phase transformations may occur during FT synthesis. Water is a primary product of the FT synthesis and may reach concentrations high enough to oxidize iron carbides to $Fe_3O_4$ (7). In addition, carbon dioxide produced by the water-gas shift reaction can reach oxidizing concentrations at high conversion (7). A thermodynamic study of the iron carbide/oxide system under typical FT conditions has shown that both $Fe_3O_4$ and iron carbide are thermodynamically favored (8).

Several iron carbides have been identified in active iron FT catalysts. Among these are: $\chi$-$Fe_5C_2$, $\epsilon'$-$Fe_{2.2}C$, $\theta$-$Fe_3C$ and $Fe_7C_3$. The thermal stability of $\chi$-$Fe_5C_2$, $\epsilon'$-$Fe_{2.2}C$, and $\theta$-$Fe_3C$ carbides with increasing temperature has been reported to be: $\epsilon'$-$Fe_{2.2}C \leq \chi$-$Fe_5C_2 < \theta$-$Fe_3C$ (9, 10). Conducting FT synthesis at moderate to low temperatures ($<270^{O}C$) generally results in $\chi$-$Fe_5C_2$ and/or $\epsilon'$-$Fe_{2.2}C$ formation (2, 3). The $\theta$-$Fe_3C$ and $Fe_7C_3$ carbides have been reported at high temperature FT synthesis with fused iron catalysts (7). The role of iron carbides in FT synthesis has been debated since Fischer and Tropsch proposed hydrocarbons were formed by the hydrogenation of bulk iron carbide (11). Emmett demonstrated that hydrocarbons synthesized over a $^{14}C$ labeled iron carbide catalyst had lower radioactivity than the catalyst thereby demonstrating that bulk iron carbide does not directly participate in hydrocarbon production; however, Emmett did not rule out the possibility that a surface carbide was involved in hydrocarbon production (12). Subsequent studies with $^{13}C$ tracers have verified that carbon on the surface of carbided catalysts does become incorporated in FT products (13).

In addition to iron carbides, $Fe_3O_4$ (magnetite) is generally found in used iron FT catalysts. Magnetite has been reported to be both active (14) and inactive for FT synthesis (1). The discrepancy may be due to oxidation of iron carbides by improper passivation prior to analysis (15). Metallic iron has also been proposed to be active for FT synthesis (5). This is unlikely because thermodynamic data predict metallic iron will either be oxidized to $Fe_3O_4$ or converted to iron carbide(s) depending on the conversion level (8).

Herein, the impact of hydrogen, carbon monoxide and syngas activation on the phase composition of precipitated iron catalysts will be presented. Correlations between phase composition and FT activity and deactivation will be discussed.

## Experimental

Catalysts with atomic composition 100Fe/4.6Si/1.0K, 100Fe/4.6Si/2.7Cu/1.0K, 100Fe/3.7Si/0.7K and an unpromoted catalyst were prepared by continuous precipitation and incipient wetness impregnation of promoters as previously described (1). A commercially prepared catalyst with mass composition 100Fe/8.9Cu/1.9K/67kaolin was obtained from United Catalysts Inc. Catalyst and Ethlyflo 164 (Ethyl) $C_{30}$ oil were charged into a one liter autoclave operated as a continuous stirred tank reactor (cstr). Hydrogen activation was conducted by heating the reactor to $220^{O}C$ at $120^{O}C/h$ with hydrogen flow of 120 l $h^{-1}$ (STP) at ambient

pressure; conditions were maintained for 24 hours. Activation with carbon monoxide was conducted at 270$^{O}$C for 24 hours at 1.3 MPa pressure with a space velocity of 2 l h$^{-1}$ g-Fe$^{-1}$ (STP). Syngas activations were conducted at 270$^{O}$C for 24 hours with $H_2$/CO=0.7 and space velocity of 3.1 l h$^{-1}$ g-Fe$^{-1}$ (STP) at either ambient pressure or 1.3 MPa. Fischer-Tropsch synthesis was conducted at 270$^{O}$C, $H_2$/CO=0.7, space velocity=3.1 l h$^{-1}$ g-Fe$^{-1}$ (STP) and 1.3 MPa pressure.

Catalyst/slurry samples were removed from the reactor periodically during activation and throughout FT synthesis. Mössbauer spectra were obtained with a conventional constant acceleration spectrometer using 30 mCi $^{57}$Co in rhodium matrix. Catalyst compositions are given as percent of total iron. For example, 80% $Fe_5C_2$ refers to 80% of the total iron in the catalyst being in $Fe_5C_2$.

**Results**

*Hydrogen activation*

Mössbauer spectroscopy data of 100Fe/4.6Si/2.7Cu/1.0K catalyst during hydrogen activation are shown in Figure 1. Exposure of the catalyst to hydrogen at 220$^{O}$C for 2 hours resulted in the catalyst being partially reduced to 20% $Fe_3O_4$ with the remaining 80% a superparamagnetic species. During the course of the activation, the $Fe_3O_4$ phase increased at the expense of the superparamagnetic species. Metallic iron (10%) was first detected after 10 hours of activation and after 24 hours of activation the catalyst composition was 65% $Fe_3O_4$, 24% metallic iron and 11% superparamagnetic species.

Exposure of the hydrogen activated catalyst to syngas at FT conditions caused rapid phase changes. Within 3 hours of starting FT synthesis, the superparamagnetic species had disappeared, the metallic iron decreased to 4% and $\epsilon'$-$Fe_{2.2}C$ (34%) was formed. Following 20 hours of FT synthesis, the $Fe_3O_4$ had decreased slightly to 59% and the remainder of the catalyst was $\epsilon'$-$Fe_{2.2}C$. Catalyst composition and syngas conversion as a function of time on stream are shown in Figure 3. The catalyst had high initial syngas conversion (85%) and deactivated slowly at the rate of 0.9% per week. The catalyst was run for over 3500 hours during which the catalyst composition remained constant at approximately 60% $Fe_3O_4$ and 40% $\epsilon'$-$Fe_{2.2}C$.

*Carbon monoxide activation*

Phase changes for a typical iron-based catalyst during carbon monoxide activation are shown in Figure 4 (16). The 100Fe/8.9Cu/1.9K/67kaolin catalyst was initially $\alpha$-$Fe_2O_3$ as determined by XRD and Mössbauer spectroscopy. The catalyst was reduced to 100% $Fe_3O_4$ during the heating from ambient temperature to 270$^{O}$C (2 hours) under carbon monoxide. Iron carbide phases began to appear after 4.5 hours of activation. The first carbide phase detected was a superparamagnetic carbide; this phase increased to approximately 10% of the iron and remained constant throughout the activation. $\chi$-$Fe_5C_2$ (26%) was first detected after 10 hours of activation and continued to increase at the expense of $Fe_3O_4$. The catalyst composition after 26 hours of activation was 90% $\chi$-$Fe_5C_2$ and 10% superparamagnetic carbide. Carbon dioxide production as a function of time on stream is also plotted in Figure 4. Carbon dioxide can be produced by the reduction of $\alpha$-$Fe_2O_3$ to $Fe_3O_4$ (equation 1), reduction of $Fe_3O_4$ to iron carbide (equation 2) and from the Boudouard reaction (equation 3).

$$3Fe_2O_3 + CO \rightarrow 2Fe_3O_4 + CO_2 \quad (1)$$
$$5Fe_3O_4 + 32CO \rightarrow 3Fe_5C_2 + 26CO_2 \quad (2)$$
$$2CO \rightarrow C + CO_2 \quad (3)$$

Figure 4 shows that enough carbon dioxide was produced after 8 hours to account for 100% carbiding of the catalyst; however, Mössbauer data reveal that the catalyst was approximately 10% iron carbide at this time. By the end of carbon monoxide activation, there was approximately 60% more carbon dioxide produced than was needed to completely carbide the catalyst. This indicates that a large amount of Boudouard carbon was produced.

Figure 5 shows that the iron carbide was partially oxidized to $Fe_3O_4$ (8%) after 20 hours of FT synthesis. Over the remainder of the run (140 h), the $Fe_3O_4$ content grew to 16% with the balance a mixture of $\chi$-$Fe_5C_2$ and superparamagnetic carbide. Catalyst activity remained high during the run with carbon monoxide conversion greater than 65%.

An unpromoted iron catalyst was also activated with carbon monoxide under identical conditions to the catalyst described above. The catalyst was reduced to 94% $\chi$-$Fe_5C_2$ and 6% $Fe_3O_4$ after 24 hours of activation; no superparamagnetic carbide was detected. This catalyst initially had high FT activity with syngas conversion of 84%; however, the catalyst was not stable and deactivated at the rate of 3.7% syngas conversion per day. The catalyst composition changed significantly during the deactivation; as the conversion decreased, the amount of $\chi$-$Fe_5C_2$ decreased and the amount of $Fe_3O_4$ increased. The catalyst was 100% $Fe_3O_4$ after 450 hours of FT synthesis and the syngas conversion had decreased to 18%.

*Syngas activation*

Catalyst composition and syngas conversion for the 100Fe/3.6Si/0.7K catalyst activated at FT synthesis conditions, syngas ($H_2$/CO=0.7) at 270$^O$C and 1.3 MPa, are shown in Figure 6 (16). Initial syngas conversion was 6% and it increased slowly to only 18% after 92 hours on stream; the catalyst was composed of 100% $Fe_3O_4$ during this time. Since the conversion was low, the catalyst was treated with carbon monoxide for 19 hours at 1.3 MPa and 270$^O$C. The catalyst was partially reduced to 42% $\chi$-$Fe_5C_2$ and superparamagnetic carbide after the carbon monoxide treatment. Fischer-Tropsch synthesis was resumed and the syngas conversion increased rapidly to the same level obtained for another FT run when the catalyst was activated with carbon monoxide (Figure 6). This run was continued for 430 hours during which the syngas conversion remained close to 80% and the catalyst composition was approximately 40% $\chi$-$Fe_5C_2$ and superparamagnetic carbide with the remainder $Fe_3O_4$.

Figure 7 shows the composition and syngas conversion for the 100Fe/3.6Si/0.7K catalyst after activation with syngas ($H_2$/CO=0.7) at ambient pressure and 270$^O$C for 24 hours (16). In contrast to activation with syngas at 1.3 MPa, activation at ambient pressure resulted in a catalyst with high syngas conversion (82%). The catalyst composition after activation was 68% $\chi$-$Fe_5C_2$ and superparamagnetic carbide and 32% $Fe_3O_4$. The total iron carbide content decreased to 53% during the first 24 hours and then slowly decreased to 40% after 400 hours. The remainder of the catalyst was $Fe_3O_4$. Syngas conversion decreased slowly to 65% after 400 hours.

**Discussion**

Activation of the 100Fe/4.6Si/2.7Cu/1.0K catalyst with hydrogen at 220$^{O}$C for 24 hours partially reduced the catalyst to 24% metallic iron, 11% superparamagnetic species and 65% $Fe_3O_4$. Exposing the activated catalyst to FT conditions caused the conversion of all of the metallic iron and superparamagnetic species and a small amount of $Fe_3O_4$ to $\epsilon'$-$Fe_{2.2}C$. Throughout 3500 hours of FT synthesis, the catalyst composition remained constant at 40% $\epsilon'$-$Fe_{2.2}C$ and 60% $Fe_3O_4$. The catalyst had high initial activity with syngas conversion greater than 80% and a deactivation rate of only 0.9% syngas conversion per week. In contrast, activation with carbon monoxide resulted in greater than 90% of an unpromoted iron catalyst and a 100Fe/8.9Cu/1.9K/67kaolin catalyst being reduced to $\chi$-$Fe_5C_2$ and a small amount of superparamagnetic iron carbide. The superparamagnetic carbide was not identified because Mössbauer data were collected at room temperature; however, this may be small particle $\epsilon'$-$Fe_{2.2}C$ (9). Activation with hydrogen lean syngas at ambient pressure was very similar to activation with carbon monoxide. The catalyst was composed of 68% $\chi$-$Fe_5C_2$ and superparamagnetic carbide following activation.

Activation with hydrogen, carbon monoxide or syngas can result in high activity if the appropriate promoters and conditions are applied (Figure 8). Activation with hydrogen requires that the catalyst be promoted with copper to lower the reduction temperature and prevent sintering; catalysts activated with hydrogen that do not contain copper generally have lower activity and require a long induction period (17). In addition, a high space velocity of hydrogen is required to maintain a low water partial pressure in the reactor and thereby prevent sintering of metallic iron (7). In the case of syngas activation, a low hydrogen partial pressure is required to minimize the water concentration in the reactor which if too high prevents $Fe_3O_4$ from being reduced to $\chi$-$Fe_5C_2$ (1). If the activation procedure is conducted properly, hydrogen, carbon monoxide or syngas activated catalysts will have similar activity. There does not seem to be a difference in the activity of hydrogen activated catalysts where the carbide phase of the active catalyst is $\epsilon'$-$Fe_{2.2}C$ and the activity of carbon monoxide or syngas activated catalysts where the predominant carbide phase is $\chi$-$Fe_5C_2$. Likewise the deactivation characteristics of hydrogen, carbon monoxide and syngas activated catalysts are very similar over the span of at least 1000 hours (8). This is surprising because it has been reported that $\epsilon'$-$Fe_{2.2}C$ is not as active as $\chi$-$Fe_5C_2$ and the transformation of $\epsilon'$-$Fe_{2.2}C$ into $\chi$-$Fe_5C_2$ has been identified as a cause of deactivation of iron catalysts (6). Although it there is no difference in activity of $\epsilon'$-$Fe_{2.2}C$ and $\chi$-$Fe_5C_2$, a strong correlation between iron carbide content and FT activity has been observed. An unpromoted iron catalyst immediately following carbon monoxide activation was composed of 92% $\chi$-$Fe_5C_2$ and 8% $Fe_3O_4$. The catalyst gradually oxidized to $Fe_3O_4$ during FT synthesis and after 450 hours was 100% $Fe_3O_4$. Catalyst activity, as measured by syngas conversion, decreased linearly from 84% to 19% as the catalyst was oxidized. Although the syngas conversion was 19% after the catalyst had been oxidized to $Fe_3O_4$, it is possible that the low activity was due to a small amount of iron carbide not detectable by Mössbauer spectroscopy (<5%) and not $Fe_3O_4$.

Catalysts which had stable activity were composed of 40% to 85% iron carbide and 60% to 15% $Fe_3O_4$ throughout FT synthesis. The question of how a catalyst can be partially and not completely oxidize during FT synthesis can be answered by thermodynamic analysis of the C/H/O/Fe system (8). A phase diagram of the C/H/O system is shown in Figure 9. The diagram is a ternary plot on the basis of mole % of C, H and O of the gases in the reactor atmosphere (CO, $CO_2$, $H_2$, $H_2O$ and $CH_x$) at 300$^{O}$C and 1.5 MPa. Iron carbide and carbon are the stable phases in

Region A, iron carbide, $Fe_3O_4$ and carbon are the stable phases in Region B, $Fe_3O_4$ and carbon are the stable phases in Region C and $Fe_3O_4$ is the stable phase in region D. Composition of the reactor atmosphere at syngas conversion ranging from 29% to 84% are shown on the phase diagram for a typical FT catalyst. The gas composition of the reactor atmosphere over this range of conversions lies close to the boundary of iron carbide/carbon and iron carbide/$Fe_3O_4$/carbon regions. Another possible explanation for the presence of both iron carbide(s) and $Fe_3O_4$ is inhomogeneity within catalyst particles. The ultimate particle size of a precipitated iron catalyst is on the order of 200 Å and these particles form agglomerates which can be smaller than 1 $\mu$m or as large as 250 $\mu$m. Conversion of carbon monoxide and hydrogen to carbon dioxide, water and hydrocarbons in the interior of these agglomerates can cause the water and carbon dioxide concentrations within the particles to be higher than at the surface of the agglomerate which is exposed to the bulk gas phase. This could lead to the formation of particles with a $Fe_3O_4$ core and an iron carbide surface.

## Conclusions

Formation of an iron carbide is necessary for high activity with precipitated iron catalysts. A precipitated iron catalyst (100Fe/4.6Si/2.7Cu/1.0K) which was activated with hydrogen at 220$^O$C and ambient pressure was partially reduced to metallic iron and $Fe_3O_4$. Metallic iron was not stable under FT conditions and exposure to syngas ($H_2$/CO=0.7) at 270ºC and 1.3 MPa converted all of the metallic iron to $\epsilon'$-$Fe_{2.2}C$. Catalysts activated with carbon monoxide (unpromoted iron and 100Fe/8.9Cu/1.9K/67kaolin) or syngas with low hydrogen partial pressure (100Fe/3.6Si/0.7K) at 270$^O$C produced predominantly $\chi$-$Fe_5C_2$ and had high initial syngas conversion. Activation with syngas at 270$^O$C and 1.3 MPa partially reduced the 100Fe/3.6Si/0.7K catalyst to 100% $Fe_3O_4$ which resulted in low FT activity. Iron carbides produced by carbon monoxide and syngas activation of promoted catalysts were partially oxidized to $Fe_3O_4$ during the first 24 hours of FT synthesis; however, these catalysts deactivated slowly. There was no difference in the activity, stability or deactivation characteristics of $\epsilon'$-$Fe_{2.2}C$ and $\chi$-$Fe_5C_2$ under the FT conditions employed in this study. Catalysts with stable activity maintained a constant iron carbide level. An unpromoted iron catalyst deactivated more rapidly than iron catalysts promoted with potassium, copper and a nonreducible metal oxide. The deactivation of the unpromoted iron catalyst was caused by oxidation of active iron carbide to inactive/less active $Fe_3O_4$.

The presence of iron carbides and $Fe_3O_4$ together can be explained by inhomogeneity of gases within individual catalyst particles. Water and carbon dioxide produced by conversion of syngas within catalyst particles can cause the environment inside a particle to be oxidizing while the surface is exposed to reducing conditions of the reactor atmosphere. This would result in the formation of a $Fe_3O_4$ core and an iron carbide outer layer. Another possibility is that under typical FT conditions the redox potential of the reactor atmosphere lies within the narrow region of the C/H/O/Fe phase diagram where $Fe_3O_4$ and iron carbides can coexist.

## Acknowledgment

This work was supported by the U.S. Department of Energy, Contract DE-FC26-98FT40308, and the Commonwealth of Kentucky.

**References**


1. R. J. O'Brien, L. Xu, R. L. Spicer, and B. H. Davis, *Energy & Fuels*, 10 (1996) 921.
2. R. J. O'Brien, L. Xu, D. R. Milburn, Y.-X. Li, K. J. Klabunde and B. H. Davis, *Topics in Catalysis*, 2 (1995) 1.
3. D. B. Bukur, M. Koranne, X. Lang, K. R. P. M. Rao and G. P. Huffman, *Applied Catal.*, 126 (1995) 85.
4. S. Soled, E. Iglesia and R. A. Fiato, *Catal. Letters*, 7 (1990) 271.
5. N. B. Jackson, A. K. Datye, L. Mansker, R. J. O'Brien, and B. H. Davis, in C. H. Bartholomew and G. A. Fuentes (Editors), Catalyst Deactivation, Elsevier Science B. V. 1997, pp. 517-526.
6. S. A. Eliason and C. H. Bartholomew, in C. H. Bartholomew and G. A. Fuentes (Editors), Catalyst Deactivation, Elsevier Science B. V. 1997, pp. 501-516.
7. M. E. Dry, in J. R. Anderson and M. Boudart (Editors), Catalysis Science and Technology, Vol 1, Springer-Verlag, New York, 1981, p. 157-255.
8. B. H. Davis, Department of Energy Final Report, Contract No. DE-AC22-94PC94055, 1998, pp. 66-82.
9. J. A. Amelse, J. B. Butt, and L. H. Schwartz, *J. Phys. Chem.*, 82 (1978) 558.
10. J. W. Niemantsverdriet, A. M. van der Kraan, W. L. van Dijk, and H. S. van der Baan, J. *Phys. Chem.*, 84 (1980) 3363.
11. F. Fischer, and H. Tropsch, *Ges. Abhandl. Kenntnis Kohle*, 10 (1932) 313.
12. J. T. Kummer, T. W. DeWitt and P. H. Emmett, *J. Am. Chem. Soc.*, 70 (1948) 3632.
13. D. M. Stockwell, D. Bianchi, and C. O. Bennett, *J. Catal.*, 113 (1988) 13.
14. J. P. Reymond, P. Mériaudeau, and S. J. Teichner, *J. Catal.*, 75 (1982) 39.
15. M. D. Shroff, D. S. Kalakkad, K. E. Coulter, S. D. Köhler, M. S. Harrington, N. B. Jackson, A. G. Sault and A. K. Datye, *J. Catal.*, 156 (1995) 185.
16. K. R. P. M. Rao, F. E. Huggins, G. P. Huffman, R. J. Gormley, R. J. O'Brien, and B. H. Davis, *Energy & Fuels*, 10 (1996) 546.
17. R. J. O'Brien, L. Xu, R. L. Spicer, S. Bao, D. R. Milburn, and B. H. Davis, Catalysis Today, 36 (1997) 325.

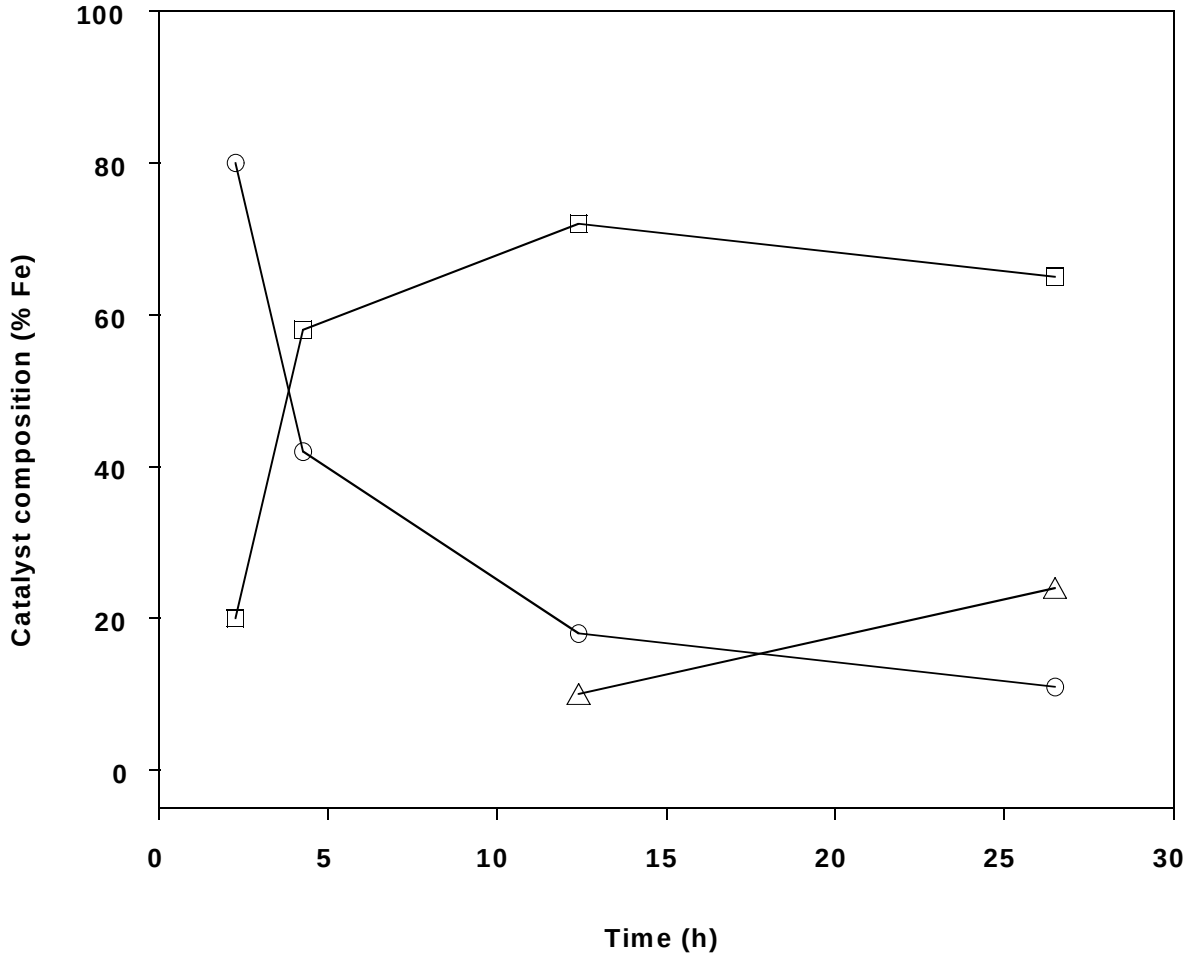


Figure 1. Phase composition changes of 100Fe/4.6Si/2.7Cu/1.0K catalyst during activation with $H_2$ at 220$^{O}$C, 0.1 MPa. (○), superparamagnetic oxide; (□), $Fe_3O_4$; (△), $Fe^{O}$.

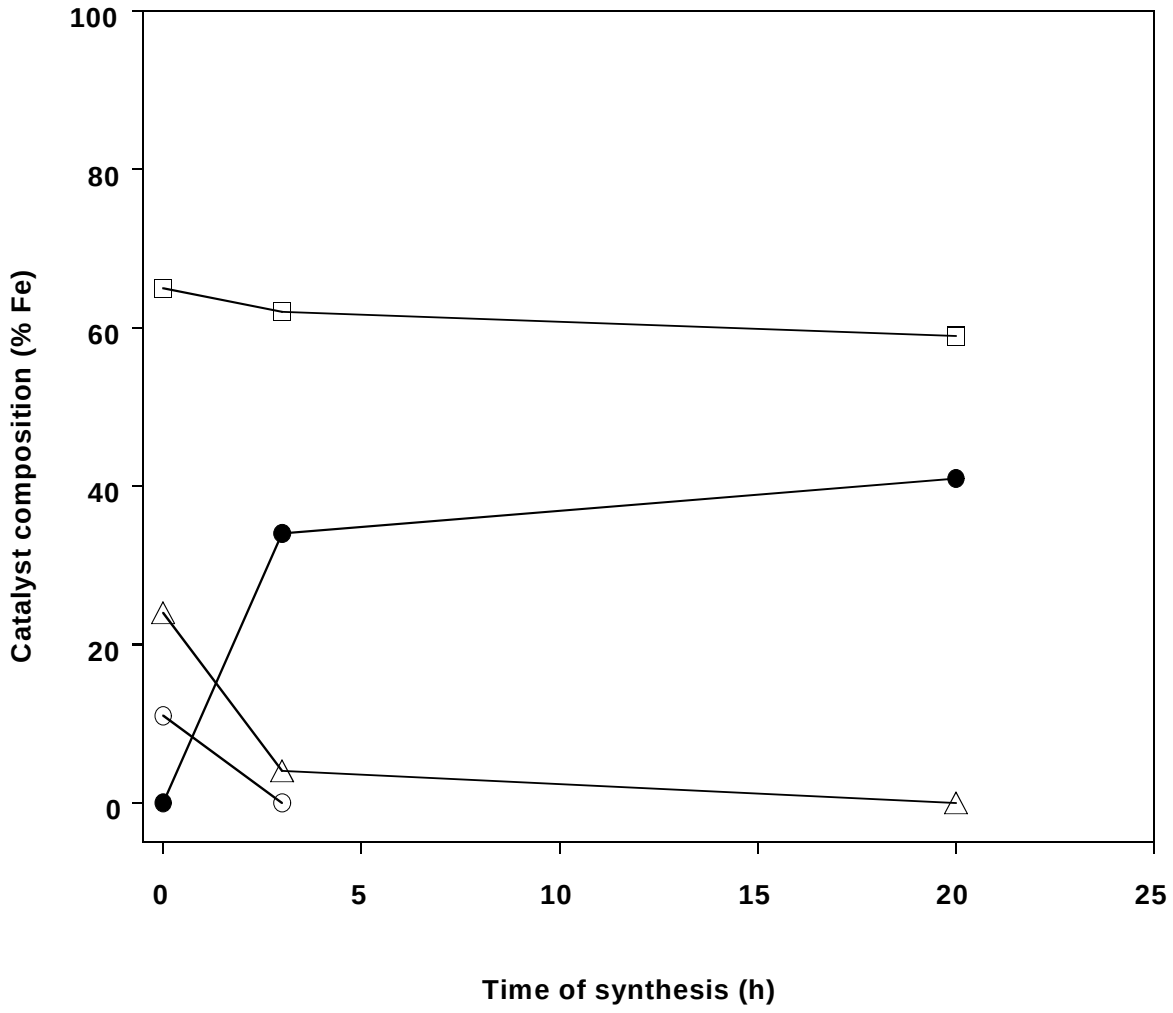


Figure 2. Phase composition changes of $H_2$ activated 100Fe/4.6Si/2.7Cu/1.0K catalyst during first 24 hours of FT synthesis (270$^{O}$C, 1.3 MPa, $H_2$/CO=0.7, whsv=3.1 sl $h^{-1}$ g-$Fe^{-1}$). (○), superparamagnetic oxide; (□), $Fe_3O_4$; (△), $Fe^{O}$; (●), $\epsilon'$-$Fe_{2.2}C$.

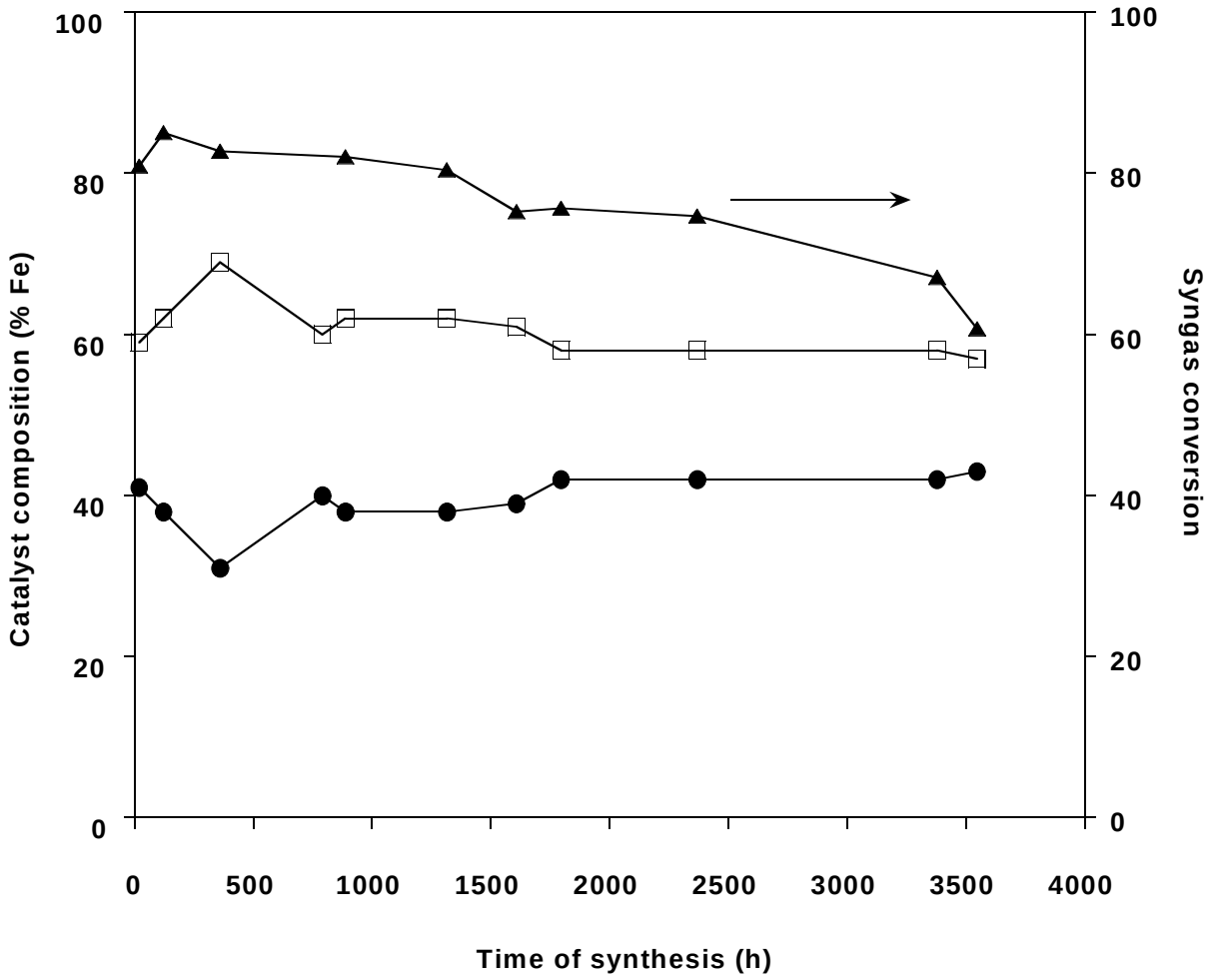


Figure 3. Long term phase composition of $H_2$ activated 100Fe/4.6Si/2.7Cu/1.0K catalyst during FT synthesis (270$^{O}$C, 1.3 MPa, $H_2$/CO=0.7, whsv=3.1 sl $h^{-1}$ g-$Fe^{-1}$). (□), $Fe_3O_4$; (●), $\epsilon'$-$Fe_{2.2}C$; (▲), syngas conversion.

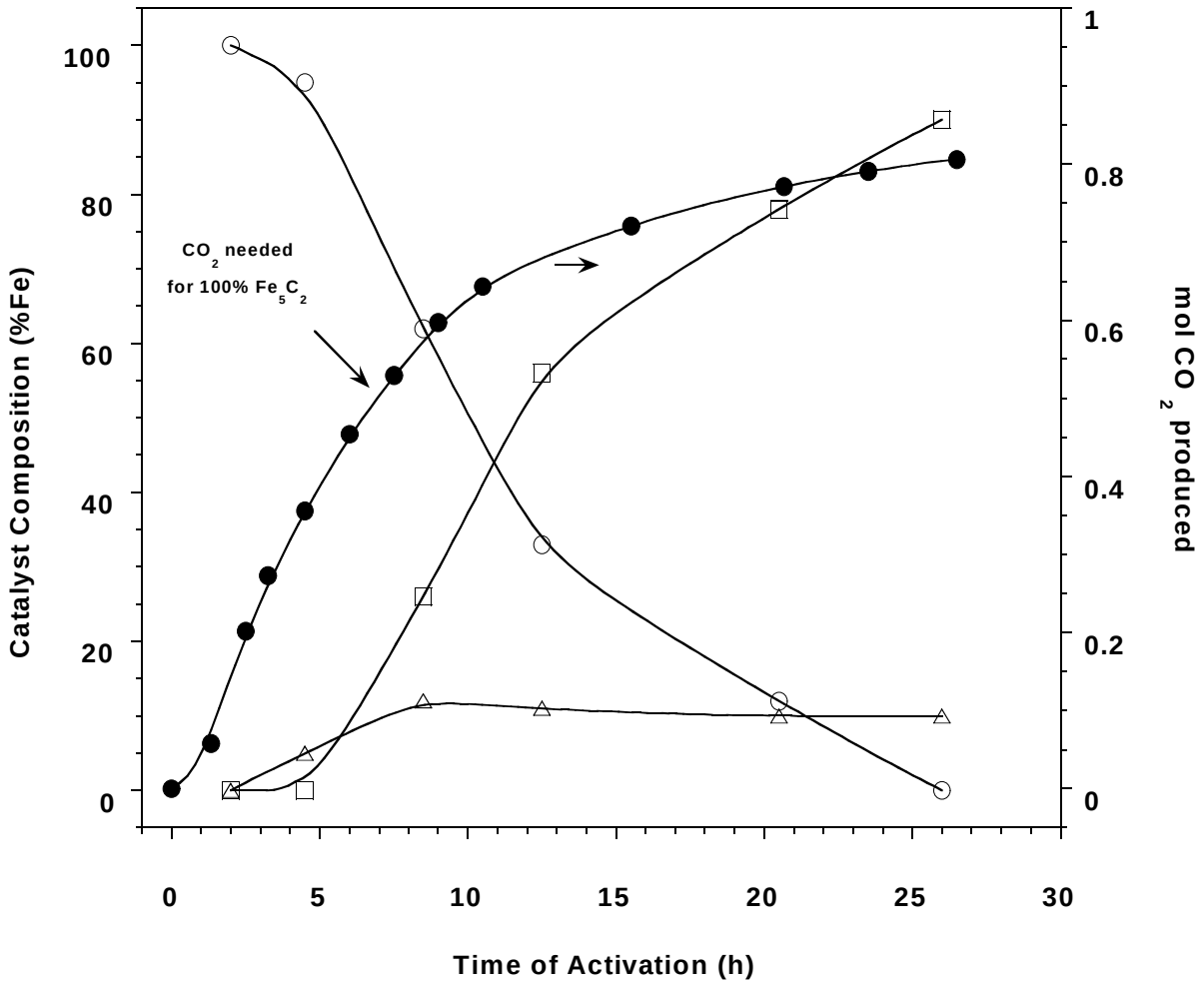


Figure 4. Phase composition changes of commercial 100Fe/8.9Cu/1.9K/67kaolin catalyst and moles of $CO_2$ generated during CO activation. (○), $Fe_3O_4$; (□), $\chi$-$Fe_5C_2$; (△), superparamagnetic carbide; (●), moles of $CO_2$. Mössbauer data from reference 16.

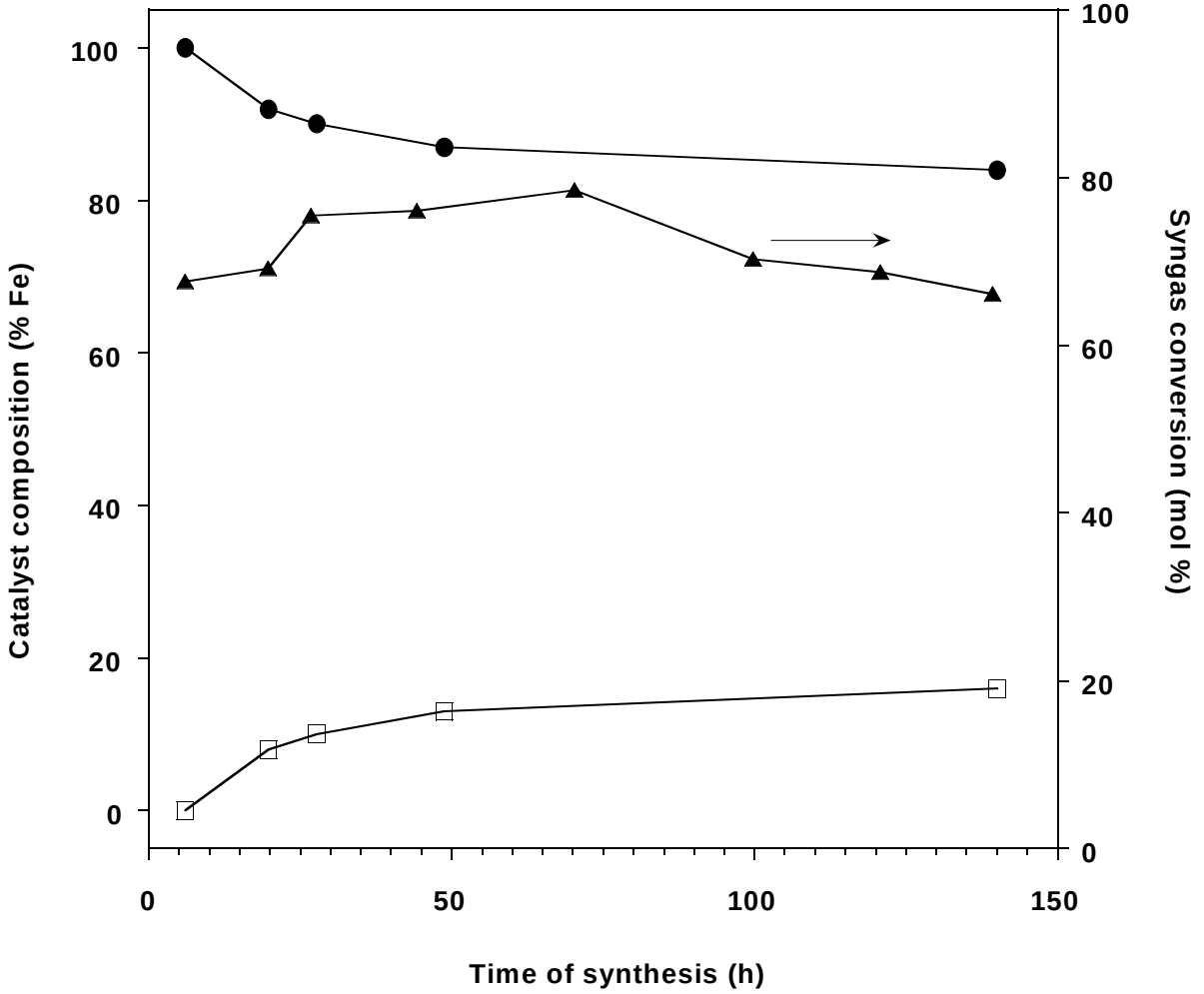


Figure 5. Phase composition of CO activated 100Fe/8.9Cu/1.9K/67kaolin catalyst during FT synthesis (270$^{O}$C, 1.3 MPa, $H_2/CO$=0.7, whsv=3.1 sl $h^{-1}$ g-$Fe^{-1}$). (●), $\chi$-$Fe_5C_2$ and superparamagnetic carbides; (□), $Fe_3O_4$; (▲), syngas conversion. Data from reference 16.

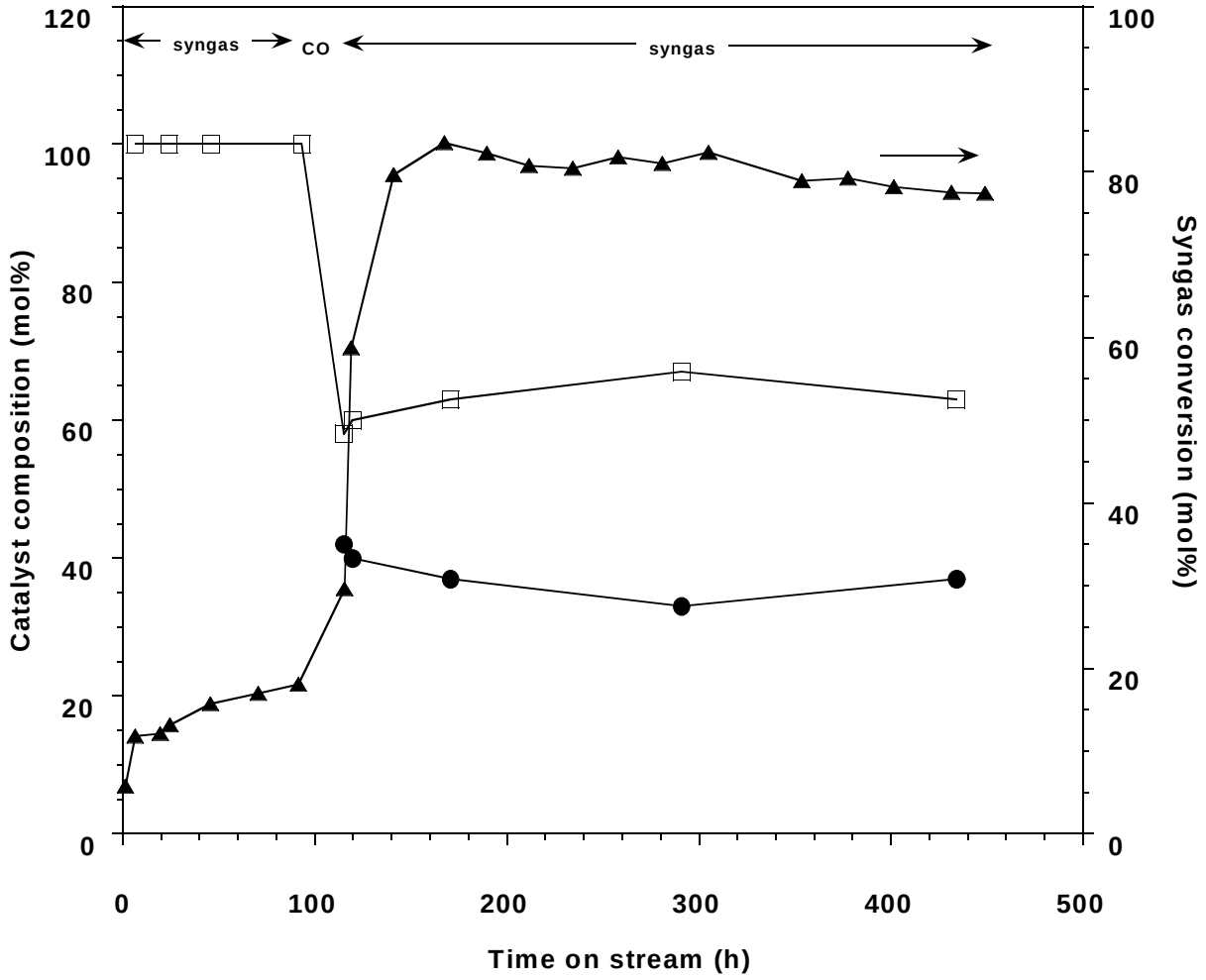


Figure 6. Phase composition of 100Fe/3.7Si/0.7K catalyst during syngas activation at 270$^{O}$C, 1.3 MPa followed by CO treatment at 270$^{O}$C, 1.3 MPa followed by FT synthesis (270$^{O}$C, 1.3 MPa, $H_2$/CO=0.7, whsv=3.1 sl $h^{-1}$ g-$Fe^{-1}$). (□), $Fe_3O_4$ and superparamagnetic oxide; (●) χ-$Fe_5C_2$ and superparamagnetic carbides; (▲) syngas conversion. Data from reference 16.

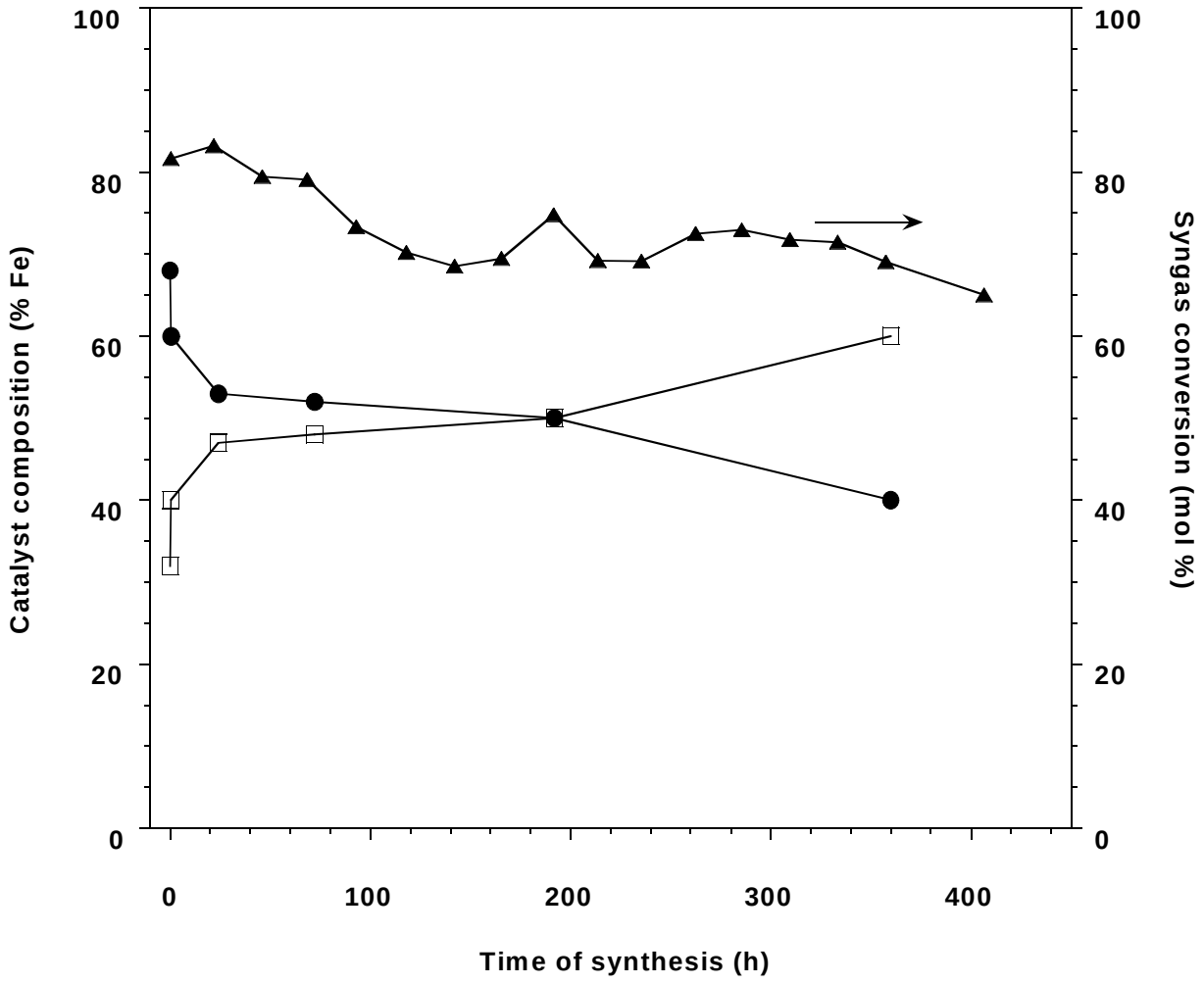


Figure 7. Phase composition of syngas activated ($H_2$/CO=0.7, 0.1 MPa, 270$^{O}$C) 100Fe/3.7Si/0.7K catalyst during FT synthesis (270$^{O}$C, 1.3 MPa, $H_2$/CO=0.7, whsv=3.1 sl $h^{-1}$ g-$Fe^{-1}$). (●), $\chi$-$Fe_5C_2$ and superparamagnetic carbides; (□), $Fe_3O_4$; (▲) syngas conversion. Data from reference 16.

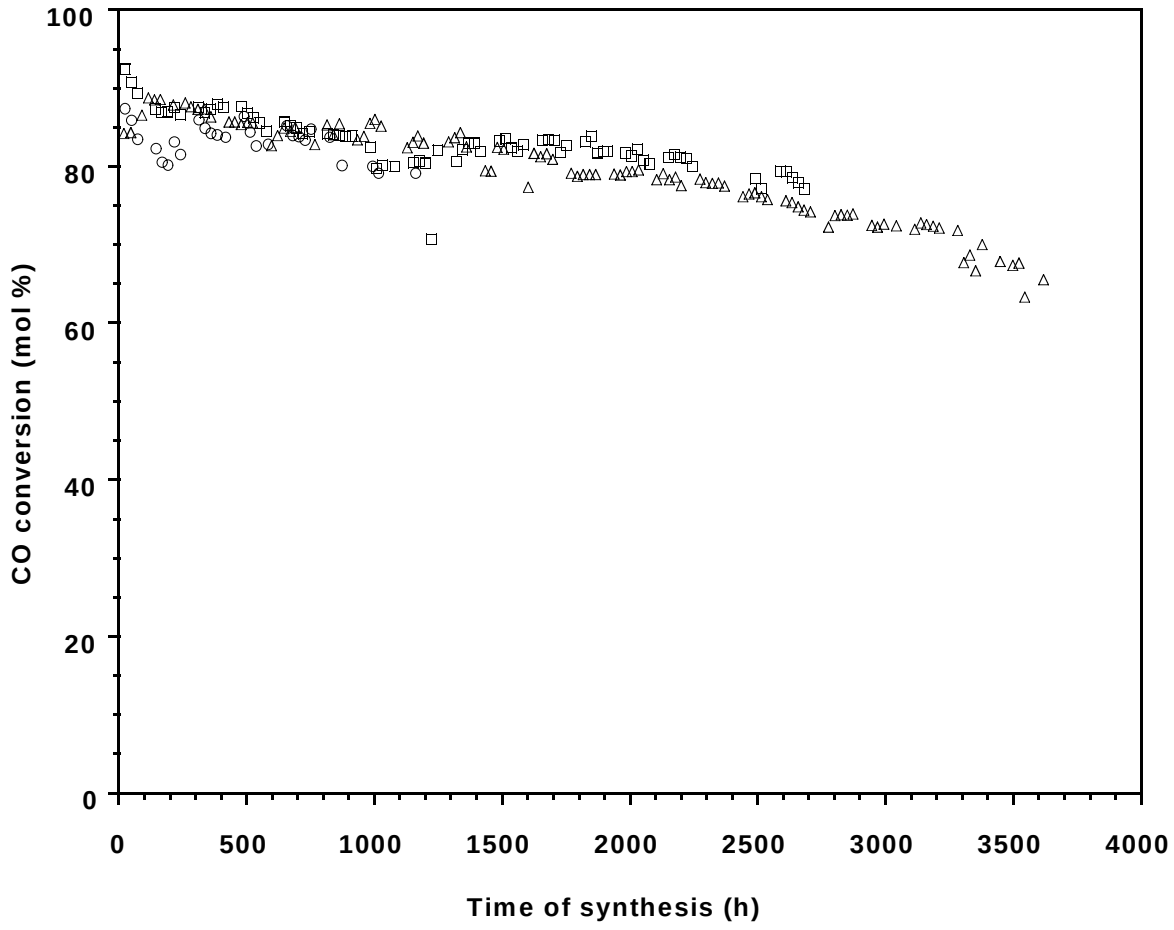


Figure 8. Comparison of CO conversion for (○), 100Fe/4.6Si/1.0K activated with CO at 270$^{O}$C, 0.1MPa; (□), 100Fe/4.6Si/1.0K, activated with syngas ($H_2$/CO=0.7) at 270$^{O}$C, 0.1 MPa; and (△) 100Fe/4.6Si/2.0Cu/1.0K activated with $H_2$ at 220$^{O}$C, 0.1 MPa. FT conditions: 270$^{O}$C, 1.3 MPa, $H_2$/CO=0.7, whsv=3.1 sl $h^{-1}$ g-$Fe^{-1}$).

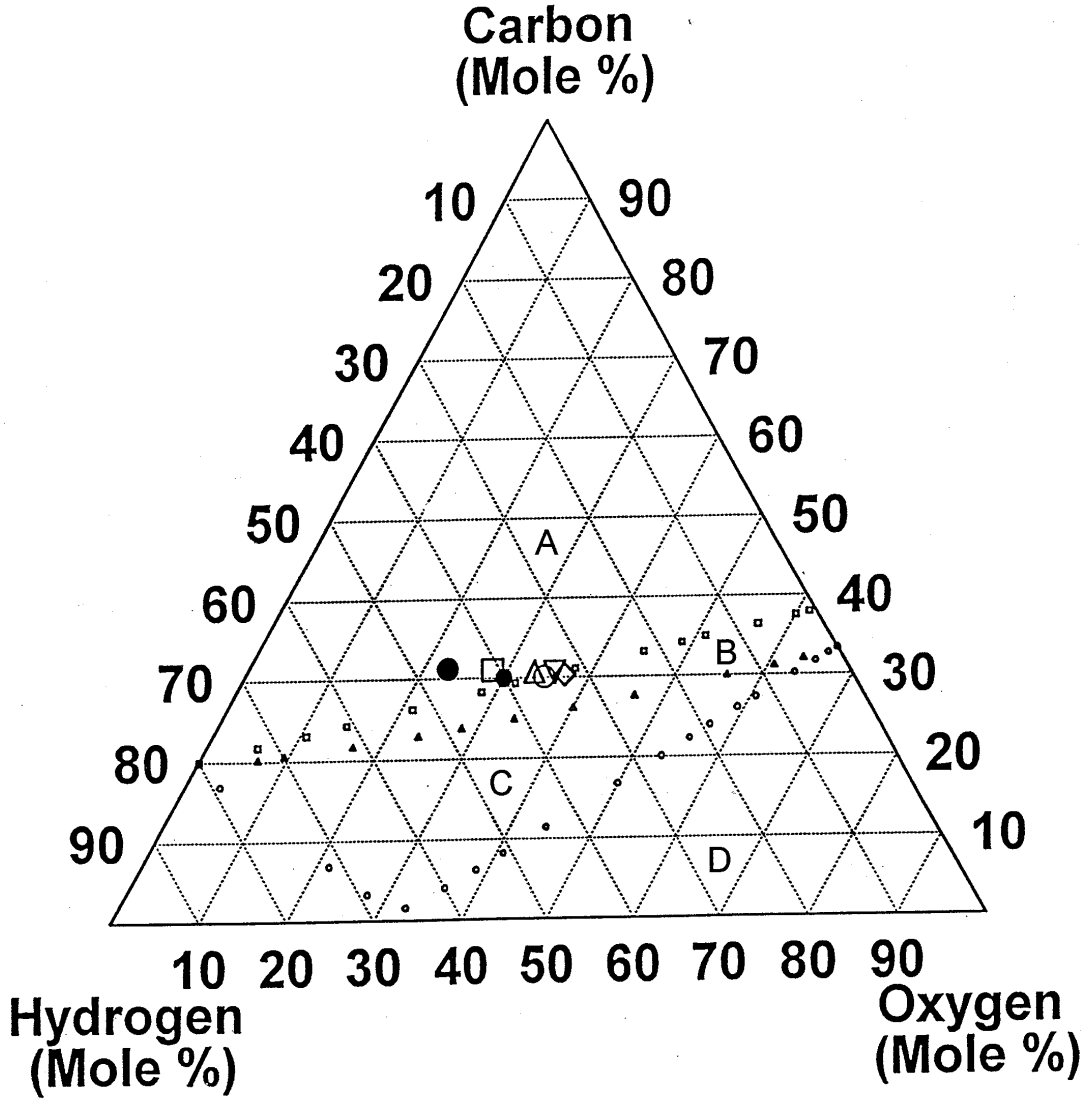


Figure 9. Ternary phase diagram for solid phase(s) present for graphite/gases (○), $Fe/Fe_3O_4$/gases (□) and $Fe/Fe_3C$/gases (△) at equilibrium at 300$^{O}$C ant 1.5 MPa. Region A: $Fe_3C$ and C; Region B: $Fe_3O_4$, $Fe_3C$ and C; Region C: $Fe_3O_4$ and C; Region D: $Fe_3O_4$. Gases = $H_2O$, CO, $CO_2$, $H_2$ and $CH_4$. Gas phase composition during FT synthesis (270$^{O}$C, 1.3 MPa) at various conversions: CO=86%, $H_2$=80% (●); CO=78%, $H_2$=76% (□); CO=68%, $H_2$=69% (△); CO=46%, $H_2$=54% (◊); CO=32%, $H_2$=45% (▽); CO=23%, $H_2$=37% (○) and syngas composition of $H_2/CO$=0.67 (●).

**Task 4. Wax/Catalyst Separation**

The objective of this task is to develop techniques for the separation of catalysts from FT reactor slurries.

No scheduled or further activity to report.

**Task 5. Oxygenates**

The objective of this task is to obtain a better understanding of the factors that affects catalyst selectivity toward oxygenates for iron-based Fischer-Tropsch catalsyts.

No scheduled or further activity to report.

**Task 6. Literature Review of Prior Fischer-Tropsch Synthesis with Co Catalysts**

The objective of this task is to prepare a critical review of prior work on cobalt Fischer-Tropsch catalysts.

This task is approximately 90% complete. Due to the size of the document, it has been submitted as a separate report to the AAD Document Control labeled Task 6.

**Task 7. Co Catalyst Preparation**

The objective of this task is to prepare a limited number of cobalt-based Fischer-Tropsch catalysts that can be used to obtain baseline data on cobalt-based Fischer-Tropsch synthesis.

No scheduled or further activity to report.

**Task 8. Cobalt Catalyst Testing for Activity and Kinetic Rate Correlations**

The objective of this task is to conduct initial screening of the cobalt catalysts prepared in Task7 to select three baseline catalysts that will then be used to generate a data base on the performance of cobalt-based Fischer-Tropsch catalysts in slurry reactors.

No scheduled or further activity to report.

**Task 9. Cobalt Catalyst Life Testing**

The objective of this task is to obtain life data on baseline cobalt Fischer-Tropsch catalysts.

No scheduled for further activity to report.

**Task 10. Cobalt Catalyst Mechanism Study**

The objective of this task is to determine the impact of secondary reactions on the relationship of cobalt Fischer-Tropsch catalysts under conditions appropriate to slurry bubble column reactors.

No scheduled or further activity to report.

**Task 11. University of California, Berkeley (Subcontract)**

The objective of this task is the characterization of the structure and function of active sites involved in the synthesis of high molecular weight hydrocarbons from CO and $H_2$ on multi-component catalysts based on Fe as the active component.

*Quarterly Research Report*

January 1, 1999 to March 31, 1999

**Structural and Catalytic Characterization of the Mechanism and Site Requirements in Fischer-Tropsch Synthesis on Fe and Co Catalysts**

**Principal Investigator** Enrique Iglesia
Laboratory for the Science and Applications of Catalysis
Department of Chemical Engineering
University of California at Berkeley
Berkeley, CA 94720

**Project Personnel:** Auwu Li (UC-Berkeley)
Mai Tu (UC-Berkeley)
Senzi Li (UC-Berkeley)
Wei Li (UC-Berkeley)

## I. FISCHER-TROPSCH SYNTHESIS ON IRON CATALYSTS

### 1. Background

*1.1. Structure and Function of Active Phases in Fischer-Tropsche Synthesis*

Fe-based oxides have been used as commercial catalysts for Fischer-Tropsch synthesis (FTS) to produce a large variety of paraffin and olefin products, ranging from methane to high molecular weight waxes [1]. During activation by synthesis gas and subsequent FTS reaction, several phases including metallic iron, iron carbides and iron oxides are known to co-exist at steady-state conditions [2-5]. The distribution and amounts of these phases depend on exposure to various activation and reaction conditions, leading to different catalytic performances in FTS. Some researchers [6] have proposed that surface iron atoms are responsible for FTS activity, while some others considered surface carbides or a mixture of carbides [7,8] and metallic iron [9] to be the active phase. There are also some reports that suggest that magnetite $Fe_3O_4$ is the active phase in FTS [10-12]. Although these studies have each provided some evidence to support their specific proposals about the active phase, the available information remains phenomenological, and a method to identify the active phase during reaction and to count the number of active sites has not yet been established.

Based on the previous research on Co [13,14] and Fe catalysts [15,16] for FTS as well as our last quarterly work on TPSR of Fe oxides in $H_2$, our characterization during this research period involves temperature-programmed reactions of Fe-based catalysts with flowing streams of CO or $H_2$-CO mixtures. We monitored the gas phase concentrations throughout the reduction and carburization processes by means of an on-line mass spectrometer, and followed the evolution of bulk phases and crystal size by X-ray

diffraction and of surface area by nitrogen physisorption measurements. In this way, we can determine the temperature required for the formation of Fe carbides as well as the stoichiometry and structure of such carbides. Our goal is to develop a new synthesis method to improve the compositional and structural purity of Fe carbides formed, and consequently to refine the structure-function relationships that we have previously proposed to interpret the catalytic behavior of Fe-based catalysts.

### *1.2. Effect of Zn, K and Cu*

Many components have been added to Fe catalysts in order to improve their mechanical and catalytic properties. Our previous studies have shown that zinc, alkali and copper [16,17] promote the catalytic properties of Fe oxides. Zinc oxide, as a non-reducible oxide in FTS conditions, appears to stabilize the surface area of Fe oxide. Alkali, as a modifier of the adsorption enthalpies of $H_2$ and CO, increases the selectivity to desired $C_{5+}$ products. Copper promotes the carburization processes and decreases the temperature required for the activation of iron oxide. Here, our efforts have focused on Fe-Zn-K-Cu catalysts. We have prepared a series of Zn and Fe co-precipitated oxides with varied Zn/Fe ratios and then introduced varying amounts of K and Cu. We are examining the surface area, bulk structure, required reduction and carburization temperatures as well as the catalytic behavior of these catalysts, in order to identify optimum Zn/Fe ratios and Cu and K contents that give maximum site density and catalytic activity.

## 2. Synthesis Procedures for Fe-Zn-K-Cu Oxides

All catalysts were prepared by co-precipitation of zinc and iron nitrates at a constant pH of 7.0 in order to to form porous mixed oxides. Then, these oxide precursors were impregnated with an aqueous solution of potassium and copper salts using incipient wetness methods. The Zn/Fe oxide precursors were prepared first. Fe nitrate (1.4 M) and Zn nitrate (3.0 M) solutions were mixed at a given atomic Zn/Fe ratio. A solution of ammonium carbonate (1 M) was prepared separately. Deionized water (ca. 50 ml) was added into a large flask, which was heated on a hot plate with a magnetic stirrer and held at 80 $^{o}$C throughout the preparation process. The mixed Zn/Fe solution was added at 2 $cm^3$/min flow into the flask through a feeding pump. At the same time, the ammonium carbonate solution was fed separately, and its flow was controlled to maintain the slurry pH at 7±0.1, as monitored by a pH meter. The resulting precipitates were washed several times with about 1 *l* water per gram of catalyst, dried at 120 $^{o}$C overnight, and then calcined at 350 $^{o}$C for 1 h. The calcined material was promoted with 2 at.% K using $K_2CO_3$ solution (0.16 M) by incipient wetness and then dried. The same process was repeated in order to promote samples with 1 at.% Cu using $Cu(NO_3)_2$ solutions (0.16 M). Finally, the dried material was treated in dry air at 400 $^{o}$C for 4 h. This final calcination temperature was chosen from temperature-programmed oxidation data, which showed that this temperature is sufficient to decompose all metal nitrates and carbonates except $K_2CO_3$. The catalysts contain CuO, ZnO, $Fe_2O_3$ and $K_2CO_3$. These catalysts were pressed at 443 MPa into pellets, lightly crushed, and then sieved to retain the 80 - 140 mesh fraction for FTS reaction.

## 3. Catalyst Characterization

### *3.1. Protocols for the Characterization of Fe-based FTS Catalysts*

This research program addresses the synthesis and the structural and catalytic characterization of the active sites of Fe-based catalysts for FTS. We have designed a matrix of samples that contains a systematic range of multi-components catalysts in order to determine the number and type of surface sites present on fresh catalysts and the samples after FTS reaction (Table 1.1). Our objective is to develop rigorous relationships between the synthesis methods, the resulting catalyst structures, and their function in FTS reactions.

### *3.2. Surface Area*

The surface areas of Fe-Zn oxides calcined at different temperatures and promoted with K and Cu are shown in Table 1.2. The calcination temperatures we used for Fe-Zn oxides and for K or Cu promoted Fe-Zn oxide samples were 350 $^{o}$C and 400 $^{o}$C, respectively. The surface area measurements on Fe-Zn oxide (Zn/Fe=0.1) at 350 $^{o}$C and 400 $^{o}$C gave similar values (56 vs 53 $m^2g^{-1}$), indicating that the calcination temperature does not influence the surface area at the investigated temperature region. The lower surface areas (ca. 20%) for K or Cu promoted samples were caused by the presence of K or Cu species.

Table 1.1 Matrix of Fe-Zn-K-Cu samples and characterization methods for FTS reaction

<table>
<tr><th colspan="3">Composition of the Catalysts</th><th rowspan="2">Characterization Before and After FTS</th><th rowspan="2">FTS reaction</th></tr>
<tr><th>Zn/Fe mole ratio</th><th>K (at.%)</th><th>Cu (at.%)</th></tr>
<tr><td rowspan="6">0</td><td rowspan="2">0</td><td>0</td><td rowspan="20">XRD<br><br>Surface area<br><br>In-situ XAS<br><br>$H_2$-TPR<br><br>CO-TPR<br><br>$(H_2+CO)$-TPR</td><td rowspan="20">Effect of reaction condition<br><br>220 $^oC$<br>21.4 atm<br><br>235 $^oC$<br>21.4 atm<br><br>270 $^oC$<br>5 atm<br><br>Effect of $CO_2$ addition</td></tr>
<tr><td>1</td></tr>
<tr><td rowspan="3">2</td><td>0</td></tr>
<tr><td>1</td></tr>
<tr><td>2</td></tr>
<tr><td>4</td><td>1</td></tr>
<tr><td rowspan="3">0.05</td><td>0</td><td>0</td></tr>
<tr><td>2</td><td>1</td></tr>
<tr><td>4</td><td>2</td></tr>
<tr><td rowspan="6">0.1</td><td rowspan="2">0</td><td>0</td></tr>
<tr><td>1</td></tr>
<tr><td rowspan="3">2</td><td>0</td></tr>
<tr><td>1</td></tr>
<tr><td>2</td></tr>
<tr><td>4</td><td>1</td></tr>
<tr><td rowspan="3">0.2</td><td>0</td><td>0</td></tr>
<tr><td>2</td><td>1</td></tr>
<tr><td>4</td><td>2</td></tr>
<tr><td rowspan="6">0.4</td><td rowspan="2">0</td><td>0</td></tr>
<tr><td>1</td></tr>
<tr><td rowspan="3">2</td><td>0</td></tr>
<tr><td>1</td></tr>
<tr><td>2</td></tr>
<tr><td>6</td><td>1</td></tr>
</table>

Table 1. 2. Surface areas ($m^2g^{-1}$) of Fe-Zn-K-Cu samples (Zn/Fe=0.1)

| Composition | Without K and Cu | | 1 at.% Cu | 2 at.% K |
|---|---|---|---|---|
| Calcination Temperature ($^oC$) | 350 | 400 | 400 | 400 |
| $S_g$ ($m^2g^{-1}$) | 56 | 53 | 44 | 40 |

### *3.3. Temperature-Programmed Surface Reaction (TPSR) of Fe-Zn and Fe-Zn-K-Cu Oxides in CO*

Temperature-programmed reduction and carburization of Fe-Zn oxides in CO have been carried out during this reporting period. Since CO either reduces metal oxides releasing $CO_2$ or carburizes metallic Fe forming carbide, we can quantitatively analyze the amount of Fe being reduced and carburized from the amount of CO consumption and $CO_2$ formation from the following formulas:

$$Fe_xO + CO = Fe_xC + CO_2 + C \text{ (graphite)}$$

Amount of oxide reduced = 2($CO_2$ formation) – (CO consumption)
Amount of carbide or free carbon formed = (CO consumption) – ($CO_2$ formation)

Combined with XRD measurements, these data allow us to get information about the temperatures and rates at which carbides are formed, about the amount of Fe oxide that is reduced or carburized, and about the stoichiometry of the carbides formed. We used several samples of typical composition from the catalyst matrix (Table 1.1) to test the effects of Zn, K and Cu on the reduction and carburization behavior of Fe oxide.

A typical TPSR of Fe-Zn-K-Cu oxides in CO is shown in Figure 1.1(A). Generally, the reduction/carburization of the oxides proceeds in three steps: $Fe_2O_3$ is first reduced to $Fe_3O_4$ at about 270 $^oC$; Then, $Fe_3O_4$ is reduced to metallic Fe followed by carburization to a mixture of $\chi$-$Fe_{2.5}C$ and $Fe_3C$ between 270 ~ 450 $^oC$; Above 450 $^oC$, CO disproportionation (Boudouard reaction) occurs, leading to the formation of excess free carbon. XRD measurements (Figure 1.1(B)) showed that a phase transformation from $\chi$-$Fe_{2.5}C$ to cementite ($Fe_3C$) occurs at about 450 $^oC$ during carburization in CO (Figure 1.1). The excess free carbon formed in this phase transformation may act as nucleation sites for the subsequent deposition of free carbon via the Boudouard reaction.

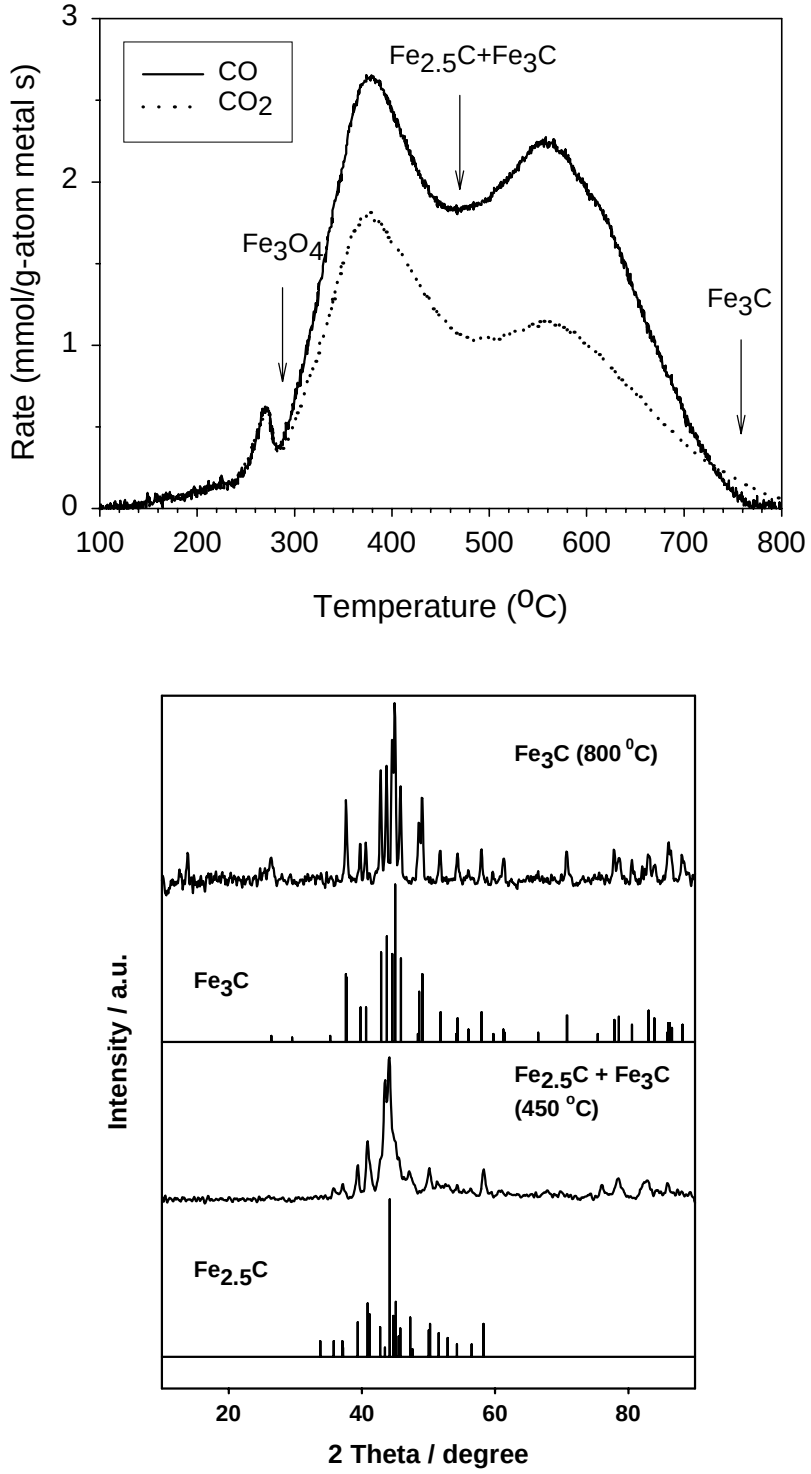


Figure 1.1 (A) TPSR of Fe-Zn-K-Cu oxide (Zn/Fe=0.1, 2 at.% K and 1 at.% Cu) in CO (0.2 g samples; 10 $^{o}$C/min ramping rate; 100 cm$^{3}$/min, 20% CO/Ar). (B) XRD showing the phase transformation from $\chi$-$Fe_{2.5}C$ to cementite $Fe_3C$ during the TPSR in CO.

3.3.1. Effect of Zn on the Reduction and Carburization of Fe Oxides in CO

Figure 1.2 shows the reduction (A) and carburization (B) of Fe-Zn oxides with different Zn/Fe ratio in CO. Stoichiometric calculations show that $Fe_2O_3$ is first reduced to $Fe_3O_4$ at around 270 $^oC$ and further reduced to metallic Fe at temperatures between 270~500 $^oC$. The carburization of metallic Fe occurs at 350 $^oC$, and the carburization rate increases dramatically following the marked increase of the reduction rate of $Fe_3O_4$.

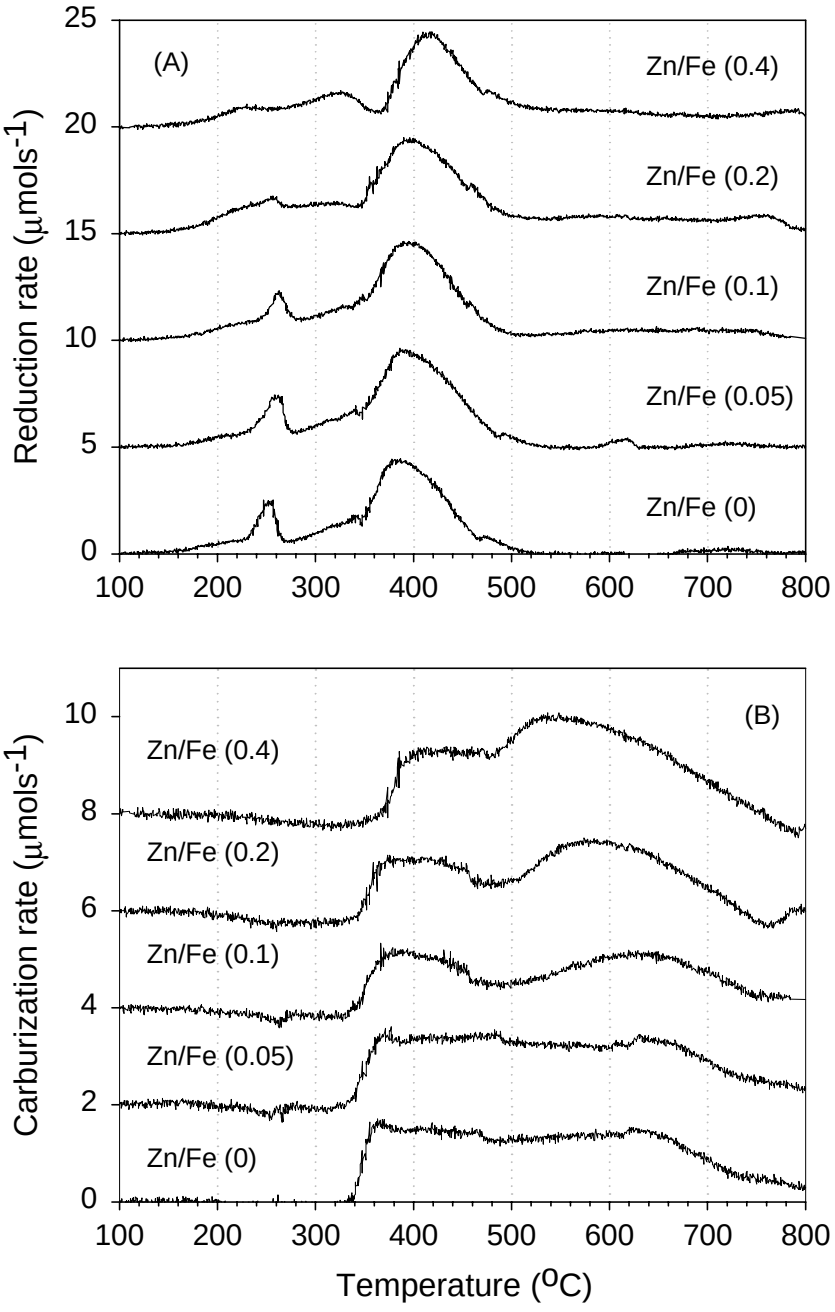


Figure 1.2 The reduction (A) and carburization (B) of Fe-Zn oxides with different Zn/Fe ratio in CO (0.2 g samples; 10 $^oC$/min ramping rate; 100 $cm^3$/min, 20% CO/Ar).

At low Zn contents (<0.2), Zn does not significantly influence the reduction/carburization of Fe oxides because of the small amount of Zn that exists in amorphous $ZnFe_2O_4$ form. However, at high Zn contents (e.g., Zn/Fe=0.4), $ZnFe_2O_4$ is the predominant bulk phase and there is small amount of $Fe_2O_3$ in amorphous form, leading to the detection of three reduction peaks. The first small peak can be ascribed to the reduction of amorphous $Fe_2O_3$ to $Fe_3O_4$; the second peak appears to reflect the reduction of $ZnFe_2O_4$ to a mixture of $Fe_3O_4$ and ZnO, and the third peak is due to the reduction of the oxide mixture. $ZnFe_2O_4$ is reduced and carburized at about 50 $^oC$ higher temperature than $Fe_2O_3$. The slight shifts of reduction/carburization steps to higher temperatures in high Zn loading samples are reasonable because $ZnFe_2O_4$ is more thermodynamically stable than $Fe_2O_3$. The residual ZnO seems to act as the sites for the Boudouard reaction, leading to more carbon deposition on samples with higher Zn contents.

### 3.3.2 Effects of K and Cu on the Reduction and Carburization of Fe Oxides in CO

Figure 1.2 shows the effect of K and Cu on the reduction and carburization behavior of Fe oxides in CO. It is found that Cu slightly decreases the temperature required to reduce $Fe_2O_3$ to $Fe_3O_4$ but markedly decreases that required to reduce $Fe_3O_4$ to metallic Fe. Also, Cu decreases the temperature required for carburization. For example, 1 at.% Cu decreases the carburization temperature about 50 $^oC$. K slightly inhibits the reduction of Fe oxide. On the 4 at.% K sample, in spite of promotion with 1 at.% Cu, the reduction temperature increases about 50 $^oC$ compared with that of pure $Fe_2O_3$.

On the pure $Fe_2O_3$ samples, initial rates of carburization are fast, but beyond this initial stage, carburization remains at a constant rate until the Boudouard reaction begins to occur at higher temperatures. This suggests that the incorporation of carbon within Fe becomes slower as soon as surface carbide forms, and that the carburization rate is limited by the diffusion of carbon into Fe interstices.

For the Fe oxide samples promoted with 1 at.% Cu or (2 at.% K + 1 at.% Cu), the carburization of Fe occurs in such a way that reduction and carburization take place simultaneously, that is, Fe is carburized as soon as $Fe_3O_4$ is reduced. It seems that Cu dissociates CO at high temperatures (>270 $^oC$), and this helps the reduction of $Fe_3O_4$ to metallic Fe. Fe may then react with dissociated carbon forming Fe carbide. However, the formed carbide appears to inhibit the diffusion of carbon species into the inner interstices. Here, Cu probably acts as a fast “transfer station” for carbon species between the outer and the inner interstitial positions, because the addition of Cu appear to facilitate the incorporation of C with Fe as well as the diffusion of C into Fe lattice interstices. This reminds us the fact that a topotactic reaction route is required in preparation for high surface area molybdenum nitride and carbides [20]. It seems that such a topotactic reaction is also required to produce high surface area Fe carbide, i.e., carbon should incorporate with Fe as soon as oxygen is removed from $Fe_3O_4$ and fill the vacancy left by the leaving oxygen. Although it is not clear why Fe oxide promoted with (2 at.% K+1 at.% Cu) shows a lower reduction/carburization temperature than those promoted with K and Cu separately, there seems to exist synergism between K and Cu components.

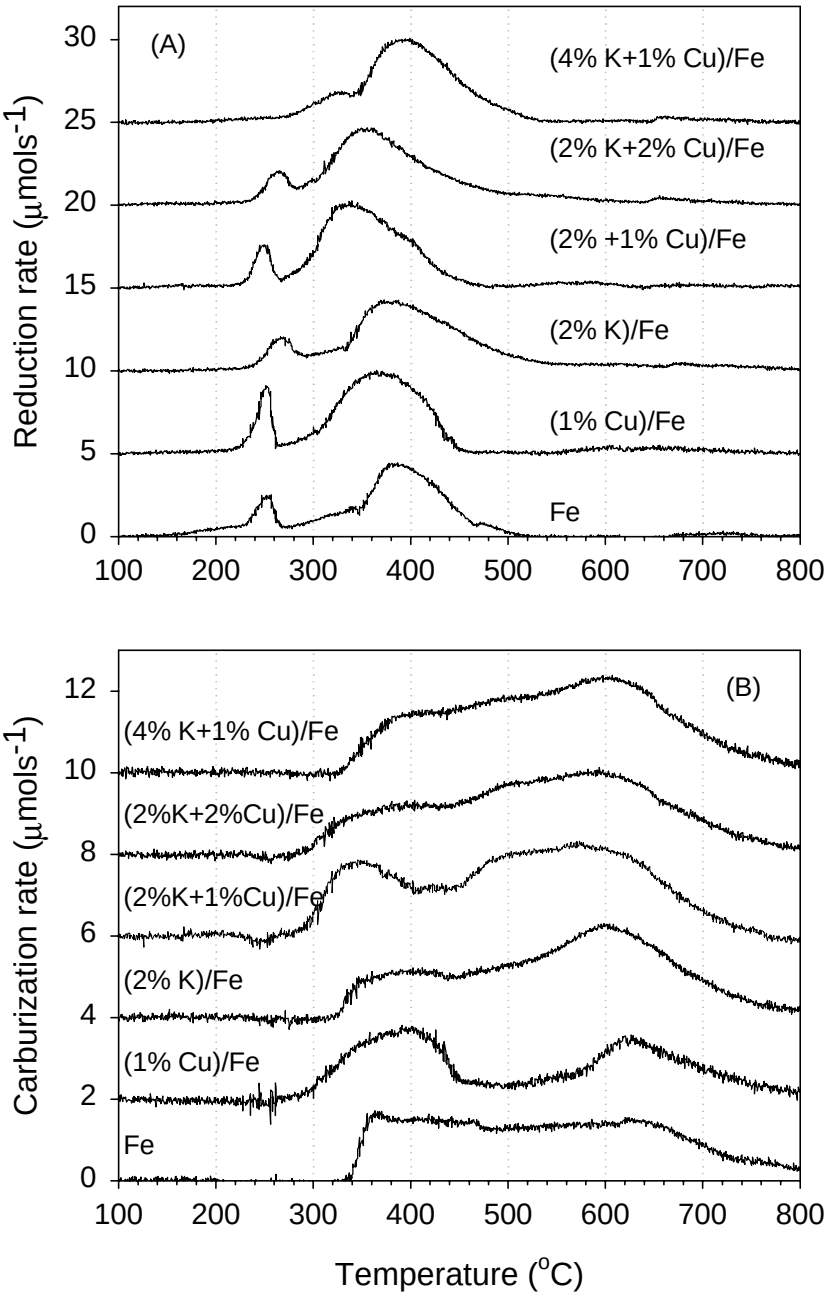


Figure 1.3 The reduction (A) and carburization (B) of Fe oxides with different K and Cu contents (0.2 g samples, 10 $^{o}$C ramping rate; 100 cm$^3$/min, 20% CO/Ar).

3.3.3 Comparison of the Reduction of Fe-Zn-K-Cu Oxides in $H_2$ and CO

Figure 1.4. shows the TPSR of Fe-Zn-K-Cu oxides in $H_2$ and in CO. As presented in our last report, Cu decreases the reduction temperature of Fe oxides in $H_2$, while K inhibits the reduction of Fe oxides. The reduction of $Fe_2O_3$ to $Fe_3O_4$ is separated into two parts because $H_2$ dissociates on Cu. Those Fe oxide crystallites that are in contact with Cu can

be readily reduced as soon as CuO is reduced. Those that are not near Cu, will not be reduced at those lower temperatures. In CO, Cu slightly decreases the temperature in the first reduction step but not as strongly as with $H_2$ as the reductant. This reflects the fact that CO dissociates on Cu at higher temperatures than $H_2$. As a result, $Fe_2O_3$ is reduced at lower temperatures in $H_2$ than in CO. However, Cu significantly decreases the temperature required for the second reduction/carburization step in the presence of CO (ca. 100 $^oC$ lower in CO than in $H_2$). K also appears to slightly inhibit the reduction of Fe oxides in CO but not as strongly as in $H_2$.

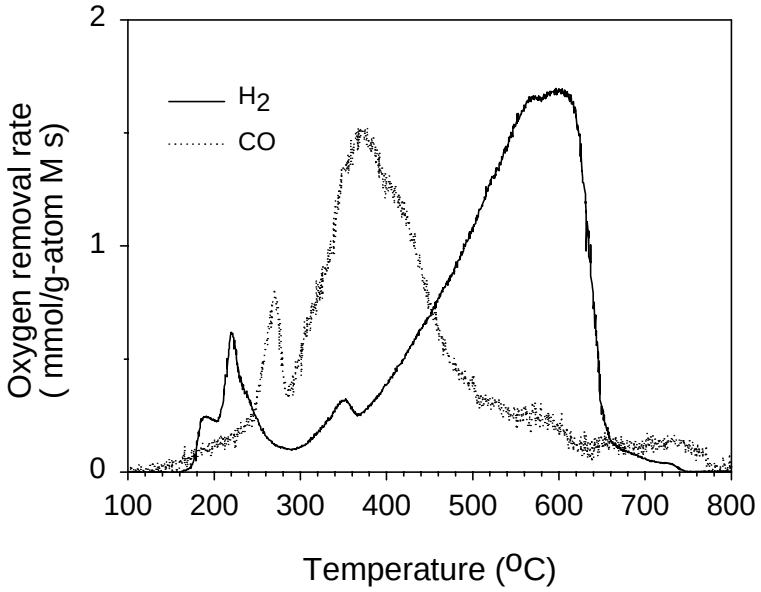


Figure 1.4 The comparison of TPSR of Fe-Zn-K-Cu oxide
(Zn/Fe=0.1, 2 at.% K and 1 at.% Cu) in CO and $H_2$.
(0.2 g samples, 10 $^oC$ ramping rate; 100 $cm^3$/min, 20% CO or $H_2$/Ar).

*3.4. In-Situ X-ray Absorption (XAS) Studies on Fe Catalysts*

X-ray adsorption near edge (XANES) and extended X-ray adsorption fine structure (EXAFS) analyses of X-ray absorption spectra are very powerful techniques to determine the oxidation state and the local structure of Fe, Cu, Zn and K in FTS catalysts, especially at the beginning of carburization and reduction processes when metal or carbides are present in amorphous or microcrystalline phases. In-situ X-ray absorption studies during the FTS reaction can establish a relationship between the catalytic activity and the structural phases of the catalysts. In-situ X-ray absorption studies on Fe-based catalysts are currently being carried out at the Stanford Synchrotron Radiation Laboratory.

*In-situ* treatments were carried out in a XAS cell of our design (Figure 1.5). This cell consists of a 0.8mm internal diameter quartz tube with 0.1mm-wall thickness connected to a gas manifold. Cartridge heaters placed in a finned copper block are used to heat the cell. The copper block is placed inside an insulating ceramic chamber. A 20mm by 4mm beam path is machined out of the copper and ceramic to allow the X-rays (6mm by

0.2mm beam) to pass through the heated zone. This design also accommodates rapid cooling of the quartz cell to room temperature by simply sliding the heated zone back from the cell. A flow trough was added beneath the copper block to rapidly cool the copper heat sink and ceramic insulation using flowing air or flowing liquid $N_2$.

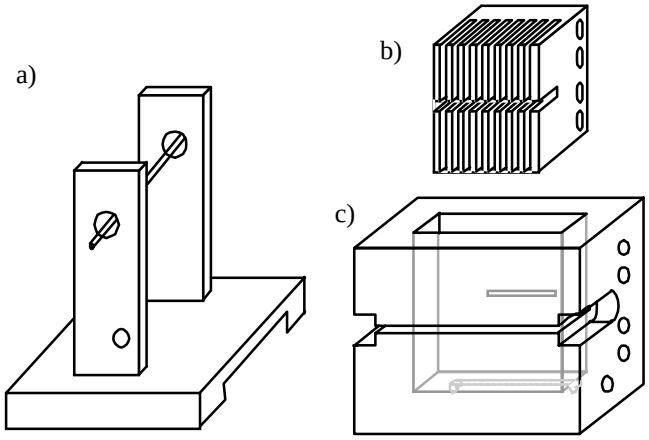


Figure 1.5 XAS cell. (a) quartz capillary cell and holder, (b) copper block, (c) Insulator (not to scale).

Our preliminary XAS studies focused on the structural evolution of Fe species during the reduction and carburization process in FTS. The catalysts we used for FTS reaction generally contain more than 60 wt.% Fe, which is too high a concentration for the acquisition of unbiased spectra. Therefore, we diluted the samples with graphite powder (surface area of ca. 1 $m^2/g$), which was shown to be inactive in synthesis gas up to 600 $^oC$. The optimum concentration of Fe for XAS measurement was found to be 7 wt.%.

Fe K-edge spectra were recorded on a typical Fe-Zn-K-Cu oxide sample (Zn/Fe=0.1, 2 at.% K and 1 at.% Cu) in CO at different temperatures. The normalized near edge spectrum at the Fe K-edge is shown in Figure 1.6. Fe K-edge spectrum of Fe-Zn oxide shows a sharp increase in absorbance at 7123 eV, caused by the excitation of Fe 1s electrons. As the carburization temperature increases, the edge energy progressively shifts from 7123 eV to 7112 eV, which is the absorption edge of metallic Fe. A principal component analysis of the near edge spectra is being carried out in order to quantity the relative concentration of various oxide, carbide and Fe metal phases during FTS. We also performed the in-situ XAS measurements for the Fe-Zn-K-Cu oxide in $H_2$ and synthesis gas. These spectra are currently being analyzed.

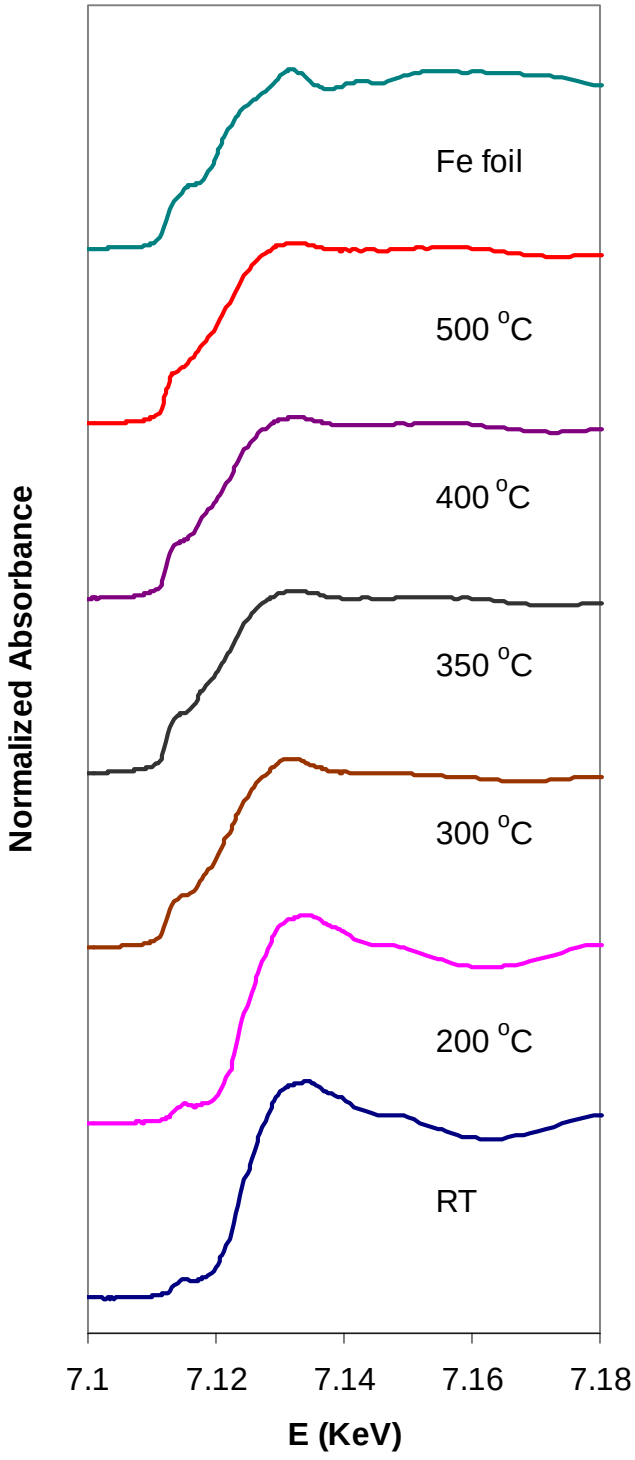


Figure 1.6 Normalized Fe K-edge spectra showing the shifts of the edge energy on Fe-Zn-K-Cu sample (Zn/Fe=0.1, 2 at.% K, 1 at.% Cu) during the carburization in CO. (8 mg samples with 7 wt.% Fe; 1.5 $cm^3$/min CO).

## 4. Fischer-Tropsch Synthesis on Fe-Based Catalysts

### *4.1. Investigation of Potassium Effects during FTS Reaction*

The addition of potassium has been found to affect the catalytic activity for both the Fischer-Tropsch synthesis and the concurrent water-gas shift reaction and the hydrocarbon selectivity on Fe-based catalysts. During this reporting period, the potassium effects on methane and higher hydrocarbon selectivities, the rates of the water-gas shift and Fischer-Tropsch synthesis and the olefin selectivity were measured on Fe-based catalysts (Zn/Fe = 0.1, 1 at.% Cu) with atomic K contents of 0%, 2% and 4% in a fixed-bed reactor at different temperatures and pressures using synthesis gas with a $H_2$/CO ratio of 2:1.

#### 4.1.1 Effects of Potassium on the Fischer-Tropsch Synthesis Activity

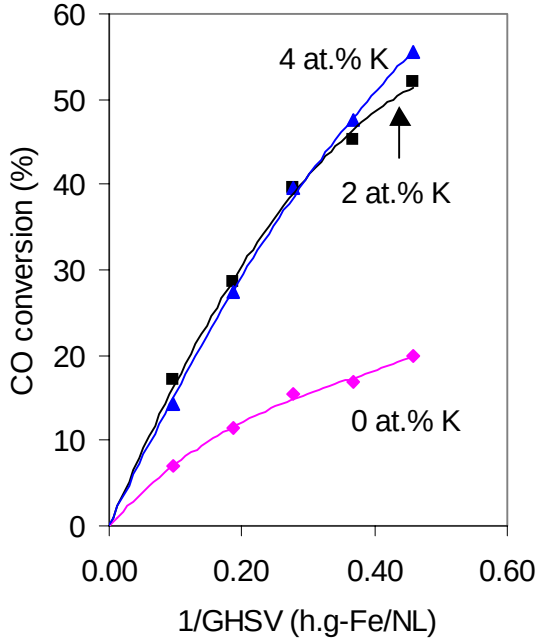


Fig. 1.7. CO conversion as a function of reciprocal space velocity on the catalysts (Zn/Fe = 0.1, 1 at.% Cu) with various potassium loading levels at 235 $^{o}$C and 21.4 atm, $H_2$/CO=2

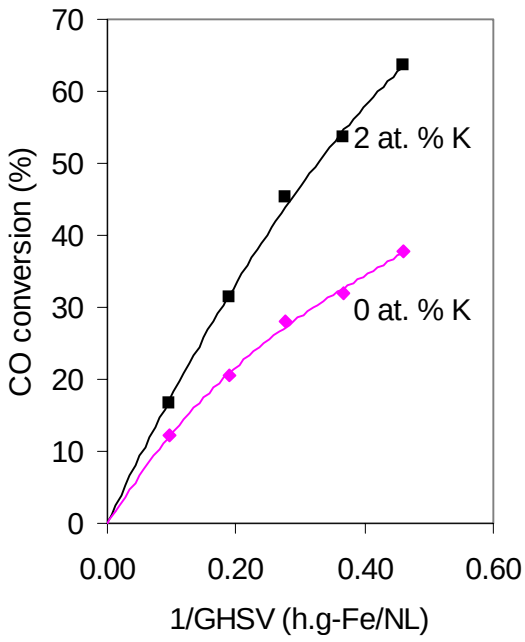


Fig. 1.8. CO conversion as a function of reciprocal space velocity on the catalysts (Zn/Fe = 0.1, 1 at.% Cu) with various potassium loading levels at 270 $^{o}$C and 5 atm, $H_2$/CO=2

CO conversion is a rough measure of FTS activity. CO conversions for the three levels of potassium loading studied at 235 $^{o}$C and 21.4 atm are shown in Fig. 1.7. The K-free catalyst showed a very low activity for CO conversion. At the same space velocity, much higher CO conversions were obtained on the K promoted catalysts (2 at.% K and 4 at.% K) than on the K-free catalyst. This result is in agreement with previous reports [16, 21]. Potassium can increase CO chemisorption and decrease $H_2$ chemisorption on Fe-based catalysts [22]. Potassium donates electrons to iron, facilitating CO chemisorption,

because CO tends to accept electrons from iron. On the other hand, hydrogen donates electrons to iron (electron affinity decreases upon $H_2$ chemisorption), and the presence of electron-donating alkali would be expected to weaken the iron-hydrogen bond. The net result of potassium promotion is the strengthening of the Fe-C bond and the weakening of the C-O and Fe-H bonds [23]. The weakening of C-O bond favors its dissociation and the removal of oxygen by hydrogen to form the monomer $CH_2$, which is an essential step in FTS. Therefore, potassium improves FTS activity.

However, the catalyst with 4 at.% K did not exhibit a further increase in FTS activity. As shown in Fig. 1.7, CO conversion was almost the same on the catalyst with 4 at.% K as on the catalyst with 2 at.% K. This suggests that high concentrations of K may cover the active sites for FTS reaction and that an increase in potassium favors carbon deposition, which can block the active surface area, leading to a further decline in the activity [21]. As a result, the promotion effects of potassium are reduced or offset at high K levels. Therefore, the FTS activity did not increase with increasing potassium concentration.

Similar promotion effects of potassium were observed at 270 $^oC$ and 5 atm. Interestingly, K promotion effects became smaller, compared to the results at 235 $^oC$ and 21.4 atm (Fig. 1.8). As discussed in the previous section, potassium favors carbon deposition. Higher temperatures (270 $^oC$) also favor carbon deposition too. More carbon is deposited at higher temperature than at lower temperature on the K-promoted catalysts. As a result, a larger fraction of the active sites in the K-promoted catalyst may be blocked at 270 $^oC$ than at 235 $^oC$. The promotion effects of potassium thus become smaller at 270 $^oC$.

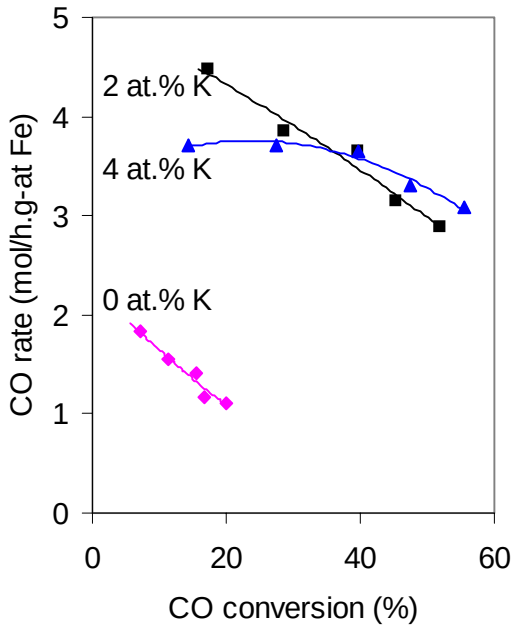


Fig. 1.9. CO conversion rate as a function of CO conversion on the catalysts (Zn/Fe = 0.1, 1 at.% Cu) with various potassium loading level at 235 $^oC$ and 21.4 atm, $H_2/CO=2$

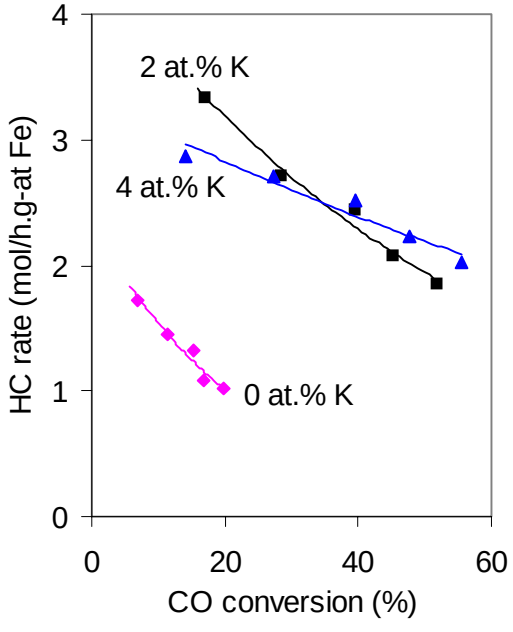


Fig. 1.10. Hydrocarbon formation rate as a function of CO conversion on the catalysts (Zn/Fe = 0.1, 1 at.% Cu) with various potassium loading level at 235 $^oC$ and 21.4 atm, $H_2/CO=2$

Figs. 1.9 and 1.10 show CO conversion rates and hydrocarbon formation rates at 235 $^{o}$C and 21.4 atm as a function of CO conversion. At the same CO conversion, the CO conversion rates are much higher on the K-promoted catalysts than on the K-free catalysts, confirming the promotion effect of potassium. It is also noted that the trends in CO conversion rates depend on the CO conversion level. At low CO conversions, a higher CO conversion rate was obtained on the catalyst with 2 % K than on the catalyst with 4 % K but the opposite trend was observed at high CO conversions.

Similar trends were observed for hydrocarbon formation rates as a function of potassium loading level (Fig. 1.10)

4.1.2. Effects of Potassium on Water-Gas Shift Reaction

Water is the primary oxygenate product, and $CO_2$ forms via a subsequent water-gas shift. Higher $CO_2$ selectivity means that more $CO_2$ is produced from water and CO, indicating that the catalyst is more active for water-gas shift reaction.

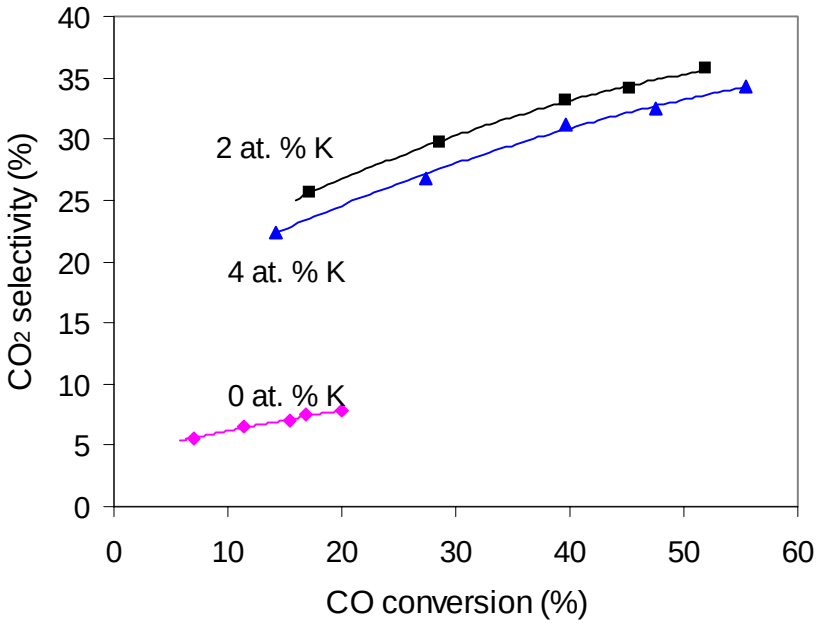


Fig. 1.11. $CO_2$ selectivity as a function of CO conversion on the catalysts (Zn/Fe = 0.1, 1 at.% Cu) with various potassium loading levels at 235 $^{o}$C and 21.4 atm, $H_2$/CO=2.

Fig. 1.11 shows $CO_2$ selectivity as a function of CO conversion with various potassium loading level at 235 $^{o}$C and 21.4 atm. $CO_2$ selectivity increased with CO conversion at all K loadings. This is expected if more water is produced at the higher CO conversion. $CO_2$ selectivity was considerably increased after potassium was introduced into the catalyst. For example, at 20% CO conversion, $CO_2$ selectivity was about 9% on the K-free catalyst while it was as high as 27% on the catalyst with 2 at.% K, indicating that potassium increased the activity of the catalyst for the water-gas shift reaction. This is in agreement with many other previous studies [16, 21].

4.1.3. Effects of Potassium on Hydrocarbon Selectivity and 1-Olefin to n-Paraffin Ratio

Fig. 1.12 shows methane selectivity as a function of CO conversion on the catalysts (Zn/Fe = 0.1, 1 at.% Cu) with various potassium loading levels at 235 $^{o}$C and 21.4 atm. Methane selectivities were almost independent of CO conversion on all three catalysts. This is expected since $H_2$/CO ratio just slightly increased with increasing CO conversion. It is clearly seen from Fig. 1.12 that potassium can inhibit the formation of methane. For example, methane selectivity was about 10% on K-free catalyst while it was only 3% on the catalyst promoted with 2 at.% K. $C_{5+}$ selectivities were 62% and 82.5% on these two catalysts, respectively (Fig. 1.13). The inhibition effect on the methane formation and the promotion effect of chain growth of potassium are in agreement with the results obtained in several earlier studies on Fe-based catalysts [16, 19]. The decrease in methane selectivity and the increase in $C_{5+}$ selectivity are due to the increased CO and lower hydrogen surface coverage in the presence of potassium, as discussed before. Low hydrogen surface concentration also reduce the probability of chain termination to paraffins and increase the possibility of the olefin formation since chain growth can terminate either by β-hydrogen abstraction to form α-olefin or by H-addition to form paraffins [24, 25]. Therefore, the addition of K can increase 1-olefin to n-paraffin ratio (Fig. 1.14).

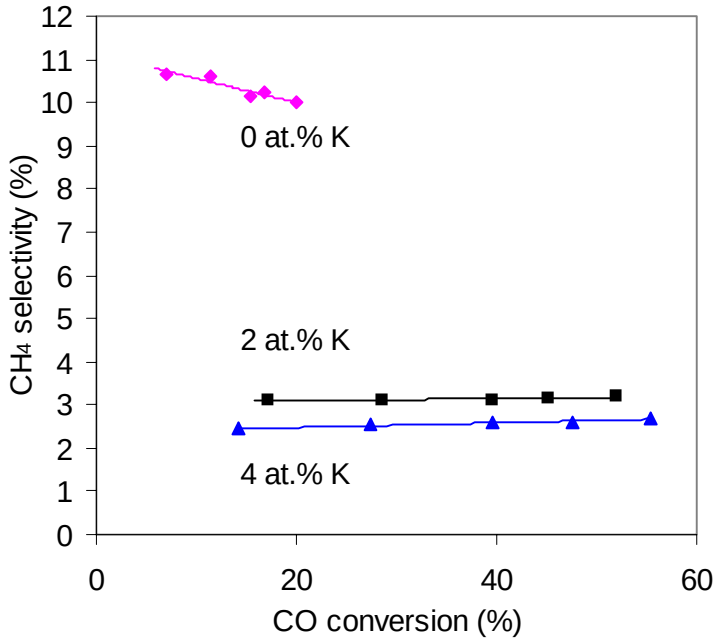


Fig. 1.12. Methane selectivity as a function of CO conversion on the catalysts (Zn/Fe = 0.1, 1 at.% Cu) with various potassium loading levels at 235 $^{o}$C and 21.4 atm, $H_2$/CO=2.

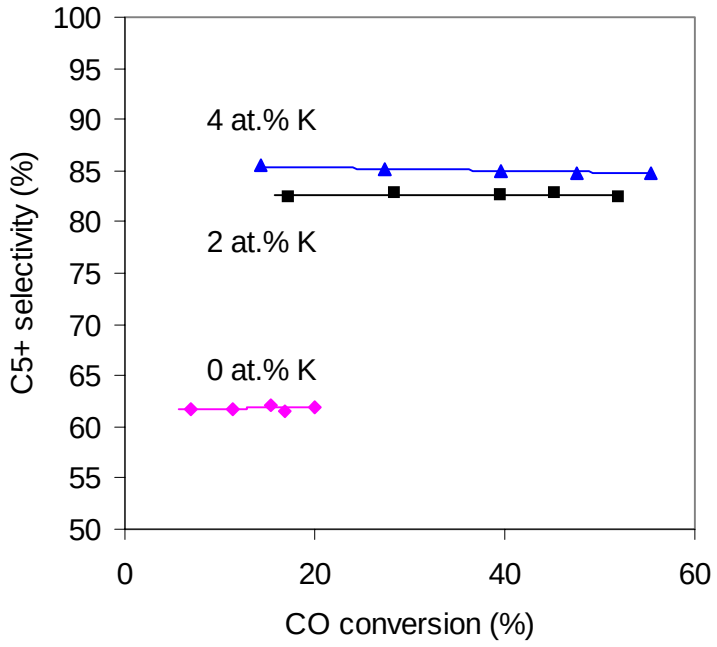


Fig. 1.13. $C_{5+}$ selectivity as a function of CO conversion on the catalysts (Zn/Fe = 0.1, 1 at.% Cu) with various potassium loading levels at 235 $^{o}$C and 21.4 atm, $H_2$/CO=2.

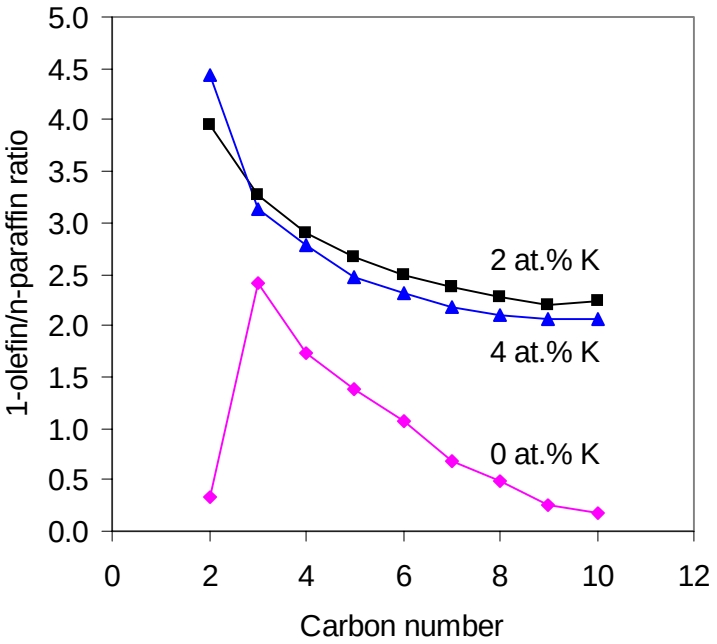


Fig. 1.14. 1-olefin to n-paraffin ratio as a function of CO conversion on the catalysts (Zn/Fe = 0.1, 1 at.% Cu) with various potassium loading levels at 235 $^{o}$C and 21.4 atm, $H_2$/CO=2.

*4.2. $CO_2$ Addition Effects*

The effects of $CO_2$ addition on the rate of water-gas shift reaction and on $CO_2$ and hydrocarbon selectivities were investigated by adding $CO_2$ at 270 $^oC$ and 5 atm on the K-free catalyst (Zn/Fe=0.1, 1 at.% Cu). The partial pressure of synthesis gas was maintained constant as the $CO_2$ pressure was varied. Fig. 1.15 shows CO conversion as a function of the added $CO_2$ pressure. Fig. 1.16 shows CO conversion rate, $CO_2$ net formation rate and hydrocarbon formation rate against the added $CO_2$ pressure. It is seen from Fig. 1.16 that the net $CO_2$ formation rate decreased with $CO_2$ pressure, suggesting that addition of $CO_2$ can inhibit $CO_2$ formation. As a result, both CO conversion and CO conversion rate decreased with $CO_2$ pressure (Figs. 1.15 and 1.16). However, hydrocarbon formation rate was almost independent of $CO_2$ pressure, indicating that the addition of $CO_2$ did not affect Fischer-Tropsch synthesis reactions.

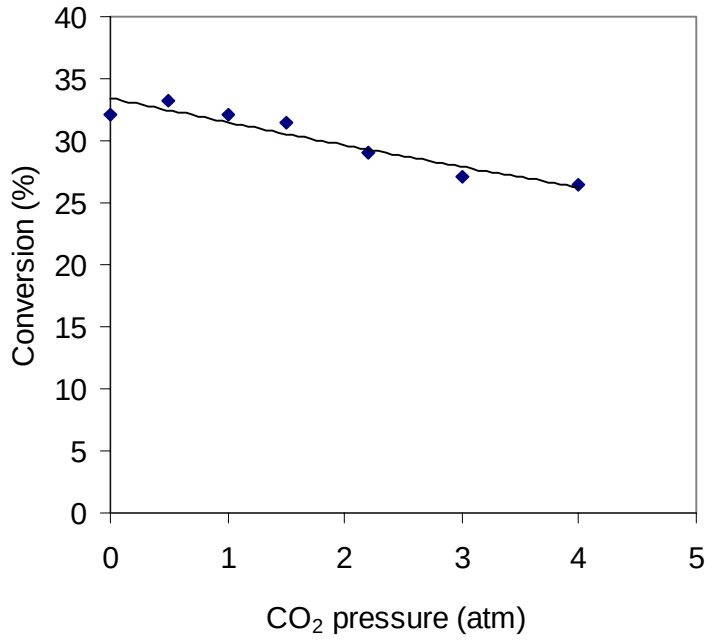


Fig. 1.15. CO conversion as a function of $CO_2$ pressure on the K-free catalyst (Zn/Fe=0.1, 1 at.% Cu) at 270 $^oC$ and 5 atm, $H_2/CO=2$.

However, even when the $CO_2$ partial pressure was 4 atm, which was much higher than CO pressure in feed (1.55 atm), some $CO_2$ was still produced during FTS reactions. This is in agreement with our calculations, which indicate that at these reaction conditions, a $CO_2/CO$ ratio of about 7.4 in the feed (e.g. $CO_2$ partial pressure about 11.4 atm) would be required by thermodynamics in order to avoid any net $CO_2$ formation via water-gas shift reactions. It shows that although $CO_2$ addition can be used to decrease $CO_2$ yields during FTS, the elimination of net $CO_2$ formation may well require levels of $CO_2$ that are impractical because of separation and re-compression costs.

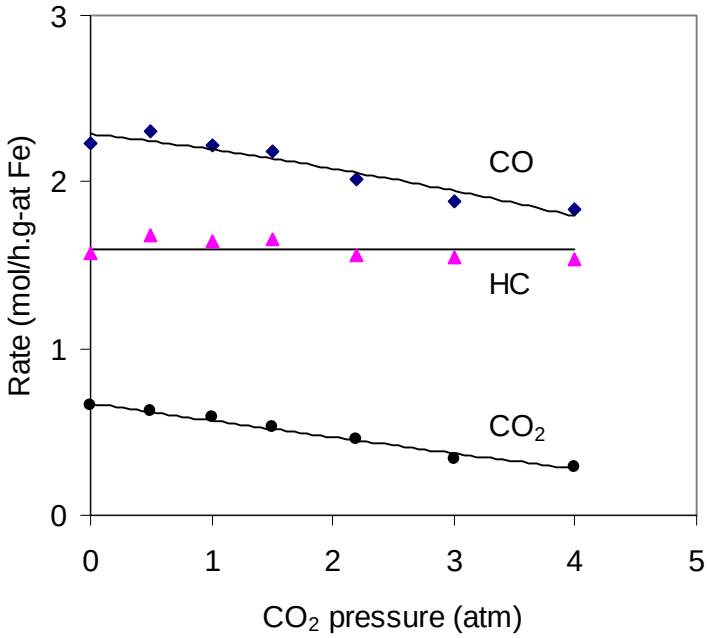


Fig. 1.16. CO conversion rate, hydrocarbon formation rate and net $CO_2$ formation rate as a function of $CO_2$ pressure on the K-free catalyst (Zn/Fe=0.1, 1 at.% Cu) at 270 $^{o}$C and 5 atm, $H_2$/CO=2.

One measure of the distance of the water-gas shift reaction from equilibrium can be obtained by the following ratio,

$$\eta = \frac{\left( \frac{P_{CO_2} P_{H_2}}{P_{CO} P_{H_2}} \right)}{K} \qquad (1)$$

where K is equilibrium constant for water-gas shift reaction. As shown in Fig. 1.17, the value of η is very small when no $CO_2$ was added into the synthesis gas and increased to about 0.5 as 4 atm $CO_2$ was added into the synthesis gas. The value of 0.5 means water-gas shift reaction remained far from equilibrium. That is the reason why $CO_2$ was still produced via water-gas shift even when 4 atm $CO_2$ was added into synthesis gas.

$CO_2$ formation rate via water-gas shift depends on the $CO_2$ forward rate $r_f$ and reverse reaction rate $r_b$ . $CO_2$ formation rate r can be expressed as the following equation,

$$r = r_f - r_b = k_1 f(P_j) - k_{-1} g(P_i) \qquad (2)$$

where $k_1$ is the rate constant for the water-gas shift reaction and $k_{-1}$ the rate constant for the reverse reaction. Since $r_f = r_b$ at equilibrium, the reaction rates must satisfy $\frac{f(P_j)}{g(P_i)} = \frac{P_{CO_2} P_{H_2}}{P_{co} P_{H_2O}}$. Then from equations (1), (2), and $K = k/k_{-1}$, we can obtain the following equation.

$$r = k_1 f(P_j)(1 - \frac{k_{-1}}{k_1} \frac{f(P_j)}{g(P_i)}) = r_f(1-\eta) \qquad (3)$$

Fig. 1.18 shows the $CO_2$ forward rate $r_f$ (= r/(1-η) as a function of η. It is seen that $CO_2$ forward rate $r_f$ was almost not changed with η within the experimental error. Therefore, the reduction in $CO_2$ net formation rate is caused by the increase in the reverse rate of water-gas shift reaction after addition of $CO_2$.

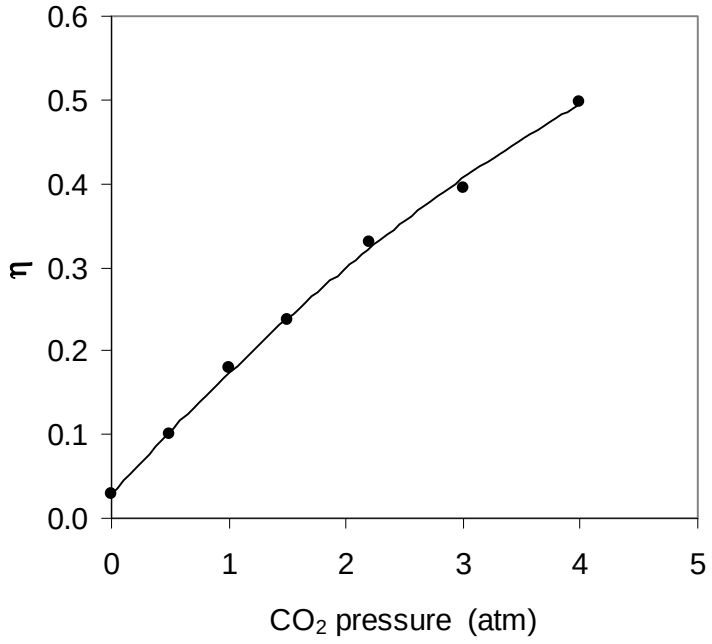


Fig. 1.17. The value of η as a function of $CO_2$ pressure on the K-free catalyst (Zn/Fe=0.1, 1 at.% Cu) at 270 $^oC$ and 5 atm, $H_2/CO=2$.

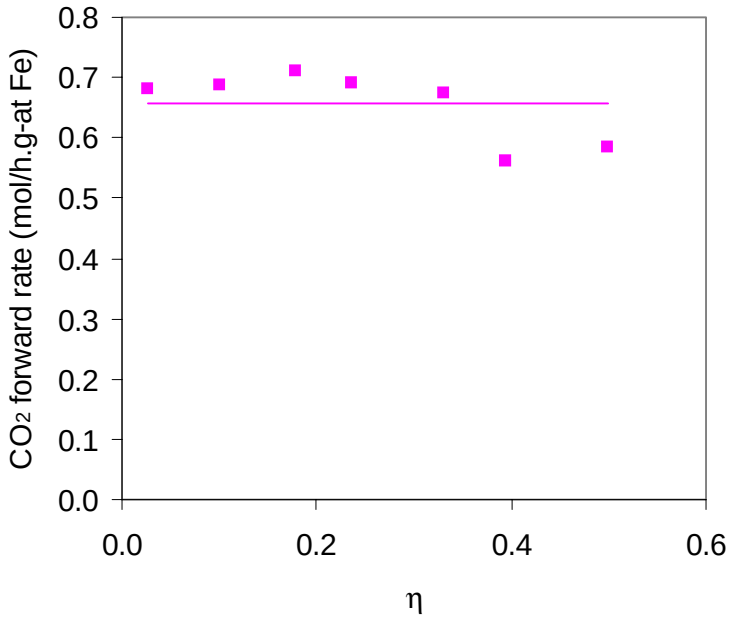


Fig. 1.18. $CO_2$ forward rate as a function of η on the K-free catalyst (Zn/Fe=0.1, 1 at.% Cu) at 270 $^{o}$C and 5 atm, $H_2$/CO=2.

# II. FISCHER-TROPSCH SYNTHESIS ON COBALT CATALYSTS

## 1. Background

In contrast with Fe, Co catalysts may work at relatively low reaction temperatures and pressures with slightly higher selectivity to linear paraffins in the $C_{5+}$ range and much lower water-gas-shift activity [4]. We have developed a *reaction-transport model* [13] of chain growth and termination for FTS with Co and Ru-based catalysts. During this reporting time, we prepared some silica-supported Co catalysts. We explored the effects of bed residence time and of water concentration on Co-catalyzed FTS. We also explored the reversibility of hydrogen and water dissociation steps by performing $D_2O$ tracer and kinetic isotope effect run.

## 2. Preparation of Cobalt Catalysts

Co catalysts were prepared by incipient wetness impregnation of $SiO_2$ (PQ Co. CS-2133) with Co nitrate (Aldrich 98%) solution (Table 2.1) [26]. The samples were dried at 60°C for 24 h. Temperature-programmed reduction (TPR) was carried out in order to determine required pretreatment conditions for all catalyst precursors. The TPR results (Figure 2.1) showed that the supported cobalt nitrate decomposes at about 160°C. The resulting cobalt oxide species reduce completely below 300°C. Thus, the catalyst precursors were pretreated following the procedures:

(1) reduced in flowing $H_2$ (20 ml $min^{-1}$ $g^{-1}$ cat) by increasing the temperature from 20°C to 150°C at 10°C $min^{-1}$ and from 150°C to 350°C at 30°C $h^{-1}$ (This low heating rate minimizes the deleterious effect of the water formed during the decomposition of Co nitrate and during the reduction of Co oxides, and it leads to higher Co dispersion [26])
(2) held at 350°C in flowing $H_2$ for 1 h
(3) passivated in a 1% $O_2$/He at 25°C before exposure to ambient air

Table 2.1. Characterization of $Co/SiO_2$ catalysts

| Co content (wt%)[a,b] | Co Dispersion (%)[a,c] | Co content (wt%)[c,d] | Co Dispersion (%)[c,d] |
|---|---|---|---|
| 12.7 | 5.8 | 13.0 | 6.3 |
| 21.9 | 4.6 | 24.8 | 4.2 |

[a] this work
[b] confirmed by ICP
[c] from $H_2$ chemisorption, measured at 100°C
[d] previous work [13]

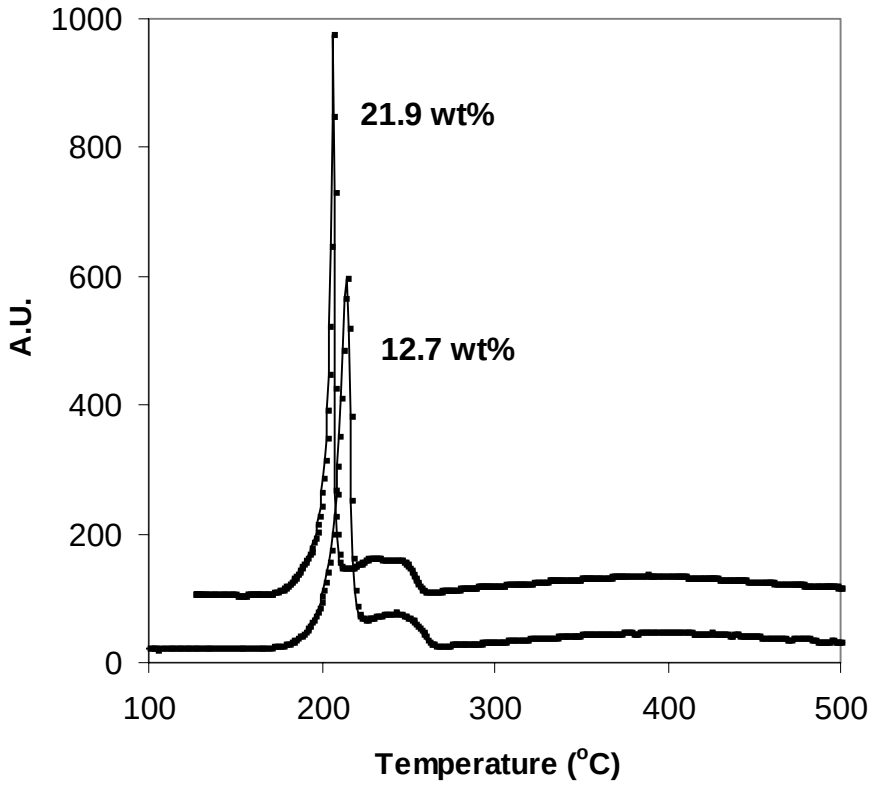


Figure 2.1. Temperature-programmed reduction of $Co/SiO_2$ catalysts (10% $H_2$/Ar, 10 °C $min^{-1}$)

## 3. Hydrogen Chemisorption

Co dispersion was measured by $H_2$ chemisorption at 100°C assuming a 1:1 H:Co surface stoichiometry. These measurements were carried out in a glass volumetric adsorption unit capable of $10^{-4}$ Pa dynamic vacuum. Pre-reduced and passivated catalysts were re-reduced in flowing $H_2$ by increasing the temperature from 20°C to 300°C at 10°C $min^{-1}$ and then holding for 10 min, evacuated at 300°C to less than $10^{-3}$ Pa, and cooled to 100°C. The chemisorption isotherms were measured at five $H_2$ pressures between 0 and 500 Torr. These isotherms (Figure 2.2) were extrapolated to zero pressure in order to calculate chemisorption uptakes. The Co dispersions calculated from the $H_2$ chemisorption uptakes are presented in Table 2.1. The dispersions of the two $Co/SiO_2$ catalysts were very similar to those reported after similar pre-treatments in the literature [13].

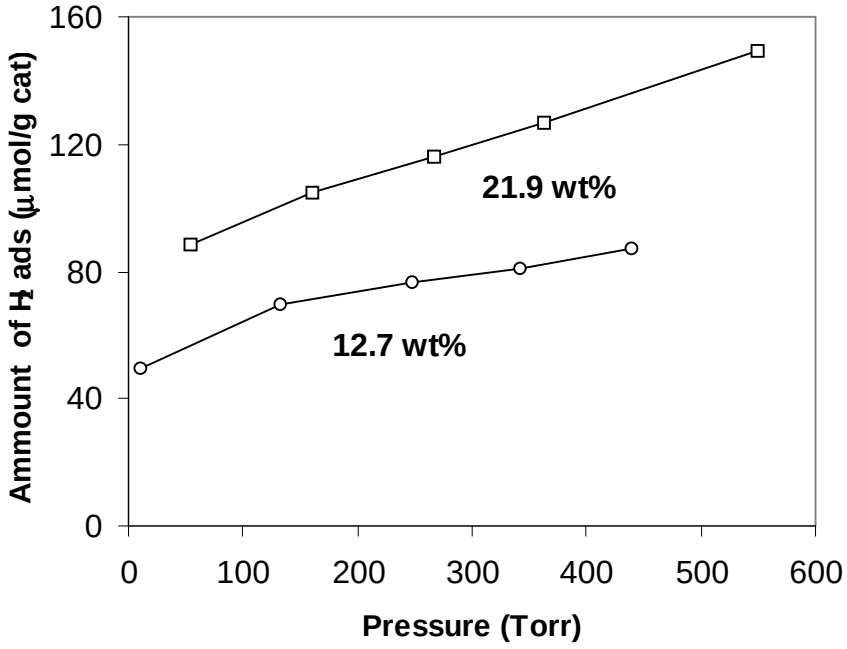


Figure 2.2. Hydrogen chemisorption on $Co/SiO_2$ catalysts (measured at 100°C)

## 4. Fischer-Tropsch synthesis on Cobalt Catalysts

### *4.1. Catalytic Reaction Unit*

Catalyst studies were performed in a fixed-bed, single-pass flow reactor, hereafter referred to as the FTS unit (FTSU) (Appendix 2.1). It consists of six feed streams, one of which introduces syngas into the reactor after passing through gas purifiers (Matheson, Model 454 and 452) for the removal of metal carbonyls and of water. Flow rates were metered using mass flow controllers (Brooks 5850). A three-zone split tube furnace was controlled with three temperature controllers (IEPS Co.). The system pressure was maintained using a back-pressure regulator (Mity Mite, Model S-91xw). Liquid reactants were introduced using a high-pressure syringe pump (Isco, Inc., Model 500D). In addition, the FTSU was equipped with an automatic six-port switching valve, which enabled the unit to carry out isotopic switch transient and temperature programmed studies.

The feed gas and the reactor effluent were analyzed on-line using a gas chromatograph (Hewlett-Parkard, Model 5890 series II) equipped with a ten-port sample valve and two sample loops. One sample was injected into a capillary column (HP-1 cross-linked methyl silicone, 50m × 0.32mm × 1.05μm film) while the other was injected into a packed column (Carboxen-1004, 2m × 1/16''). A TCD was used to analyze CO, $N_2$, $CO_2$, Ar, $H_2O$, and light hydrocarbons ($C_1$-$C_3$). A FID analyzed all products except for permanent gases and water. A typical separation of reaction products is given in Appendix 4.1-4.3.

## *4.2. FTS on $Co/SiO_2$ Catalysts*

### 4.2.1. FTS conditions

FTS was running at 200°C using 20 atm syngas ($H_2/CO/N_2$ = 62/31/7). Bed residence time was defined as catalyst volume divided by space velocity at standard conditions. Selectivity of hydrocarbon is based on carbon and $CO_2$-free.

### 4.2.2. Space Velocity Effects

Space velocity effects on reaction rates and selectivities were examined by changing the syngas flow rate while maintaining other conditions constant. The results are shown in Figures 2.3 to 2.8. The two $Co/SiO_2$ catalysts exhibited similar behaviors in the space velocity run. The CO conversion increases with increasing bed residence time (Figure 2.3, 2.4), but surprisingly the apparent FTS reaction rate also increases with increasing bed residence time (Table 2.2). This is unusual in view of the fact that the partial pressures of CO and $H_2$ reactants decrease as CO conversion increases by increasing bed residence time. It appears that one of the reaction products ($H_2O$) has an accelerating effect on the FTS rate, since the water partial pressure is higher at higher conversion (Tables 2.2). The details of these unusual autocatalytic effects will be the subject of future studies. As shown in Figures 2.5 to 2.8, $CH_4$ selectivity decreases, $C_{5+}$ selectivity increases, and $\alpha$-olefin to *n*-paraffin ratio decreases with increasing bed residence time. These trends were previously attributed to a greater probability of olefin readsorption and growth as CO conversion and bed residence time increased [14]. Both the catalysts have very low $CO_2$ selectivities (Figure 2.5, 2.6), consistent with very low water-gas-shift reaction rates at the conditions. In general, the results of space velocity studies are in agreement with a *reaction transport model* [13]. This model proposes that diffusion-enhanced olefin resorption increases the probability of chain growth and leads to heavier and more paraffinic products [13].

Table 2.2. Effects of bed residence time on FTS rate[a]

| Catalyst | Space velocity ($ml\ g^{-1}min^{-1}$) | Bed residence time (s) | CO conv (%) | Water partial pressure (atm)[b] | Site-time yield ($h^{-1}$) |
|---|---|---|---|---|---|
| 12.7 wt% $Co/SiO_2$ | 11.4 | 15.8 | 49.0 | 2.2 | 34.1 |
| | 17.1 | 10.5 | 29.0 | 1.1 | 30.3 |
| | 34.2 | 5.3 | 12.8 | 0.4 | 26.8 |
| | 51.4 | 3.5 | 8.7 | 0.3 | 26.9 |
| 21.9 wt% $Co/SiO_2$ | 30.0 | 6.2 | 54.9 | 2.6 | 71.4 |
| | 45.0 | 4.1 | 33.0 | 1.3 | 64.5 |
| | 60.0 | 3.1 | 21.6 | 0.8 | 56.4 |
| | 90.0 | 2.0 | 12.9 | 0.4 | 50.5 |
| | 180.0 | 1.0 | 5.7 | 0.2 | 44.7 |

[a] reaction conditions: 200°C, 20 atm, $H_2/CO$ = 2.0

[b] average of the inlet and the exit water pressures

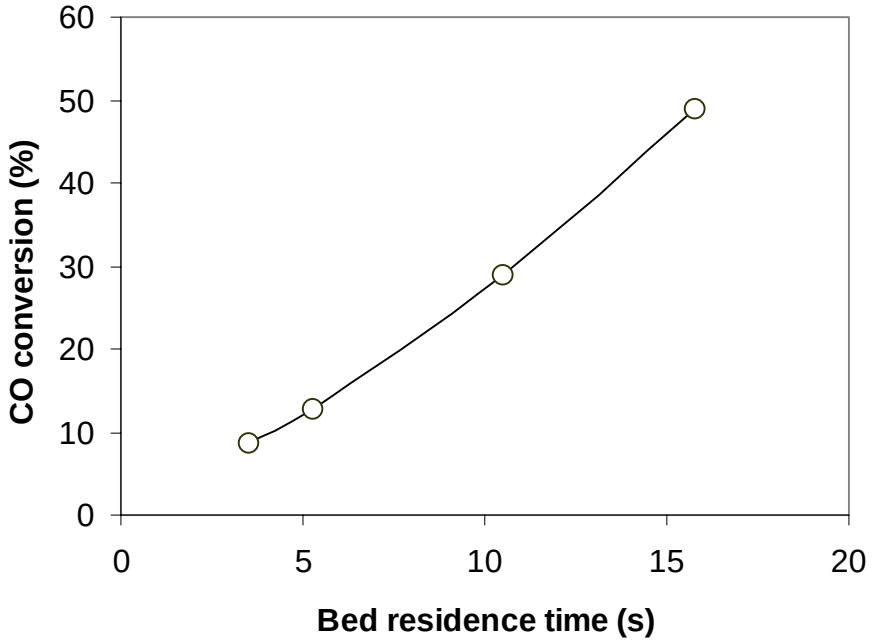


Figure 2.3. Space velocity effect on CO conversion
(12.7 wt% $Co/SiO_2$, 200°C, 20 atm, $H_2/CO = 2.0$)

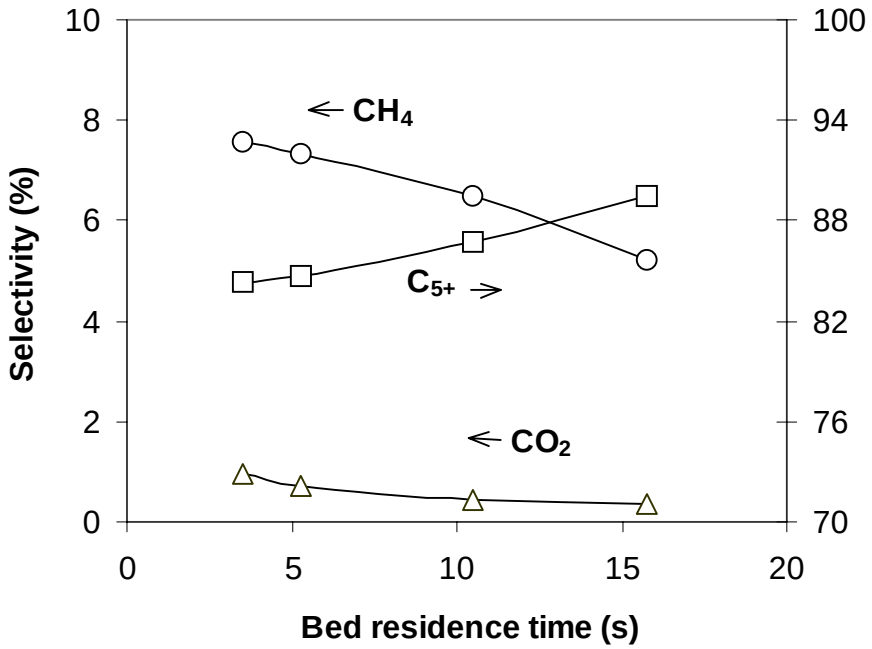


Figure 2.4. Space velocity effect on $CH_4$, $C_{5+}$, and $CO_2$ selectivities
(12.7 wt% $Co/SiO_2$, 200°C, 20 atm, $H_2/CO = 2.0$)

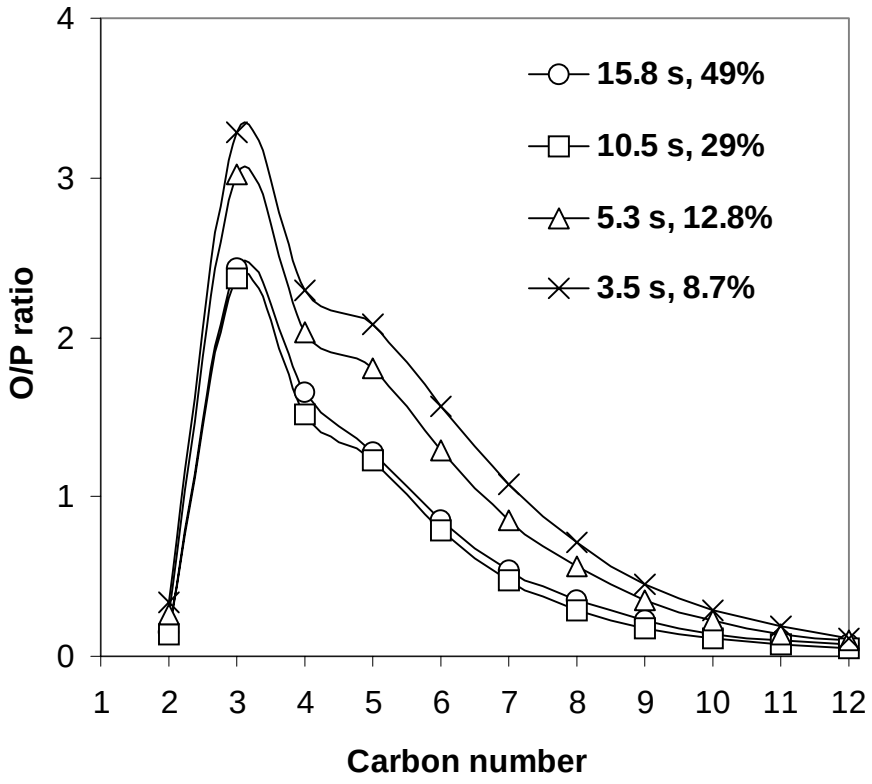


Figure 2.5. Space velocity effect on *a*-olefin to *n*-paraffin ratio
(12.7 wt% $Co/SiO_2$, 200°C, 20 atm, $H_2/CO = 2.0$)

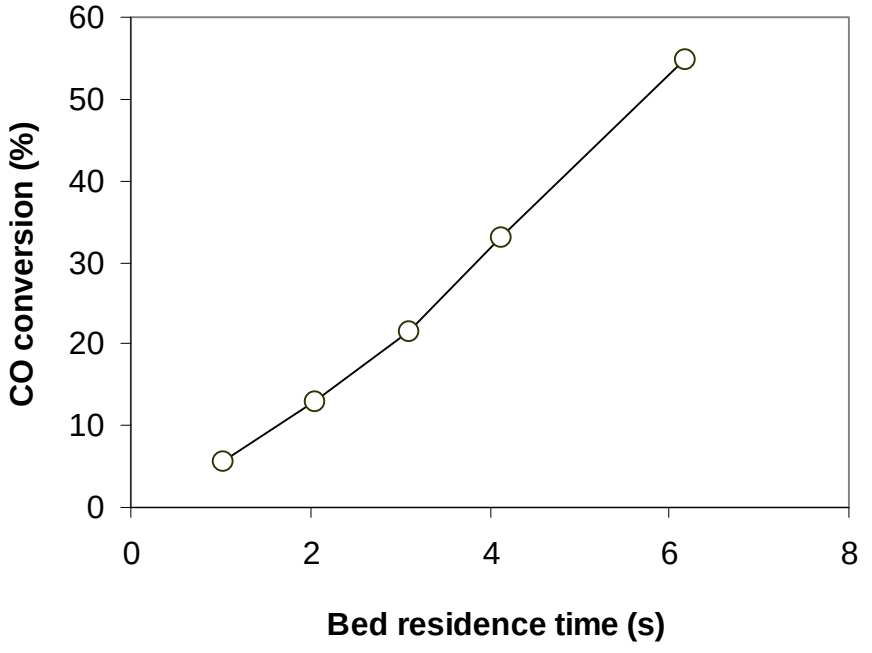


Figure 2.6. Space velocity effect on CO conversion
(21.9 wt% $Co/SiO_2$, 200°C, 20 atm, $H_2/CO = 2.0$)

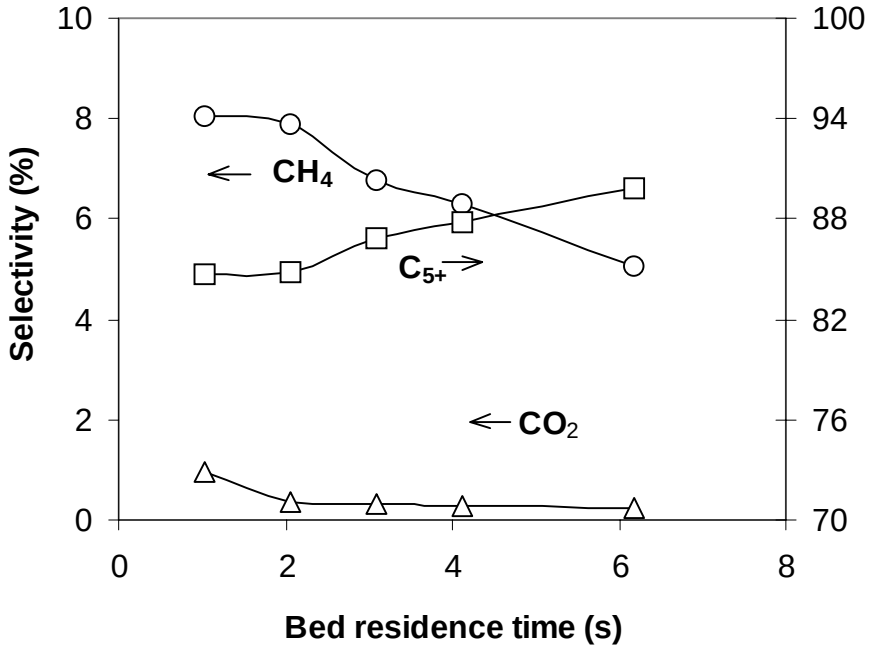


Figure 2.7. Space velocity effect on $CH_4$, $C_{5+}$, and $CO_2$ selectivities (21.9 wt% $Co/SiO_2$, 200°C, 20 atm, $H_2/CO$ = 2.0)

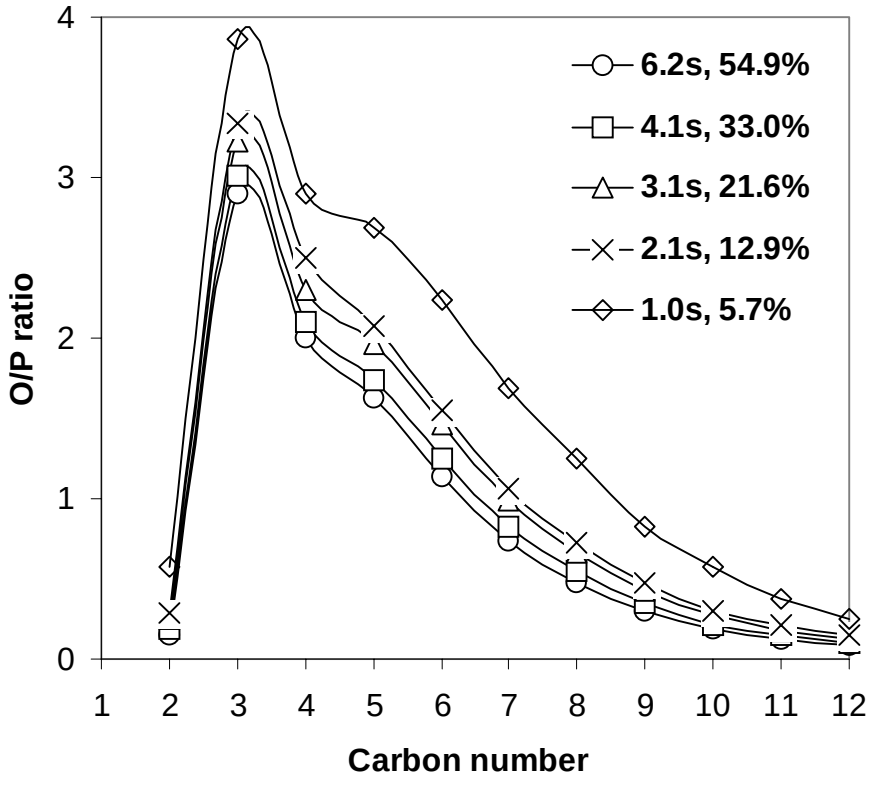


Figure 2.8. Space velocity effect on *a*-olefin to *n*-paraffin ratio (21.9 wt% $Co/SiO_2$, 200°C, 20 atm, $H_2/CO$ = 2.0)

4.2.3. Effects of Water on FTS Reaction Rate and Selectivity

So far, most of kinetic rate equations for Co-catalyzed FTS do not include the influence of water [27]. Water is usually considered to have little effect on the overall rate of CO consumption on Co catalysts [28]. But in the above space velocity studies, water has been found to promote the CO conversion rate. We have examined the water effects on FTS rate and selectivities by adding 2, 4, and 8 atm $H_2O$ at low CO conversions while maintaining the $H_2$ and CO partial pressures constant. The results are shown in Figures 2.9 to 2.12. CO conversion rates increase with increasing water partial pressure (Figure 2.9). We suggest that water may affect FTS by changing the relative concentrations of kinetic-relevant species on surface. The nature of this kind of water effect is being studied by using $D_2O$ isotopic tracers. It should be noted that the high loading Co catalyst is deactivated when the water partial pressure reaches 8 atm (Figure 2.9). The deactivation is probably due to the high concentration of water, which could oxidize active Co sites. On the other hand, water has a positive effect on the product distribution. The methane selectivity decreases (Figure 2.10), the selectivity to desired $C_{5+}$ increases (Figure 2.11), and the products become more olefinic (Figure 2.12) with increasing water partial pressure. All these beneficial modifications of FTS selectivities were reported previously [14] and they are consistent with the literature [28]. It appears that water inhibits all termination steps leading to paraffins (*e.g.*, secondary hydrogenation) with a consequent increase in the selectivity of $\alpha$–olefins. $\alpha$–Olefins possess higher probability of readsorption and of chain growth, resulting in heavier products.

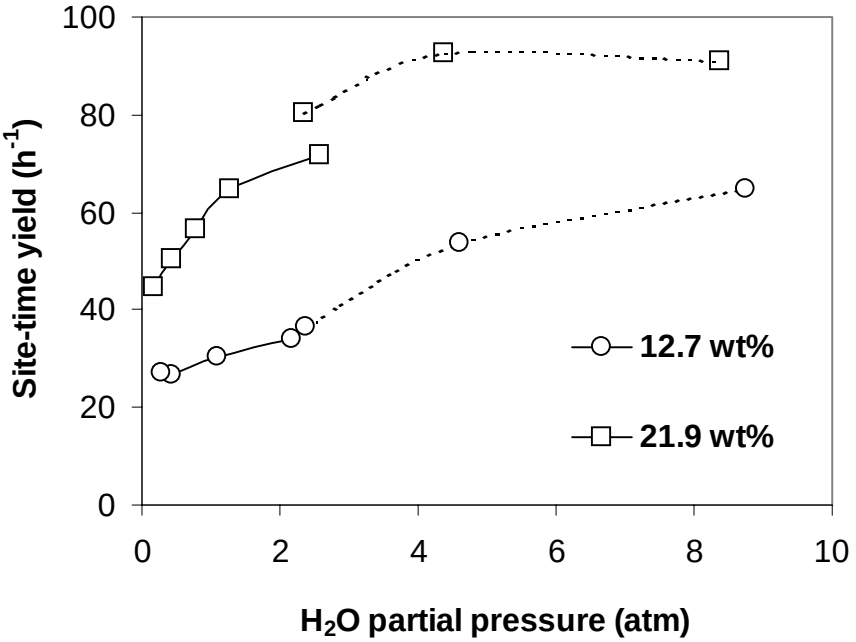


Figure 2.9. Water effect on FTS reaction rate ($Co/SiO_2$ catalysts, 200°C, $H_2/CO$ = 2.0; solid lines, space velocity runs, 20 atm; dash lines, water added at the lowest conversions; water partial pressure is the average of the inlet and the exit water pressures)

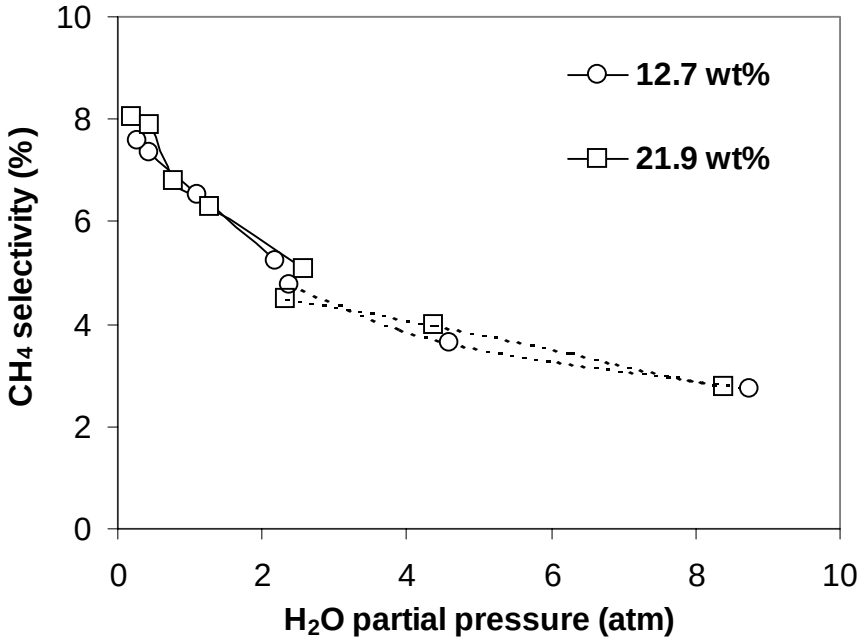


Figure 2.10. Water effect on $CH_4$ selectivity ($Co/SiO_2$ catalysts, 200°C, $H_2/CO = 2.0$; solid lines, space velocity runs, 20 atm; dash lines, water added at the lowest conversions; water partial pressure is the average of the inlet and the exit water pressures)

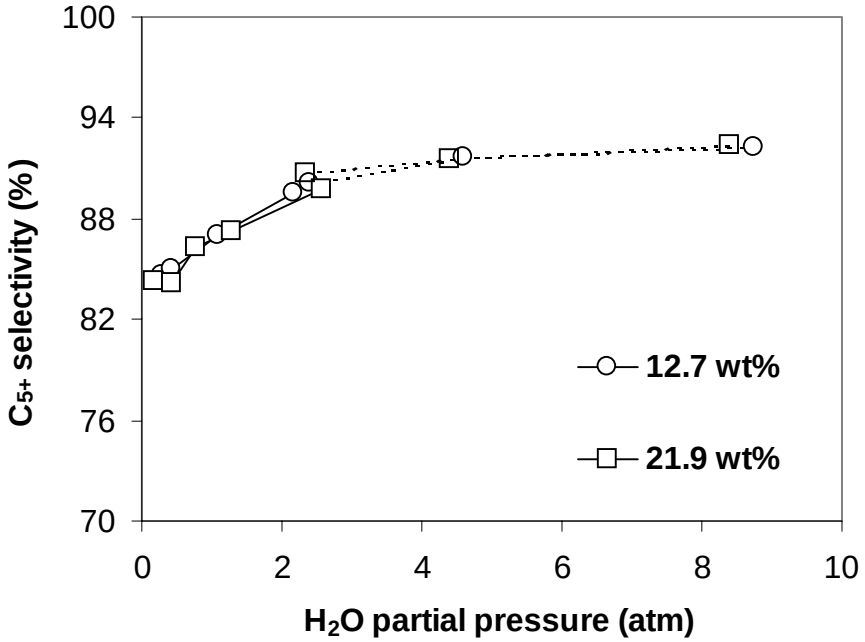


Figure 2.11. Water effect on $C_{5+}$ selectivity ($Co/SiO_2$ catalysts, 200°C, $H_2/CO = 2.0$; solid lines, space velocity runs, 20 atm; dash lines, water added at the lowest conversions; water partial pressure is the average of the inlet and the exit water pressures)

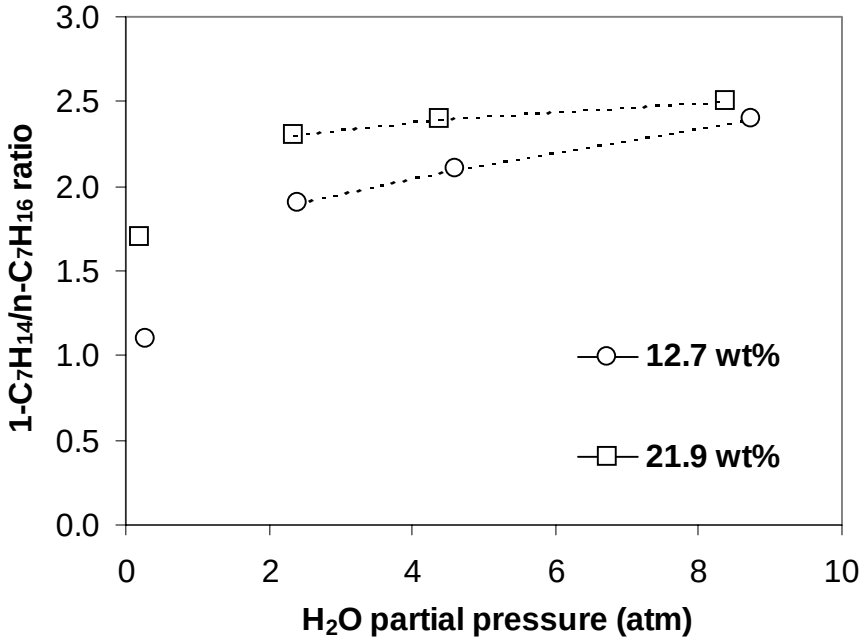


Figure 2.12. Water effect on olefin to paraffin ratio ($Co/SiO_2$ catalysts, 200°C, $H_2/CO$ = 2.0; points, at the lowest conversion of each space velocity run, 20 atm; dash lines, water added at the lowest conversions; water partial pressure is the average of the inlet and the exit water pressures)

4.2.4. $D_2O$ tracer and kinetic isotope effect studies

In order to explore the reversibility of water dissociation step during FTS, $D_2O$ tracer studies were carried out by co-feeding 2 atm $D_2O$ with 20 atm syngas (13.8% D in the feed). The deuterium content in hydrocarbon products (up to $C_8$) and in water were measured by a GC-MS (Hewlett-Packard 5972), while the D content in hydrogen isotopomers was determined by mass spectrometry (Leybod Inficon Instruments Co., Inc.). The D contents were calculated using matrix techniques that correct for ion fragmentation [29]. The results are shown in Table 2.3 and in Figure 2.13. The D content in the water decreases with increase in the bed residence time, because more $H_2O$ formed at longer bed residence time, *i.e.*, higher conversion. The D contents in all the primary products ($C_4$-$C_8$) and in the $H_2$ isotopomers increase as increasing bed residence time, suggesting the D content in surface H-D pool changes with bed residence time. The water dissociation steps during FTS consist:

$O^* + H^* \rightarrow OH^* + *$ (1)
$OH^* + H^* \rightarrow OH_2^* + *$ (2)
$OH_2^* \leftrightarrow H_2O + *$ (3)

which may influence the H/D ratio on surface. Assuming the step (3) is quasi-equilibrated, at least one of the steps (1) and (2) should be not quasi-equilibrated. Otherwise, D contents in the hydrocarbons and in the $H_2$ isotopomers should be

independent of bed residence time. Further, extrapolating the lines in Figure 2.13 to zero bed residence time, we find D contents in the hydrocarbons and in the $H_2$ isotopomers are around 3%. This is an evidence that water dissociation is reversible, although it is not quasi-equilibrated during FTS. Thus, water in the gas phase influences FTS probably by consuming surface vacant site (step 3). This will depress the dissociation of CO (forming the predominant species on surface) in which vacant sites are required. This may account for the CO conversion rate increasing with increase in the water partial pressure, since the rate is mildly negative order in CO partial pressure [13].

Table 2.4. Deuterium content in hydrocarbon products, water and hydrogen isotopomers[a]

| Bed residence time (s) | | 1 | 1.5 | 3 |
|---|---|---|---|---|
| Water | Frct of D (%) | 0.37 | 0.29 | 0.25 |
| | Dev from binomial | 0.03 | 0.04 | 0.00 |
| $H_2$-iso | Frct of D (%) | 0.05 | 0.06 | 0.09 |
| | Dev from binomial[b] | 0.00 | 0.00 | 0.01 |
| *1*-$C_4H_8$ | Frct of D (%) | 5.2 | 6.3 | 9.3 |
| | Dev from binomial | 0.02 | 0.01 | 0.01 |
| *n*-$C_4H_{10}$ | Frct of D (%) | 5.1 | 5.8 | 9.2 |
| | Dev from binomial | 0.04 | 0.01 | 0.02 |
| *1*-$C_5H_{10}$ | Frct of D (%) | 5.5 | 6.2 | 9.6 |
| | Dev from binomial | 0.00 | 0.02 | 0.01 |
| *n*-$C_5H_{12}$ | Frct of D (%) | 4.6 | 6.0 | 9.5 |
| | Dev from binomial | 0.01 | 0.01 | 0.02 |
| *1*-$C_6H_{12}$ | Frct of D (%) | 4.3 | 6.0 | 9.7 |
| | Dev from binomial | 0.01 | 0.02 | 0.02 |
| *n*-$C_6H_{14}$ | Frct of D (%) | 4.7 | 5.8 | 8.8 |
| | Dev from binomial | 0.02 | 0.02 | 0.02 |
| *1*-$C_7H_{14}$ | Frct of D (%) | 4.8 | 6.3 | 9.7 |
| | Dev from binomial | 0.02 | 0.02 | 0.02 |
| *n*-$C_7H_{16}$ | Frct of D (%) | 4.4 | 5.7 | 8.6 |
| | Dev from binomial | 0.01 | 0.02 | 0.02 |
| *1*-$C_8H_{16}$ | Frct of D (%) | 4.8 | 6.2 | 9.7 |
| | Dev from binomial | 0.03 | 0.01 | 0.02 |
| *n*-$C_8H_{18}$ | Frct of D (%) | 4.3 | 5.4 | 8.4 |
| | Dev from binomial | 0.02 | 0.02 | 0.03 |

[a] reaction conditions: 21.9 wt% $Co/SiO_2$ catalyst; 200°C; 20 atm syngas, $H_2/CO = 2.0$; 2 atm $D_2O$ added;

[b] deviation from statistic distribution at each D content

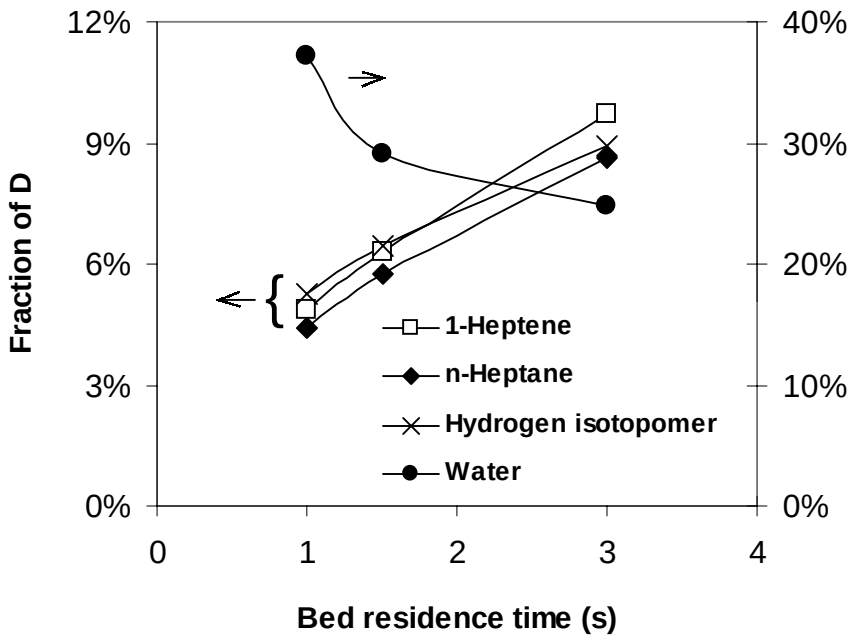


Figure 2.13. Deuterium content in FTS products (21.9 wt% $Co/SiO_2$ catalysts, 200°C; $H_2/CO/N_2$ = 62/31/7, 20 atm; $D_2O$ added, 2 atm)

The kinetic isotope effect (KIE) was studied by comparing the rates of FTS using $H_2/CO/N_2$ (62/31/7) and $D_2/CO/N_2$ (62/31/7). All the conditions were same as those of the previous space velocity run. This KIE study can probe the reversibility of hydrogen dissociation steps and the role of hydrogen-containing species in the rate-determining step during FTS. As shown in Table 2.5, the ratio of CO conversion rate ($k_{CO(H)}/k_{CO(D)}$) is 0.92. Since the CO conversion rate sums the formation of all carbon-based products, rigorous analysis of the formation rate of each primary product (non-deuterated and per-deuterated) is being performed in order to make conclusions about the mechanisms. First we consider the formation of methane during FTS, which involves the following steps: [28]

(1) (2) (3) (4) (5) (6)

$$CO \leftrightarrow CO^* \leftrightarrow C^* \rightarrow CH^* \rightarrow CH_2^* \rightarrow CH_3^* \rightarrow CH_4$$

CO dissociation (1, 2) is usually taken as a reversible step [13]. So the rate of methane formation depends on the subsequent hydrogen addition steps. If one of these steps is rate-determining, the methane formation rate should increase when we replace $H_2$ with $D_2$. However, the observed ratio ($k_{CH4}/k_{CD4}$) is 1.34, suggesting that none of the hydrogen addition steps are rate-determining. We may then infer the $H_2$ dissociation is rate-determining. If this is true, switching from $H_2$ to $D_2$ (with other conditions unchanged) would lower the surface D* concentration compared with the H* concentration, leading to the lower formation rate of $CD_4$. Thus the preliminary results of the KIE run suggest the involvement of hydrogen dissociation in the rate-determining step.

Table 2.5. Results of kinetic isotope effect run[a]

| Feed | $H_2/CO/N_2$ (62/31/7) | $D_2/CO/N_2$ (62/31/7) |
|---|---|---|
| Bed residence time (s) | 5.6 | 5.1 |
| CO conversion (%) | 48.6 | 47.4 |
| CO conversion rate ($s^{-1}$) | 70.1 | 75.8 |
| $k_{CO(H)}/k_{CO(D)}$ | 0.92 | |
| Methane selectivity (%) | 6.1 | 4.2 |
| Methane formation rate ($s^{-1}$) | 4.3 | 3.2 |
| $k_{CH4}/k_{CD4}$ | 1.34 | |

[a] reaction conditions: 21.9 wt% $Co/SiO_2$ catalyst; 200°C; 20 atm syngas, $H_2/CO$ = 2.0; 2 atm $D_2O$ added;

# III. APPENDIX

## 1. Reference


1. M. E. Dry, The Fisher-Tropsch Synthesis, in *Catalysis-Science and Technology*, Vol. 1, p. 160, J. R. Anderson and M. Boudart eds., Springer Verlag, New York, 1981.
2. F. Fischer and H. Tropsch, *Brennstoff-Chem.* **7** (1926) 97.
3. R. B. Anderson, in *Catalysis* Vol. 4, p. 29, P. H. Emmett eds., Van Nostrand-Reinhold, New York, 1956.
4. H. H. Storch, N. Golumbic and R. B. Anderson, *The Fischer-Tropsch and Related Syntheses*, Wiley, New York, 1951; R. B. Anderson, *The Fischer-Tropsch Synthesis*, Wiley, New York, 1984.
5. H. Kolbel and M. Ralek, *Catal. Rev.-Sci. Eng.* **21** (1980) 225.
6. J. W. Niemantsverdriet and A. M. van der Kraan, *J. Catal.* **72** (1981) 385.
7. J. A. Amelse, J. B. Butt and L. J. Schwartz, *J. Phys. Chem.* **82** (1978) 558.
8. G. B. Raupp and W. N. Delgass, *J. Catal.* **58** (1979) 348.
9. R. Dictor and A. T. Bell, *J. Catal.* **97** (1986) 121.
10. J. P. Reymond, P. Meriaudeau and S. J. Teichner, *J. Catal.* **75** (1982) 39.
11. C. S. Kuivila, P. C. Stair and J. B. Butt, *J. Catal.* **118** (1989) 299.
12. C. S. Huang, L. Xu and B. H. Davis, *Fuel Sci. Tech. Int.* **11** (1993) 639.
13. E. Iglesia, and S. C. Reyes, R. J. Madon and S. L. Soled, *Advances in Catalysis*, Vol. 39, p. 221, Academic Press, 1993.
14. E. Iglesia, *Appl. Catal. A: General* **161** (1997) 59.
15. S. Soled, E. Iglesia and R. A. Fiato, *Catal. Lett.* **7** (1990) 271.
16. S. Soled, E. Iglesia, S. Miseo, B. A. DeRites and R. A. Fiato, *Topics in Catal.* **2** (1995) 193.
17. E. Iglesia, A research proposal submitted to the Division of Fossil Energy.
18. M. T. Xu, E. Iglesia, *J. Phys. Chem. B* **102(6)**, 961-966, 1998.
19. A. P. Raje, R. J. O'Brien and B. H. Davis, *J. Catal.* **180** (1998) 36.
20. J. S. Lee, L. Volpe, F. H. Ribeiro, M. Baudart, *J. Catal.* 44, **112** (1988).
21. D.B. Bukur, D. Mukesh and S.A. Patel, *Ind. Eng. Chem. Res.* 1990, **29**, 194-204.
22. H. Kolbel, In Actes du Deuxieme Congres International de Catalyse; Tchnip: Paris, 1960; Vol. II, p 2075-2099.
23. J. Benziger and R. Madix. *Surf. Sci.* 1981, **109**, L527.
24. H. Olive and S. Olive, *Chem. Int. Ed.* **15** (1976) 136.
25. C. K. Rofer-DePooter, *Chem. Rev.* **81**, 447 (1981).
26. E. Iglesia, S. L. Soled, J. E. Baumgartner, and S. C. Reyes, *J. Catal.* **153** (1995) 108.
27. B. Wojciechowsky, *Catal. Rev. Sci. Eng.*, **30** (1988) 678.
28. H. Schulz, M. Claeys, S. Harms, *Stud. Surf. Sci. Catal.* **107** (1997) 193.
29. J. A. Biscardi, G. D. Meitzner, and E. Iglesia, *J. Catal.* **179** (1998) 192.


## 2. Schematic Diagram of Experimental Apparatus

*2.1. Catalytic Microreactor Unit (FTSU) for FTS on Co-based Catalyst*

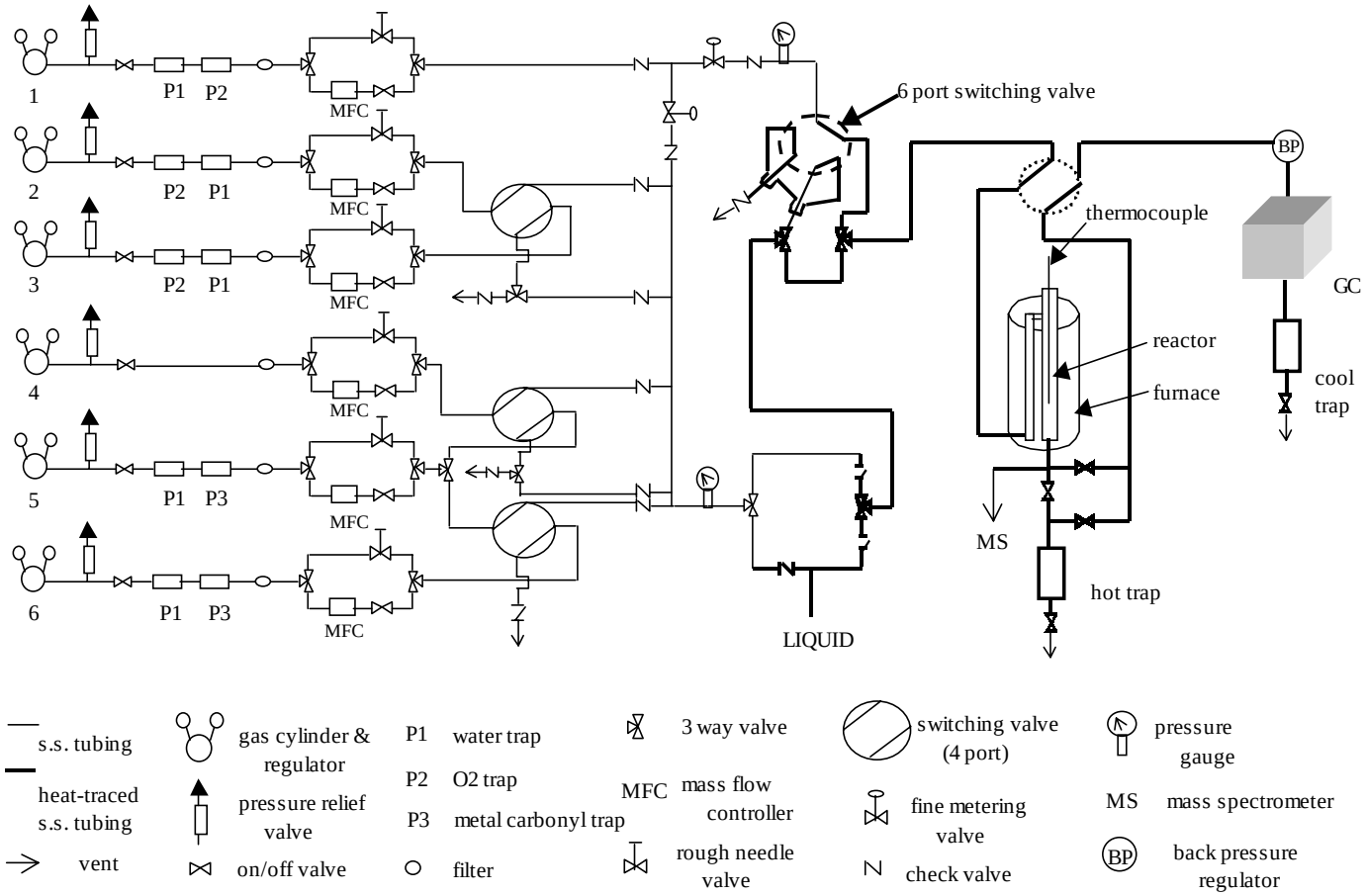


**Appendix 2.1 Schematic diagram of the Fischer-Tropsch synthesis unit**

## 3. Peak Identification on Gas-Chromatograph

Appendix 3.1. Gas chromatograph conditions and typical products of Co-based catalysts with retention time[a]

[a]Reaction conditions: 21.9 wt% $Co/SiO_2$ Catalyst, 200°C, 20 atm, $H_2/CO/N_2$ = 62/31/7

TCD

| Column | | Carboxen-1004, 2m × 1/16'' | | |
|---|---|---|---|---|
| Oven | Initial Temperature ($^oC$) | - 60 | Initial Time (min) | 3 |
| | Ramping Rate ($^oC$/min) | 10 | | |
| | Final Temperature ($^oC$) | 230 | Final Time (min) | 20 |
| Detector Temperature ($^oC$) | | 250 | Injector Temperature ($^oC$) | 250 |
| Inlet Pressure (atm) | | 4 | | |
| He Flow Rate (ml/min) | | 30 | Reference Flow Rate (ml/min) | 30 |

| Index Number | Carbon Number | Products | Retention Time (min) |
|---|---|---|---|
| 1 | | $H_2$ | 0.87 |
| 2 | | $N_2$ | 7.26 |
| 3 | C1 | CO | 8.77 |
| 4 | C1 | $CH_4$ | 13.57 |
| 5 | C1 | $CO_2$ | 17.39 |
| 6 | | $H_2O$ | 18.62 |
| 7 | C2 | $C_2H_6$ | 25.40 |
| 8 | C3 | $C_3H_6$ | 34.07 |
| 9 | C3 | $C_3H_8$ | 35.58 |

FID

| Column | | HP-1, crosslinked methyl silicone, 50m × 0.32mm × 1.05μm | | |
|---|---|---|---|---|
| Oven | Initial Temperature ($^oC$) | - 60 | Initial Time (min) | 3 |
| | Ramping Rate ($^oC$/min) | 10 | | |
| | Final Temperature ($^oC$) | 230 | Final Time (min) | 20 |
| Detector Temperature ($^oC$) | | 250 | Injector Temperature ($^oC$) | 250 |
| Inlet Pressure (psi) | | 23.2 | Split Ratio | 25: 1 |
| He Flow Rate (ml/min) | | 100 | Make-up He Flow Rate (ml/min) | 20 |
| $H_2$ Flow Rate (ml/min) | | 30 | Air Flow Rate (ml/min) | 300 |

| Index Number | Carbon Number | Products | Retention Time (min) |
|---|---|---|---|
| 1 | C1 | $CH_4$ | 2.25 |
| 2 | C2 | $C_2H_4$ | 2.53 |
| 3 | C2 | $C_2H_6$ | 2.76 |
| 4 | C3 | $C_3H_6$ | 5.02 |
| 5 | C3 | $C_3H_8$ | 5.23 |
| 6 | | unknown | 8.07 |
| 7 | C4 | 1-$C_4H_8$ | 8.77 |
| 8 | C4 | 1-$C_4H_{10}$ | 9.04 |
| 9 | C4 | *Cis*-2-$C_4H_8$ | 9.45 |
| 10 | C4 | *Trans*-2-$C_4H_8$ | 9.91 |
| 11 | C5 | $C_5H_{10}$-isomer | 10.86 |
| 12 | C5 | $C_5H_{12}$-isomer | 11.38 |
| 13 | C5 | $C_5H_{12}$-isomer | 11.49 |
| 14 | C5 | 1-$C_5H_{10}$ | 11.82 |
| 15 | C5 | 1-$C_5H_{12}$ | 12.13 |
| 16 | C5 | $C_5H_{10}$-internal | 12.38 |
| 17 | C5 | $C_5H_{10}$-internal | 12.58 |
| 18 | C6 | $C_6H_{12}$-isomer | 13.57 |
| 19 | C6 | $C_6H_{14}$-isomer | 14.08 |
| 20 | C6 | 1-$C_6H_{12}$ | 14.49 |
| 21 | C6 | 1-$C_6H_{14}$ | 14.77 |
| 22 | C6 | $C_6H_{12}$-internal | 14.89 |
| 23 | C6 | $C_6H_{12}$-internal | 15.11 |
| 24 | C7 | $C_7H_{14}$-isomer | 15.99 |

| | | | |
|---|---|---|---|
| 25 | C7 | $C_7H_{16}$-isomer | 16.55 |
| 26 | C7 | 1-$C_7H_{14}$ | 16.86 |
| 27 | C7 | 1-$C_7H_{16}$ | 17.11 |
| 28 | C7 | $C_7H_{14}$-internal | 17.21 |
| 29 | C7 | $C_7H_{14}$-internal | 17.40 |
| 30 | C8 | $C_8H_{16}$-isomer | 18.20 |
| 31 | C8 | 1-$C_8H_{16}$ | 19.00 |
| 32 | C8 | 1-$C_8H_{18}$ | 19.23 |
| 33 | C8 | $C_8H_{16}$-internal | 19.30 |
| 34 | C8 | $C_8H_{16}$-internal | 19.47 |
| 35 | C9 | $C_9H_{18}$-isomer | 20.23 |
| 36 | C9 | 1-$C_9H_{18}$ | 20.96 |
| 37 | C9 | $C_9H_{18}$-isomer | 21.08 |
| 38 | C9 | 1-$C_9H_{20}$ | 21.18 |
| 39 | C9 | $C_9H_{18}$-internal | 21.39 |
| 40 | C10 | $C_{10}H_{20}$-isomer | 22.10 |
| 41 | C10 | 1-$C_{10}H_{20}$ | 22.77 |
| 42 | C10 | $C_{10}H_{20}$-isomer | 22.87 |
| 43 | C10 | 1-$C_{10}H_{22}$ | 22.97 |
| 44 | C10 | $C_{10}H_{20}$-internal | 23.17 |
| 45 | C11 | $C_{11}H_{22}$-isomer | 23.84 |
| 46 | C11 | 1-$C_{11}H_{22}$ | 24.45 |
| 47 | C11 | $C_{11}H_{22}$-isomer | 24.52 |
| 48 | C11 | 1-$C_{11}H_{24}$ | 24.63 |
| 49 | C11 | $C_{11}H_{22}$-internal | 24.82 |
| 50 | C12 | $C_{12}H_{24}$-isomer | 25.46 |
| 51 | C12 | 1-$C_{12}H_{24}$ | 26.01 |
| 52 | C12 | $C_{12}H_{24}$-isomer | 26.07 |
| 53 | C12 | 1-$C_{12}H_{26}$ | 26.18 |
| 54 | C12 | $C_{12}H_{24}$-internal | 26.36 |
| 55 | C13 | $C_{13}H_{26}$-isomer | 26.98 |
| 56 | C13 | 1-$C_{13}H_{26}$ | 27.48 |
| 57 | C13 | $C_{13}H_{26}$-isomer | 27.52 |
| 58 | C13 | 1-$C_{13}H_{28}$ | 27.63 |
| 59 | C13 | $C_{13}H_{26}$-internal | 27.81 |
| 60 | C14 | $C_{14}H_{28}$-isomer | 28.40 |
| 61 | C14 | 1-$C_{14}H_{28}$ | 28.85 |
| 62 | C14 | 1-$C_{14}H_{30}$ | 28.99 |

| | | | |
|---|---|---|---|
| 63 | C14 | $C_{14}H_{28}$-internal | 29.16 |
| 64 | C15 | $C_{15}H_{30}$-isomer | 29.74 |
| 65 | C15 | 1-$C_{15}H_{30}$ | 30.14 |
| 66 | C15 | 1-$C_{15}H_{32}$ | 30.27 |
| 67 | C15 | $C_{15}H_{30}$-internal | 30.44 |
| 68 | C16 | 1-$C_{16}H_{34}$ | 31.48 |

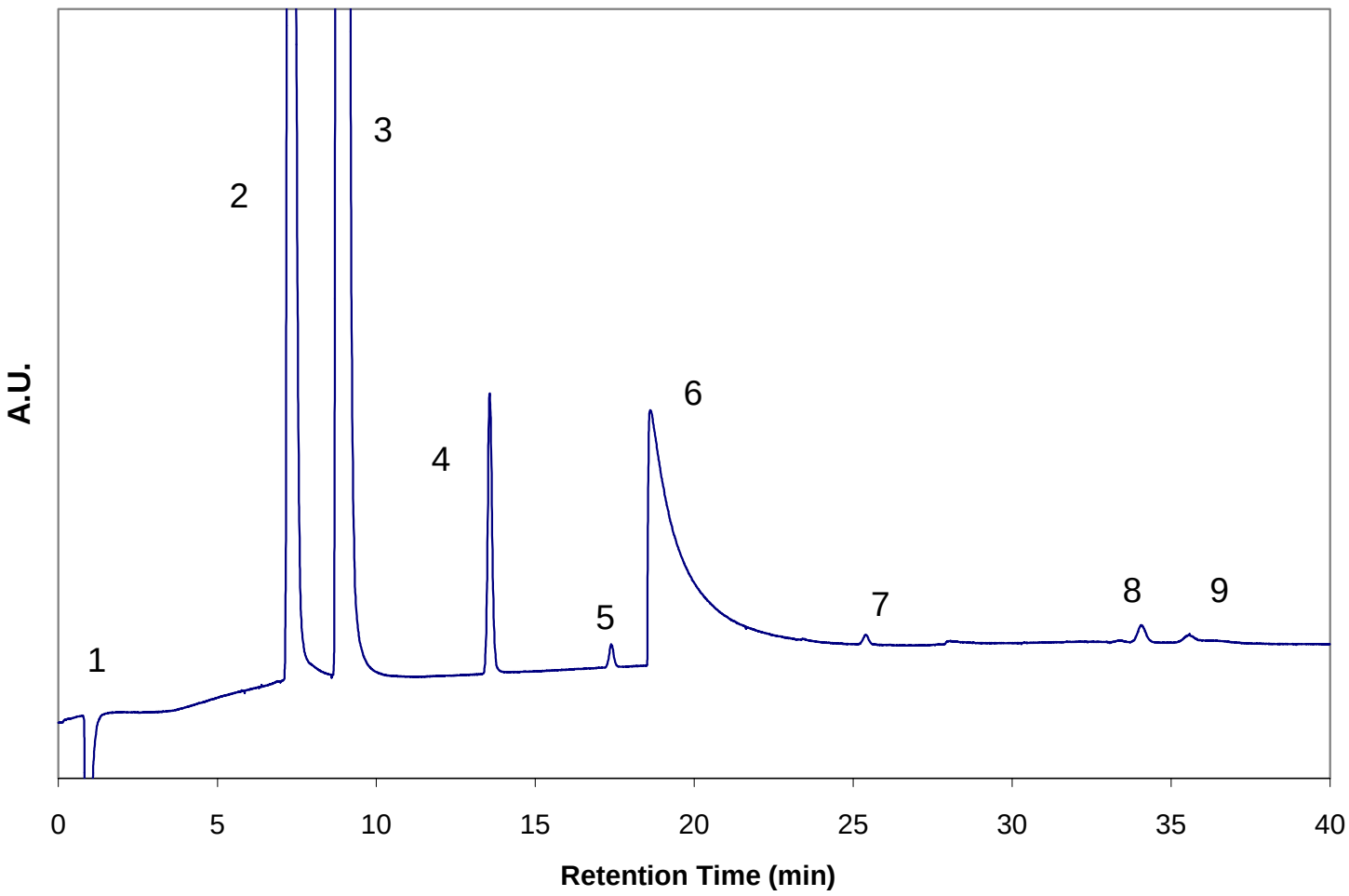


**Appendix 3.2. TCD chromatogram**

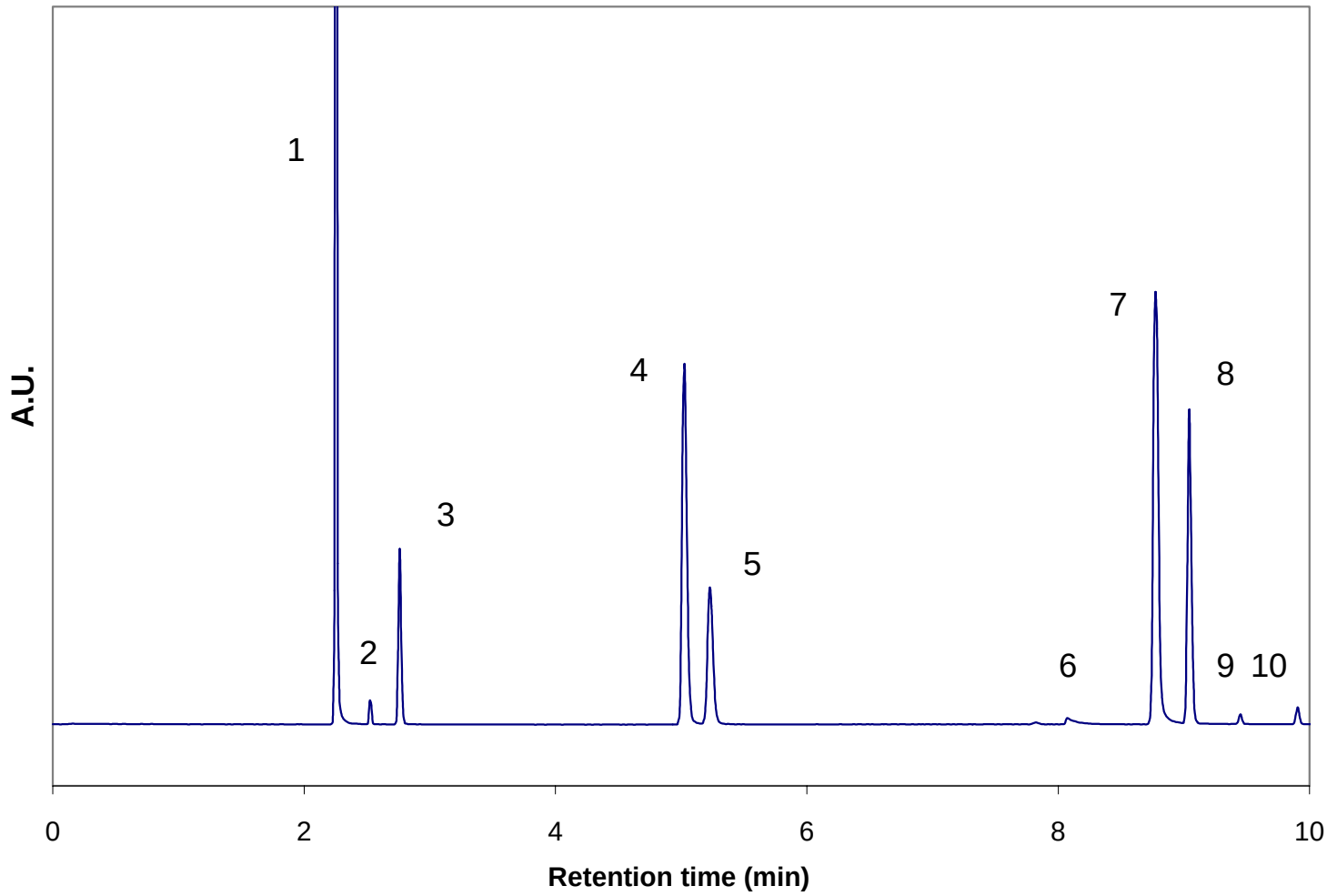


**Appendix 3.3. FID chromatogram**

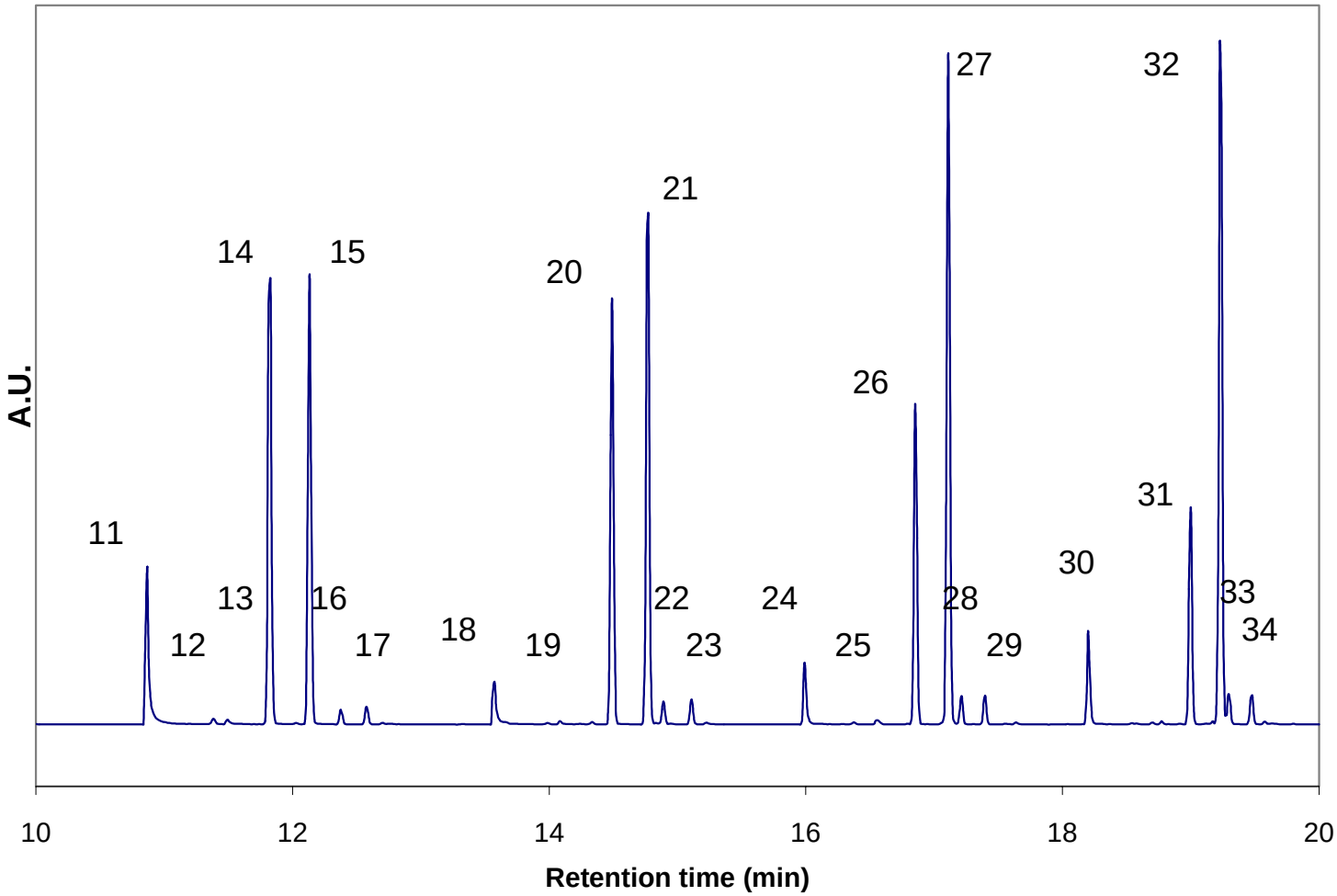


**Appendix 3.3. FID chromatogram (continued)**

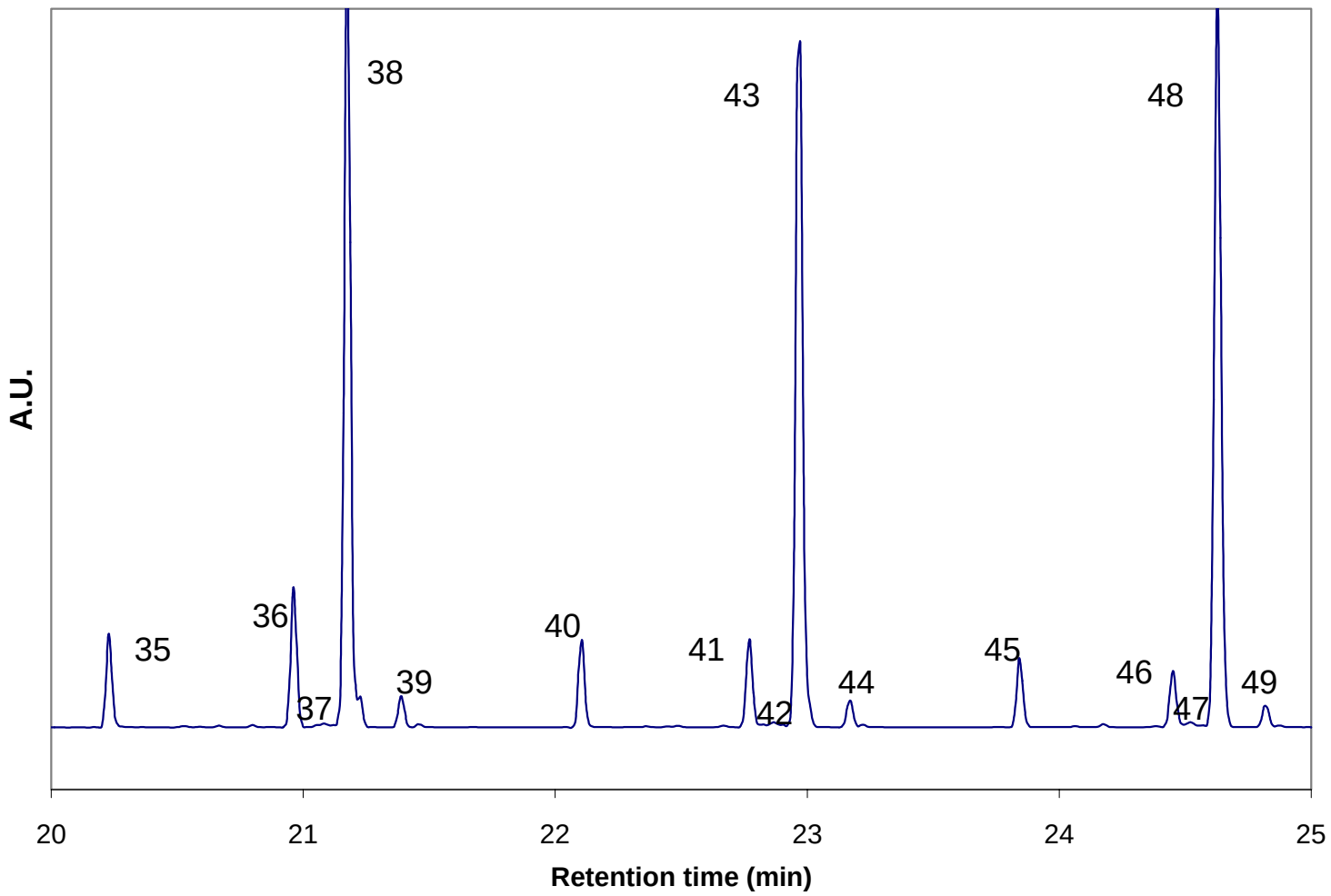


**Appendix 3.3. FID chromatogram (continued)**

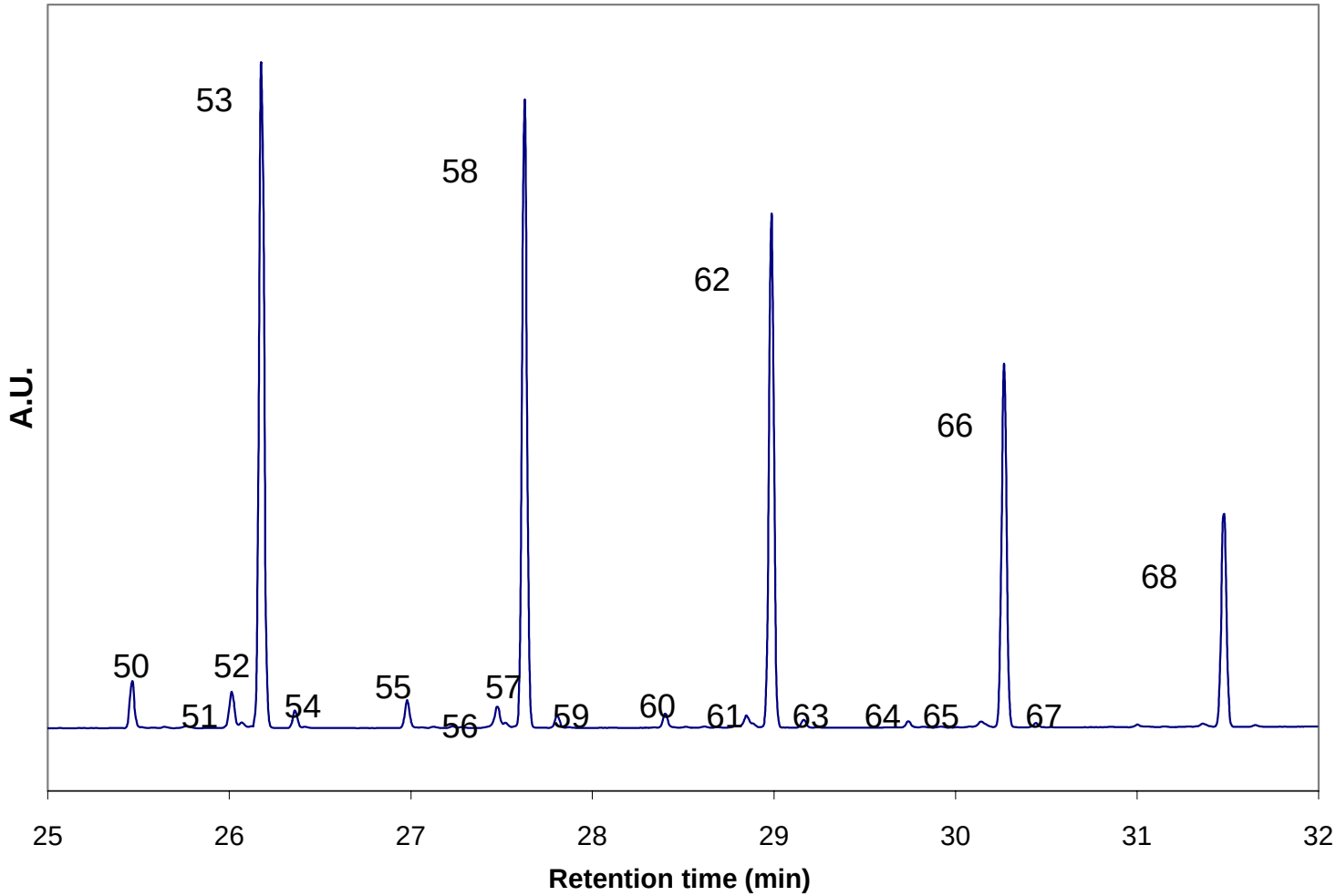


**Appendix 3.3. FID chromatogram (continued)**

## Task 12. Reporting/Project Management

Three monthly and one quarterly reports have been completed.